

UNIVERSITÁ DEGLI STUDI DI NAPOLI FEDERICO II

FACOLTÁ DI INGEGNERIA

SCUOLA DI DOTTORATO IN INGEGNERIA INDUSTRIALE



DOTTORATO DI RICERCA IN

INGEGNERIA ELETTRICA

(XX CICLO)

**A SUB-OPTIMAL ENERGY MANAGEMENT
STRATEGY FOR HYBRID ELECTRIC VEHICLES**

Tutor:

Prof. Ing. Santolo Meo

Addottorando:

Ing. Francesco Esposito

Coordinatore del corso di dottorato:

Prof. Ing. Guido Carpinelli

A mia moglie

Contents

<i>Abstract</i>	1
1. Present status and future trends in light transport technologies	
1.1 Introduction	3
1.2 Current status of private transport sector.....	5
1.2.1 Environmental pollution and energy primary sources emergency.....	7
1.3 Future trends in transports	10
1.3.1 The actual government policies	11
1.4 New vehicular technologies for a “sustainable” transport.....	12
1.4.1 Hystorical evolution of automotive electrical power systems	15
1.4.2 More Electric Vehicles (MEV).....	16
1.4.3 X-by-wire technologies.....	18
1.5 Hybrid electric vehicles	21
1.5.1 Series hybrid architecture.....	22
1.5.2 Parallel hybrid architecture	23
1.5.3 Series-parallel and power-split hybrid architectures.....	24
1.5.4 A commercial power-split hybrid vehicle: the Toyota Prius	25
2. State of the art of energy management strategies for automotive power systems	
2.1 Introduction	27
2.2 Energy management strategy for conventional vehicles	28
2.3 Energy management strategies for hybrid electric vehicles	30
2.3.1 Parallel and series-parallel hybrid vehicles.....	31
2.3.1.1 Charge sustaining parallel hybrids	31
2.3.1.2 Charge depleting parallel hybrids.....	32
2.3.2 Series hybrid vehicles	33
2.3.2.1 Charge sustaining series hybrids	33
2.3.2.2 Charge depleting series hybrids.....	34
2.3.3 Real control strategy of Toyota Prius	35
2.3.4 Real control strategy of Honda Insight	35
2.3.5 Choice of the suitable control strategy.....	36

2.3.6	Innovative energy management strategies	36
3.	Comparative evaluation of automotive power bus architectures	
3.1	Introduction	42
3.2	State of the art of automotive power bus architectures.....	43
3.3	Modelling of classical on-board loads.....	52
3.3.1	Subspace methods for the parameter identification of linear systems ..	53
3.3.2	Torque estimation for the considered models	56
3.3.3	Definition of the model's parameters.....	56
3.3.3.1	Electric window winder model's parameters	56
3.3.3.2	Electric fans model's parameters.....	57
3.3.3.3	Front electric windscreen wiper model's parameters.....	59
3.3.3.4	Rear electric windscreen wiper model's parameters	60
3.3.4	Electric window winder model validation	61
3.3.5	Air conditioner's electric fan model validation	63
3.3.6	Radiator's electric fan model validation	65
3.3.7	Front electric windscreen wiper model validation.....	66
3.3.8	Rear electric windscreen wiper model validation.....	68
3.4	Modelling of innovative on-board electric loads.....	69
3.4.1	EPAS (Electrical Power Assisted Steering).....	69
3.5	Modelling of the power supply system for conventional vehicles	71
3.5.1	Lead-acid batteries	72
3.5.2	Lundell alternator	72
3.6	A tool for the comparative analysis of power bus architectures.....	78
3.6.1	Critical drive cycles maker	79
3.6.2	Critical loads activation sequences maker	80
3.6.3	Power bus simulator.....	81
3.7	Case-study for the testing of Evaluator	82
4.	The proposed energy management strategy for conventional vehicles	
4.1	Introduction	88
4.2	Energetic model of the vehicle	89
4.2.1	Basic assumptions	90
4.2.2	Engine model	90
4.2.3	Power train model	92
4.2.4	Alternator model	93

4.2.5	Battery model.....	94
4.2.6	Schematic of the power bus	95
4.3	Analytic formulation of the proposed optimal control strategy	96
4.4	Case-study: an application to a real vehicle	101
4.4.1	Simulations and results	103
5.	The proposed energy management strategy for hybrid power-split vehicles	
5.1	Introduction	108
5.2	Energetic model of the vehicle	109
5.2.1	The considered hybrid architecture.....	109
5.2.2	Basic assumptions	111
5.2.3	Engine model	112
5.2.4	Electric motor model.....	114
5.2.5	Power train model	116
5.2.6	CVT model.....	116
5.2.7	ISA model	118
5.2.8	Battery model.....	120
5.2.9	Schematic of the power bus	122
5.3	Analytic formulation of the proposed optimal control strategy	123
5.4	Case-study: an application to a real vehicle	130
5.4.1	Simulations and results of the proposed strategy.....	132
5.4.2	Comparisons with ADVISOR simulations results.....	136
	Conclusions.....	140
	References	143

Abstract

The research activity performed in this dissertation focussed on the development of enhanced solutions for the architectures and the relative control of hybrid or conventional vehicles' power buses, with the aim to minimize the fuel consumption and the pollutant emissions. These goals would have to be obtained either improving the efficiency of every components in the vehicle or adopting a suitable energy management strategy, able to operate the "vehicle" system at its maximum global efficiency, while ensuring the fulfillment of the performances required from the driver, leaving unaffected the drivability of the vehicle and the on-board electrical loads supplies, as much as possible leaving the battery SOC at a constant level.

Two research activity lines have been followed: the first one concerns a comparative analysis of the power bus architectures in vehicles with conventional or hybrid propulsion, for the detection of innovative solutions with high quality-of-electric-service and reliability performances, able to satisfy specific requests. The second activity involves the development and implementation of an algorithm for the management and control of the power bus in conventional and hybrid propulsion vehicles.

Employing some acquired methodologies, the first research activity has led to the modeling of automotive components (power supply system, electro-mechanical drives and electrical loads) of the vehicle power system, the detection of critical drive cycles and critical loads activation sequences, the simulation of the power bus

architecture for the analysis in steady-state and transient conditions, with the purpose to realize a comparative evaluation among several existing or innovative power bus architectures. The comparative evaluation among different architectures has been made achievable with the design of the software so-called *Evaluator*, implemented in MATLAB environment: starting from the value of several performance indexes such as volume, weight, cost, reliability of the individual components and of whole system, quality of the bus voltage, *Evaluator* provides a global index that defines the adaptability of the evaluated architecture to a fixed application.

The second research activity includes the energetic modelling of the propulsor and electric generation/storage/conversion devices of the vehicle with conventional and hybrid propulsion. It has also involved the analysis of energy management strategies currently available in the literature, adopted on road vehicles.

Then, it has been formulated an “off-line” energy management algorithm, that is based on the knowledge of a fixed electric loads activation sequence and a fixed drive cycle of the vehicle. The related activity has been the formulation and the solution of a global optimization problem (particularly for conventional and hybrid power-split vehicles), the solution of finite dimensional nonlinear convex optimization problems, with equality and inequality constraints.

A case-study for testing the proposed new strategy on a real commercial hybrid power-split vehicle (Toyota Prius) has been reported.

1. Present status and future trends in light transport technologies

1.1 Introduction

In recent years, due to the continuous increase in demand of energy for the development, the alarm about the reduction of fossil fuels stocks is growing. Beside this context, to preserve the environmental quality, the governments of countries such as USA, Japan and European countries have imposed stringent restrictions on emissions of pollutants from vehicles.

In terms of light transport, which regards an important part of world fuel consumption and pollutant emissions, the research has moved towards more "efficient" and "clean" propulsion systems, and although the new engine technologies have greatly reduced the impact, a more drastic reduction is expected with the use of alternative propulsion systems.

The electric vehicles, the hybrid electric vehicles and the fuel cells as storage/generator system offer the possibility of using alternative energy resources.

The initial thrust towards the reduction of pollutant emissions had encouraged the development of electric vehicles, but the historical defects of these vehicles, related to the limited autonomy and long recharging time, has strongly affected the market penetration.

On the other hand, hybrid vehicles, that join the advantages of the electric vehicles to the highest traditional vehicles autonomy, allow more efficient use of energy, thus reducing also the pollutant emissions.

Furthermore, hybrid vehicles can play an important role in the development of power electronics technology, applied to vehicles in management systems of electric motors and storage systems, allowing a reduction in costs and a more rapid market penetration of the future fuel cells vehicle with zero emissions.

The hybrid propulsion is part of the hybrid thermal-electric category, which combines an internal combustion engine with one or more electrical machines. The choice of joining an electric motor to a thermal engine offers many advantages: the possibility to drive "electric only", switching off the engine when it is not necessary, the "regenerative braking" that recovers kinetic energy accumulated in the vehicle, and the possibility of operation of the engine under conditions of maximum efficiency.

The difficulties of managing in a better way the generic "vehicle energy system", especially the on-board electric power system, are growing even for the trend of the manufacturers to replace mechanical devices on board with electrically assisted technologies and X-By-Wire actuators (the electric power demand are growing for these reasons from actual 1 kW for conventional vehicles towards about 5 kW of luxury vehicles), in order to increase the "comfort" and the benefits provided to the end user.

This determines the necessity to analyze the actually available vehicular technologies, included the so defined "more electric vehicle", where the presence of electrical devices besides those for traction (EV and HEV) is considerable and for the correct and reliable management is necessary to redesign the vehicular power system topology.

For this purpose in this chapter, in addition to the recall of existing hybrid vehicles architectures, will be described the state of the art of the innovative no-propulsion electrical loads.

1.2 Current status of private transport sector [1]

Mobility is an essential human need. Human survival and societal interaction depend on the ability to move people and goods. Efficient mobility systems are essential facilitators of economic development. Cities could not exist and global trade could not occur without systems to transport people and goods cheaply and efficiently.

Since motorized transport relies on oil for virtually all its fuel and accounts for almost half of world oil consumption, the transport sector faces a challenging future, given its dependence on oil.

Pollutant emission reduction will be only one of several key issues in transport during the coming decades and will not be the foremost issue in many areas. In developing countries especially, increasing demand for private vehicles is outpacing the supply of transport infrastructure – including both road networks and public transit networks. The result is growing congestion and air pollution, and a rise in traffic fatalities.

Further, the predominant reliance on private vehicles for passenger travel is creating substantial societal strains as economically disadvantaged populations are left out of the rapid growth in mobility. In many countries, concerns about transport will likely focus on the local traffic, pollution, safety and equity effects. The global warming issue in transport will have to be addressed in the context of the broader goal of sustainable development.

The transport sector plays a crucial and growing role in world energy use and emissions of greenhouse gases (GHG). In 2004, transport energy use amounted to 26% of total world energy use and the transport sector was responsible for about 23% of world energy-related GHG emissions. The 1990–2002 growth rate of energy consumption in the transport sector was highest among all the end-use sectors. Of a total of 77 EJ (exaJoule) of total transport energy use, road vehicles account for more than three-quarters, with light-duty vehicles and freight trucks having the lion's share (see Table 1.1). Virtually all (95%) of transport energy comes from oil-based fuels, largely diesel (23.6 EJ, or about 31% of total energy) and gasoline (36.4 EJ, 47%). One consequence of this dependence, coupled with the only moderate differences in carbon content of the various oil-based fuels, is that the CO₂ emissions from the

different transport sub-sectors are approximately proportional to their energy use (Fig. 1.1 – OECD: Organisation for Economic Co-operation and Development).

Mode	Energy use (EJ)	Share (%)
Light-duty vehicles (LDVs)	34.2	44.5
2-wheelers	1.2	1.6
Heavy freight trucks	12.48	16.2
Medium freight trucks	6.77	8.8
Buses	4.76	6.2
Rail	1.19	1.5
Air	8.95	11.6
Shipping	7.32	9.5
Total	76.87	100

Source: WBCSD, 2004.

Table 1.1: world transport energy use in 2000, by mode.

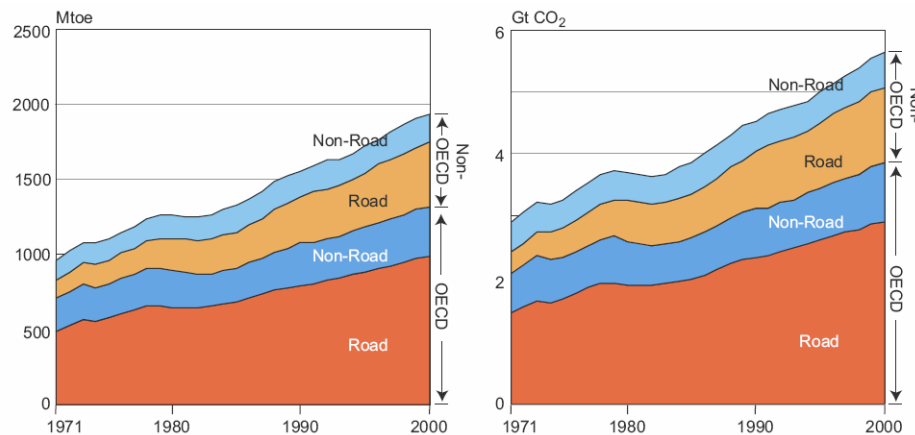


Fig. 1.1: energy consumption and CO₂ emission in the transport sector (Source: IEA, 2006).

Economic development and transport are inextricably linked. Development increases transport demand, while availability of transport stimulates even more development by allowing trade and economic specialization. Industrialization and growing specialization have created the need for large shipments of goods and materials over substantial distances; accelerating globalization has greatly increased these flows.

Urbanization has been extremely rapid in the past century. About 75% of people in the industrialized world and 40% in the developing world now live in urban areas. Also, cities have grown larger, with 19 cities now having a population over 10 million. A parallel trend has been the decentralization of cities – they have spread out

faster than they have grown in population, with rapid growth in suburban areas and the rise of ‘edge cities’ in the outer suburbs. This decentralization has created both a growing demand for travel and an urban pattern that is not easily served by public transport. The result has been a rapid increase in personal vehicles – not only cars but also 2-wheelers – and a declining share of transit. Further, the lower-density development and the greater distances needed to access jobs and services have seen the decline of walking and bicycling as a share of total travel.

Another factor that has accelerated the increase in transport energy use and carbon emissions is the gradual growth in the size, weight and power of passenger vehicles, especially in the industrialized world. Although the efficiency of vehicle technology has improved steadily over time, much of the benefit of these improvements have gone towards increased power and size at the expense of improved fuel efficiency. For example, the US Environmental Protection Agency has concluded that the US new Light-duty Vehicle (LDV) fleet fuel economy in 2005 would have been 24% higher had the fleet remained at the weight and performance distribution it had in 1987. Instead, over that time period, it became 27% heavier and 30% faster in 0–60 mph (0–97 km/h) time, and achieved 5% poorer fuel economy. In other words, if power and size had been held constant during this period, the fuel consumption rates of light-duty vehicles would have dropped more than 1% per year.

1.2.1 Environmental pollution and energy primary sources emergency

The main goal of all energy transformations is to provide energy services that improve quality of life (e.g. health, life expectancy and comfort) and productivity. A supply of secure, equitable, affordable and sustainable energy is vital to future prosperity. Approximately 45% of final consumer energy is used for low-temperature heat (cooking, water and space heating, drying), 10% for high-temperature industrial process heat, 15% for electric motors, lighting and electronics and 30% for transport. The CO₂ emissions from meeting this energy demand using mainly fossil fuels account for around 80% of total global emissions. Demands for all forms of energy continue to rise to meet expanding economies and increases in

world population. Rising prices and concerns about insecure energy supplies will compromise growth in fossil fuel consumption.

There are risks to being unprepared for future energy-supply constraints and disruptions. Currently, fossil fuels provide almost 80% of world energy supply; a transition away from their traditional use to zero- and low-carbon-emitting modern energy systems (including carbon dioxide capture and storage, as well as improved energy efficiency, would be part solutions to GHG-emission reduction.

In all regions of the world energy demand has grown in recent years (Fig. 1.2). A 65% global increase above the 2004 primary energy demand (464 EJ, 11,204 Mtoe) is anticipated by 2030 under business as usual.

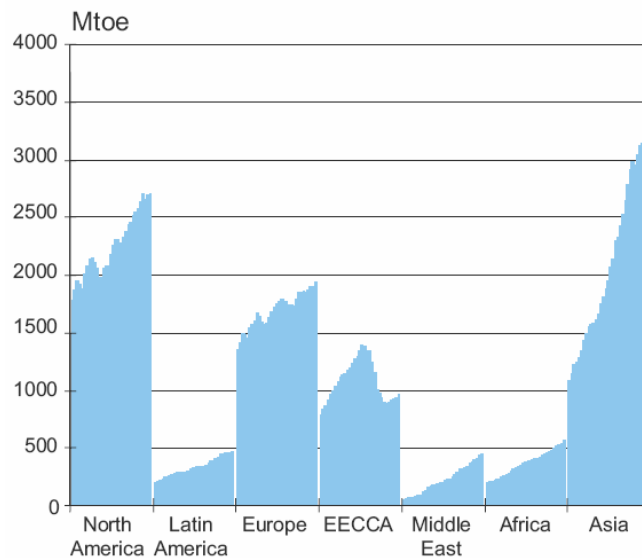


Fig. 1.2: global annual primary energy demand (including traditional biomass), 1971 – 2003 by region (Source: IEA, 2004).
Notes: EECCA = countries of Eastern Europe, the Caucasus and Central Asia. 1000 Mtoe = 42 EJ.

Major investment will be needed, mostly in developing countries. As a result, without effective mitigation, total energy-related carbon dioxide emissions (including transformations, own use and losses) will rise from 26.1 GtCO₂ (7.2 GtC) in 2004 to around 37–40 GtCO₂ (11.1 GtC) in 2030, possibly even higher, assuming modest energy-efficiency improvements are made to technologies currently in use. This means that all cost-effective means of reducing carbon emissions would need to be deployed in order to slow down the rate of increase of atmospheric concentrations.

Since 1971, oil and coal remain the most important primary energy sources with coal increasing its share significantly since 2000 (Fig. 1.3). Growth slowed in 2005 and the total share of fossil fuels dropped from 86% in 1971 to 81% in 2004, excluding wind, solar, geothermal, bioenergy and biofuels, as well as non-traded traditional biomass.

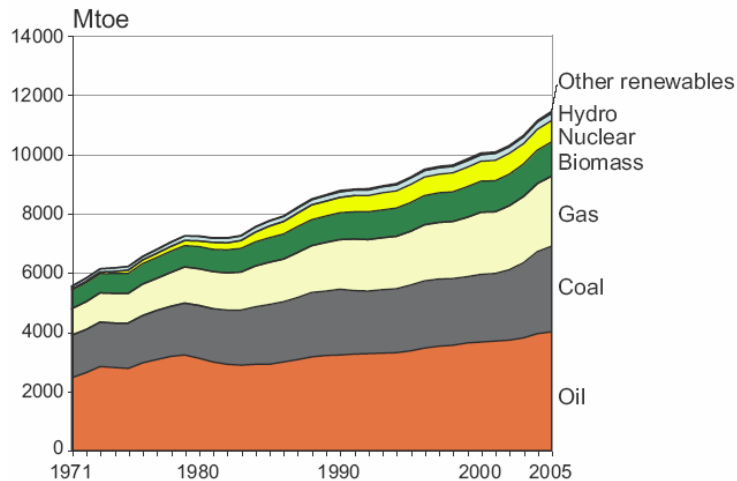


Fig. 1.3: world primary energy consumption by fuel type. (Source: IEA, 2006).

Regarding the use of oil in different industrial sectors, the following Tab. 1.2 and 1.3 provide an overview on the use of oil in various fields, and show how the main use is done in the transport sector, especially in the automotive sector.

Sector	% of oil use
Transport	57.7
Industry	20.1
Residential	7.0
No-energy uses	5.9

Table 1.2: percentual employment of oil per sector.

Transport sector	% of oil use
Road vehicles	80
Air transport	13
Sea transport	1.8
Railways	1.4

Table 1.3: percentual employment of oil per transport sector.

As can be noted from Tabs. 1.2 and 1.3, oil is the most used road vehicles' fuel and in this sector is practically irreplaceable.

As reported in literature, use of oil is continuously growing, actually the annual rated growing is about 2%, while the discovered new oil deposits are decreasing about 4% per year.

1.3 Future trends in transports [1]

There seems little doubt that, short of worldwide economic collapse, transport activity will continue to grow at a rapid pace for the foreseeable future. However, the shape of that demand and the means by which it will be satisfied depend on several factors.

For first, transport technology has been evolving rapidly. The energy efficiency of the different modes, vehicle technologies, and fuels, as well as their cost and desirability, will be strongly affected by technology developments in the future. For example, although hybrid electric drive trains have made a strong early showing in the Japanese and US markets, their ultimate degree of market penetration will depend strongly on further cost reductions. Other near-term options include the migration of light-duty diesel from Europe to other regions. Longer term opportunities requiring more advanced technology include new biomass fuels beyond those made from sugar cane in Brazil and corn in the USA, fuel cells running on hydrogen and battery powered electric vehicles.

Another important issue is that, as incomes in the developing nations grow, transport infrastructure will grow rapidly. Current trends point towards growing dependence on private cars, but other alternatives exist.

Also, as seen in Fig. 1.4, the intensity of car ownership varies widely around the world even when differences in income are accounted for, so different countries have made very different choices as they have developed. The future choices made by both governments and travellers will have huge implications for future transport energy demand and CO₂ emissions in these countries.

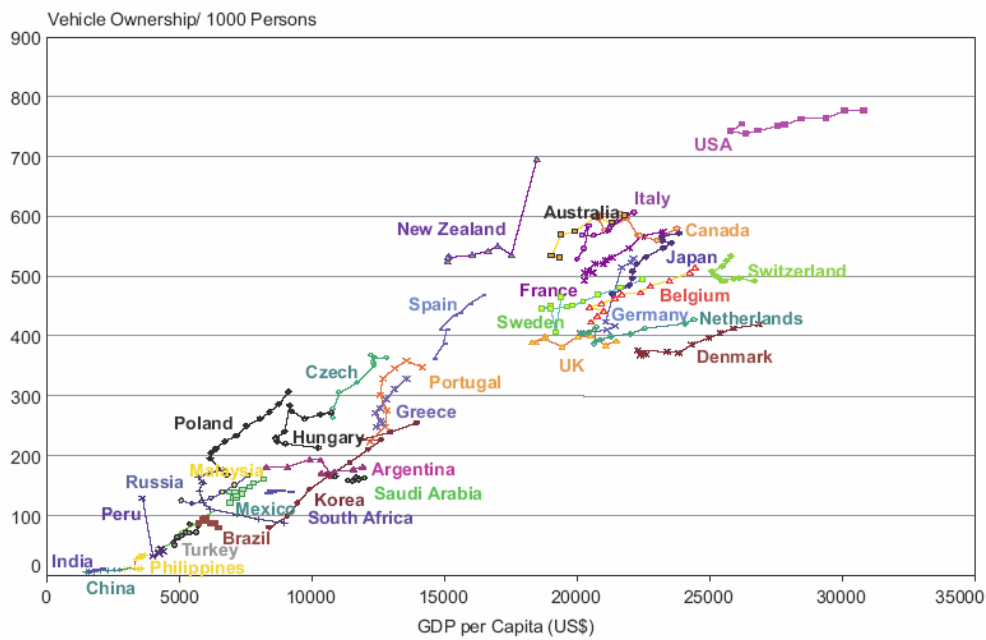


Fig. 1.4: vehicle ownership as a function of per capita income (Source: World Bank, 2004).

1.3.1 The actual government policies

The reduction of GHG emissions from energy-supply systems is being actively pursued through a variety of government policies and private sector research. There are many technologies, behavioural changes and infrastructural developments that could be adopted to reduce the environmental impacts of current energy-supply systems. Whereas planning policies provide background for climate change mitigation programmes, most climate policies relating to energy supply tend to come from three policy ‘families’:

- economic instruments (e.g. subsidies, taxes, tax exemption and tax credit);
- regulatory instruments (e.g. mandated targets, minimum performance standards, vehicle-exhaust emission controls);
- policy processes (e.g. voluntary agreements and consultation, dissemination of information, strategic planning).

In addition, governments support R&D programmes with financial incentives or direct investment to stimulate the development and deployment of new innovative energy conversion technologies and create markets for them.

Most industrialized nations now impose fuel economy requirements (or their equivalent in CO₂ emissions requirements) on new light-duty vehicles. The first

standards were imposed by the United States in 1975, requiring 27.5 mpg (8.55 L/100 km) corporate fleet averages for new passenger cars and 20.7 mpg (11.36 L/100 km) for light trucks by 1985. The passenger car standard remains unchanged, whereas the light truck standard has recently been increased to 22.2 mpg (10.6 L/100 km) for the 2007 model year and to 23.5 mpg (10.0 L/100 km) in model year 2010.

Additional standards (some voluntary) include:

- European Union: a 2008 fleet wide requirement of 140gCO₂/km, about 41 mpg (5.74 L/100 km) of gasoline equivalent, using the New European Driving Cycle (NEDC), based on a Voluntary Agreement between the EU and the European manufacturers, with the Korean and Japanese manufacturers following in 2009. Recent slowing of the rate of efficiency improvement has raised doubts that the manufacturers will achieve the 2008 and 2009 targets.
- Japan: a 2010 target of about 35.5 mpg (6.6 L/100 km) for new gasoline passenger vehicles, using the Japan 10/15 driving cycle based on weight-class standards.
- The State of California has established GHG emission standards for new light-duty vehicles designed to reduce per-vehicle emissions by 22% in 2012 and 30% by 2016. Several US states have decided to adopt these standards, as well.

Fig. 1.5 shows the comparison of standards. Recent studies of the costs and fuel savings potential of technology improvements indicate considerable opportunity to achieve further fleet fuel economy gains from more stringent standards.

1.4 New vehicular technologies for a “sustainable” transport

Many technologies and strategies are at hand to reduce the growth or even, eventually, reverse transport GHG emissions. The most promising strategy for the near term is incremental improvements in current vehicle technologies. Advanced technologies that provide great promise include greater use of electric-drive technologies, including hybrid-electric power trains, fuel cells and battery electric vehicles. The use of alternative fuels such as natural gas, biofuels, electricity and

hydrogen, in combination with improved conventional and advanced technologies; provide the potential for even larger reductions.

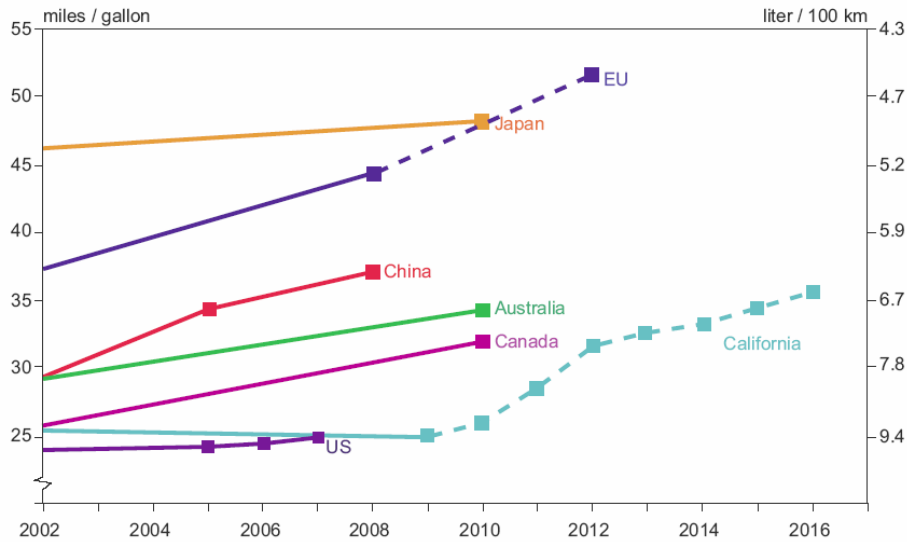


Fig. 1.5: fuel economy and GHG emission standards (Source: World Bank, 2004).

Note: all the fuel economy targets represent test values based on artificial driving cycles. The standards in the EU and Australia are based on voluntary agreements. In most cases, actual on-road fuel economy values will be lower; for example, the US publishes fuel economy estimates for individual LDVs that are about 15% lower than the test values and even these values appear to be optimistic. Miles/gallon is per US gallon.

Emissions associated with vehicles can be reduced by several types of measures, particularly increasing the efficiency of converting the fuel energy to work, by improving drive train efficiency and recapturing energy losses.

Increasing the efficiency with which the chemical energy in the fuel is transformed into work, to move the vehicle and provide comfort and other services to passengers, will also reduce GHG emissions. This includes measures to improve engine efficiency and the efficiency of the rest of the drive train and accessories, including air conditioning and heating. The range of measures here is quite great; for example, engine efficiency can be improved by three different kinds of measures, increasing thermodynamic efficiency, reducing frictional losses and reducing pumping losses (these losses are the energy needed to pump air and fuel into the cylinders and push out the exhaust) and each kind of measure can be addressed by a great number of design, material and technology changes. Improvements in transmissions can reduce losses in the transmission itself and help engines to operate in their most efficient modes. Also, some of the energy used to overcome inertia and accelerate the vehicle

– normally lost when the vehicle is slowed, to aerodynamic forces and rolling resistance as well to the mechanical brakes (as heat) – may be recaptured as electrical energy if regenerative braking is available [1].

Hybrid-electric drive trains combine a fuel-driven power source, such as a conventional internal combustion engine (ICE) with an electric drive train – electric motor/generator and battery (or ultracapacitor) - in various combinations. In current hybrids, the battery is recharged only by regenerative braking and engine charging, without external charging from the grid.

‘Plug-in hybrids,’ which would obtain part of their energy from the electric grid, can be an option but require a larger battery and perhaps a larger motor. Hybrids save energy by:

- Shutting the engine down when the vehicle is stopped (and possibly during braking or coasting);
- Recovering braking losses by using the electric motor to brake and using the electricity generated to recharge the battery;
- Using the motor to boost power during acceleration, allowing engine downsizing and improving average engine efficiency;
- Using the motor instead of the engine at low load (in some configurations), eliminating engine operation during its lowest efficiency mode;
- Allowing the use of a more efficient cycle than the standard Otto cycle (in some hybrids);
- Shifting power steering and other accessories to (more efficient) electric operation.

Hybridization can yield benefits in addition to directly improving fuel efficiency, including (depending on the design) enhanced performance (with reduced fuel efficiency benefits in some designs), less expensive 4-wheel drive systems, provision of electric power for off-vehicle use, and ease of introducing more efficient transmissions such as automated manuals (using the motor to reduce shift shock).

1.4.1 Historical evolution of automotive electrical power systems

Developments of the automobile electrical system remained relatively static in the years between 1930 and 1960. There were improvements in ignition to match the demands of higher compression engines and durability of components was improved but no real changes in concepts. By the 1950's, the ever present issue of reliable ignition again came to the forefront to challenge the automobile electrical system. With newer engines and higher compression ratio, the 6V ignition was exhibiting signs of becoming overwhelmed and durability was becoming a major obstacle. In 1952, during a meeting of the chief engineers of all the automobile companies in North America, the realization was present that unless something was done to improve the ignition system, there would be an epidemic of failed engines on the streets due to welded breaker points.

The decision was made to increase the electrical system voltage from a 6V battery with 7V DC nominal distribution potential to a 12V battery with 14V DC distribution level. The first 12V systems were introduced by General Motors in 1955 followed by Ford and Chrysler. The same rationale was present in Europe and soon all but VW would switch to 12V systems.

During the period from 1960 to 1980, the most significant change was the replacement of the DC generator with the Lundell alternator. The driving force behind the change was the increasing demand for electrical power. Electrical system demand had risen from the 100W of 1912 to typically 500W in 1960 and, by 1980, it increased even more to 1500W as more and more electrically power devices were installed. From 1980 to the present, the capability and pervasiveness of electronic engine controls have increased to the point of taking complete control of the engine combustion process, air and fuel metering, exhaust gas treatment, alternator control, and recently transmission control.

The conventional electrical system in an automobile can be divided into the architectural elements of energy storage, generation, starting, and distribution. Electrical distribution systems provide electrical power to connected consumers including ignition, interior and exterior lighting, electric motor driven fans pumps and compressors, and instrumentation subsystems. In order for the power available at

the sources to be made available at the terminals of the loads, some organized form of distribution throughout an automobile is essential. At present, most automobiles use a 14V DC electrical system. This has a single voltage level, i.e., 14V DC, with the loads being controlled by manual switches and relays. Because of the point-to-point wiring, the wiring harness is heavy and complex [2].

The present average power demand in an automobile is approximately 2.5 kW, as shown in Fig. 1.6 [11], with an annual rate increase of 5%. The voltage in a 14V system actually varies between 9V and 16V at the battery terminals, depending on the alternator output current, battery age, state of charge, and other factors. This results in overrating the loads at nominal system voltage.

Besides all the disadvantages, the present 14V system cannot handle future electrical loads to be introduced in the more electric environment of the future cars, as it would be expensive and inefficient to do so. All these reasons have led to the development of new power system architectures which will replace the antiquated 12 V system with a more reliable one.

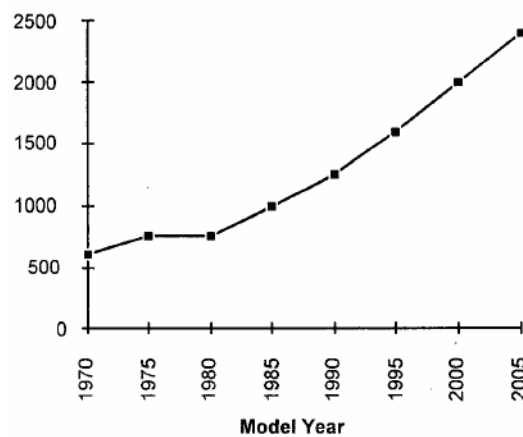


Fig. 1.6: growing of electric power demand in vehicles (W).

1.4.2 More Electric Vehicles (MEV)

In more electric vehicles (MEV) [2], there is a trend towards expanding electrical loads and replacement of more engine driven mechanical and hydraulic systems with electrical systems. These loads include the well-known lights, pumps, fans, and electric motors for various functions. They will also include some less wellknown

loads, such as electrically assisted power steering, electrically driven air conditioner compressor, electromechanical valve control, electrically controlled suspension and vehicle dynamics, and electrically heated catalytic converter. In fact, electrical subsystems may require a lower engine power with higher efficiency.

Furthermore, they can be used only when needed. Therefore, the MEV can have optimum fuel economy and performance. There are also other loads such as anti-lock braking, throttle actuation, ride-height adjustment, and rear-wheel steering, which will be driven electrically in the future.

Fig. 1.7 [3] shows electrical loads in MEV power systems. Most of the future electric loads require power electronic controls. In future automobiles, power electronics will be used to perform three different tasks. First task is simple on/off switching of loads, which is performed by mechanical switches and relays in conventional cars. Second task is the control of electric machines. Third one is not only changing the system voltage to a higher or lower level, but also converting electrical power from one form to another using DC/DC, DC/AC, and AC/DC converters.

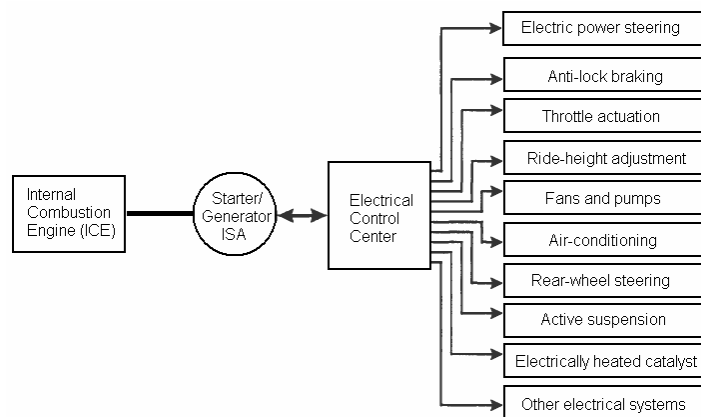


Fig. 1.7: electrical loads in the MEV power systems.

Due to the increasing electrical loads, automotive systems are becoming more electric. Therefore, MEV will need highly reliable, fault-tolerant, autonomous controlled electrical power systems to deliver high quality power from the sources to the loads. The voltage level and form in which power is distributed are important. A higher voltage (such as the proposed 42V) will reduce the weight and volume of the wiring harness, among several other advantages [6], [7], [12]. In fact, increasing the

voltage of the system, which is 14V in the conventional cars, is necessary to cope with the greater loads associated with the more electric environments in future cars.

In chapter 3, an overview on the possible substitutes of architectures for automotive power systems will be presented.

1.4.3 X-by-wire technologies

Vehicle manufacturers are seeking ways to reduce substantially vehicle weight, because lower weight means less fuel consumption, which in turn means lower emissions. Electronic systems have helped manufacturers toward this goal because these are often lighter than the mechanical systems that they replace. Additionally, electronic systems have proven to be precise in their functioning, reliable, with low need of maintenance and to have best performances, in terms of dynamic response and their natural integration in the electrical system respect to the hydraulic or mechanical actuators. Thus, engines, transmissions, airbags, brakes, and many other systems are now controlled electronically on many vehicles [13].

Another important issue is that the automobile industry is always concerned with safety related issues. It is always trying to develop methods that keep increasing the safety standards, for example, intelligent driver assistance. However, such systems need to be computer controlled to deliver maximum efficiency. With this comes the need to replace all the mechanic or hydraulic backup with electric/electronic components. This can be done only when it has been ascertained that the systems that are replacing the mechanical or hydraulic backups are very safe.

X-by-wire technologies refer right to the electric/electronic controls that are replacing traditional automotive mechanical or hydraulic systems such as steering, braking, suspension and throttle control. By placing electronic controls (a computer) between the driver and the system, automakers can gain design flexibility, shave weight and decrease the manufacturing complexity of both system components and vehicle assembly.

A consortium comprising of Daimler-Benz, Centre Ricerche Fiat, Ford Europe, Volvo, Robert Bosch, Mecel, Magneti Marelli, University of Chalmers, and Vienna Institute of Technology has carried on work on this field. The system comprises of

actuators and sensors connected to electronic control units (ECUs). The sensors and actuators are used for taking measurements, which are in turn fed to the ECUs for driver feedback. Based on the measurements taken, the driver can make suitable modifications which are then relayed to the actuators for implementation. It must always be ensured that the measurements taken are always accurate

Following [14], [15] are reported some of x-by-wire applications that can be actually found on board of few prototype cars (Figs. 1.8, 1.9).

Electronic Throttle Control: with this new technology, a sensor measures the position of the accelerator pedal to determine the driver's intentions. An actuator appropriately sets the fuel injection system.

Steer-by-Wire: the mechanical linkages of a steering system can be replaced by sensors, wires, an electric motor, and an electronic control unit. The steering wheel can be replaced by a joystick. Substantial weight savings results from the elimination of the steering column.

Brake-by-Wire: because electric actuators can be controlled very precisely by a brake management system, electrically actuated brakes are particularly suited for use with technologies such as antilock braking and stability control.

Shift-by-Wire: shift-by-wire refers to automated manual transmissions, in which computer-controlled actuators handle the shifting. Shifting occurs at the optimal moment.

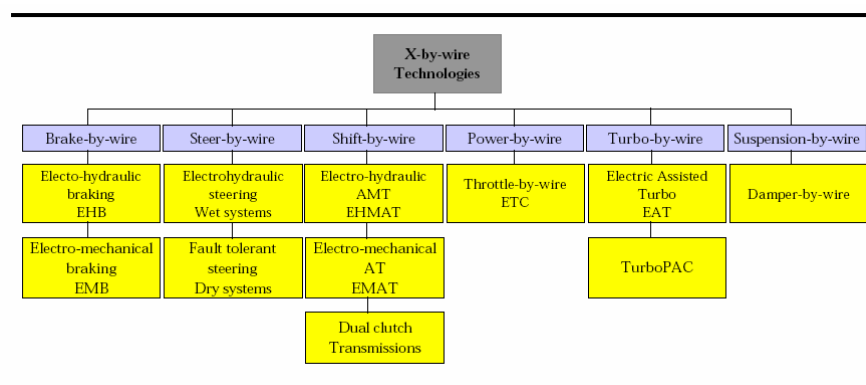


Fig. 1.8: x-by-wire technologies' applications (Source: Frost & Sullivan).

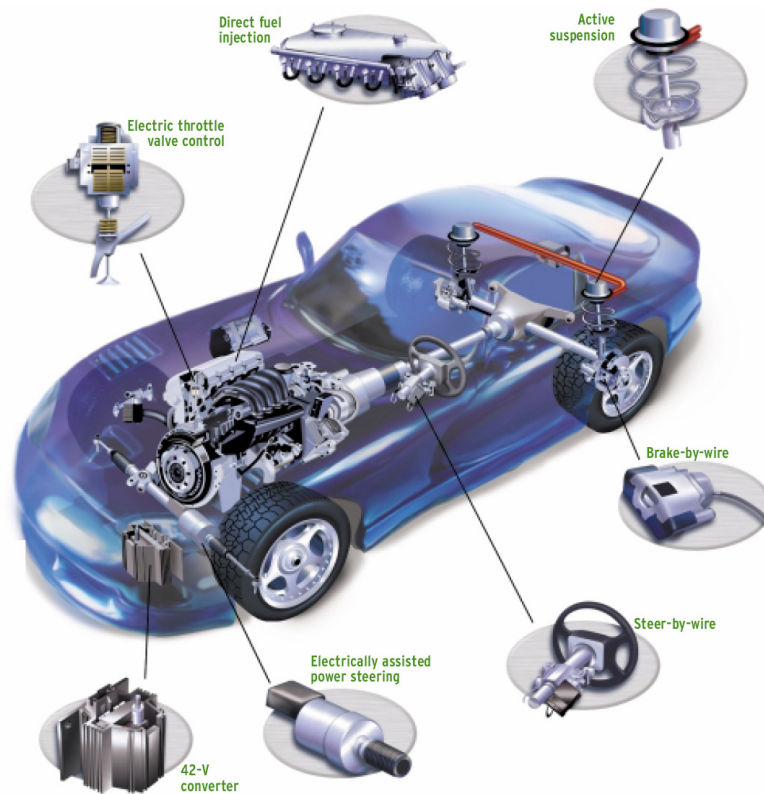


Fig. 1.9: mechanical systems replaced by x-by-wire systems [14].

As it can be easily supposed, x-by-wire systems must be powered taking into account safety, reliability, availability, and maintainability aspects. Electric and electronic components in a x-by-wire system can always fail and therefore it is important to have redundancy in order to avoid loss of alimentation caused by failure. Everyone would ideally want as much redundancy as possible but there are limits of cost and weight.

In a x-by-wire system each component must tolerate a single failure; if there are more failures the driver must be able to operate the system manually.

Some electric loads in a x-by-wire vehicle are mission and safety-critical [16]. They require uninterruptible power availability at all times. It is advantageous to have one or more back-up batteries in the automotive power system to meet the power demand for these mission-critical loads for at least a short time period in case of a primary power source interruption. The back-up or secondary battery usually has a limited energy and power capacity to minimise its weight and cost. The charging and discharging cycles of the backup battery should be minimised to maintain a long

operational life. It should also be disconnected via a PCU when not needed to maintain its state of charge.

1.5 Hybrid electric vehicles

As before introduced, due to the environmental concerns, there is a definite development towards new propulsion systems for future cars in the form of electric and hybrid electric vehicles (EV and HEV). Electric vehicles are known as zero emission vehicles. They use batteries as electrical energy storage devices and electric motors to propel the automobile. Hybrid vehicles combine more than one energy source for propulsion. In heat engine/battery hybrid systems, the mechanical power available from the heat engine is combined with the electrical energy stored in a battery to propel the vehicle. These systems also require an electric drivetrain to convert electrical energy into mechanical energy, just like in an EV [2].

There is now significant interest in HEV propulsion systems globally. Economics play a major role as evidenced by oil prices in North America pressing upwards of \$100/Bbl coupled with a customer preference for full size crossover and sport utility vehicles. The situation in Oceania is milder, but emerging markets such as China are experiencing automotive sector growth rates of 37%/year. Europe remains least affected by hybrids since nearly 47% of all new vehicles sold are diesel fueled and have economy ratings on par with that of gasoline-electric hybrids. In the global economy there are presently some 57 Mil new vehicles manufactured each year. Toyota and Honda have projected that HEVs will be 10% to 15% of the U.S. market by 2009, with Toyota raising the bar further by stating they will produce 1 Mil hybrids a year in the 2012 time frame [17].

Generally, there are two types of HEVs, namely 1) the series hybrid system (Fig. 1.10) [18], [19], [25] and 2) the parallel hybrid system (Fig. 1.11) [18], [19], [25].

The more recent type of complex HEV, i.e., the power-split hybrid system (Fig. 1.13) [20]–[24], combines the benefits of both the parallel- and series-type hybrid systems without sacrificing the cost effectiveness of this hybrid system. This system consists of two kinds of power sources, a gasoline engine, a motor, a generator, and a

high-voltage battery. This system also has the capability of driving the vehicle on electric power as well (a full HEV) [20]–[24].

1.5.1 Series hybrid architecture

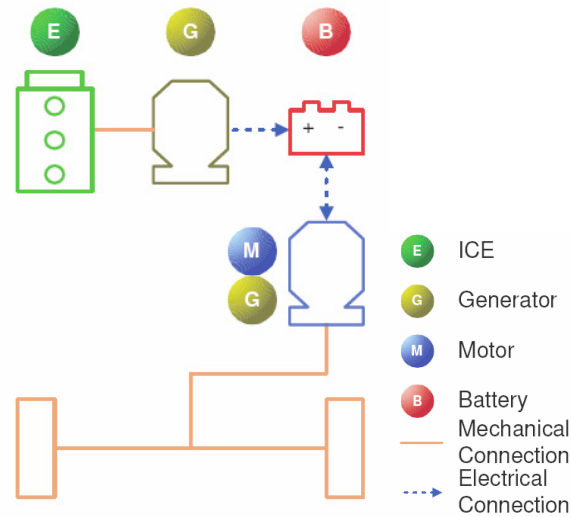


Fig. 1.10: series hybrid vehicle schema.

In the series hybrid, there is no mechanical connection between the ICE and the wheels. Only the electric motor drives the wheels and the engine is used to generate electricity (through a generator) for charging the battery. The electricity from the generator can be used either to charge the battery or to provide the propulsive power to the wheels through the motor. Due to the decoupling between the ICE and the wheels, the ICE can be operated in its efficient operating region, while maximizing fuel efficiency for generating electricity [18], [25]. While this configuration is simple, there are two issues that must be considered in this design - efficiency and cost:

1. The energy conversion (transformation) losses among components (from the ICE through the generator, the battery, and the motor to the wheels in the form of chemical energy through mechanical energy and electrical energy to mechanical energy) deteriorates the efficiency of the series drivetrain;
2. Components sizing to cover high power demand, such as in heavy acceleration or uphill climbing, causes the series hybrid to be expensive.

1.5.2 Parallel hybrid architecture

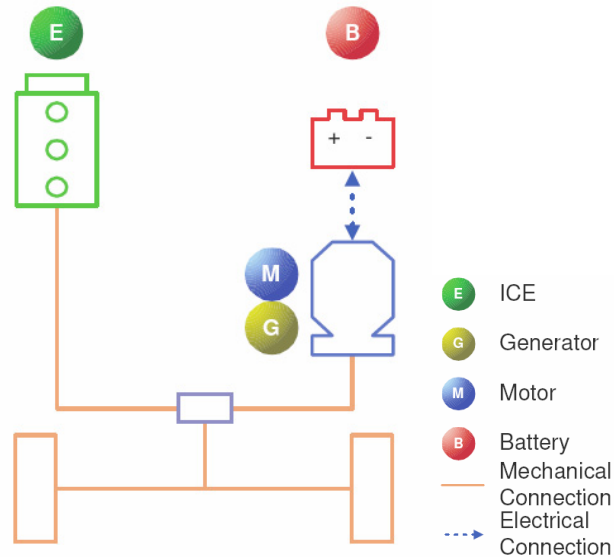


Fig. 1.11: parallel hybrid vehicle schema.

Direct delivery of propulsion power from both energy sources to the wheels is available in the parallel hybrid due to the (mechanical) coupling of both the ICE and the motor to the wheels. In the parallel hybrid, the ICE, the motor, or both power sources can be utilized to provide power to the wheels. The ICE can power the vehicle and recharge the battery using the motor as a generator. For instance, one portion of the engine power directly drives the wheels and the rest of the power goes through the electric path if surplus power from the engine is available [18], [25]. The regeneration of electric energy during braking is accomplished in the motor (functioning as a generator) that would otherwise be wasted, as in a series hybrid.

The main advantages of the parallel hybrid over the series hybrid are in:

1. its energy conversion efficiency due to the mechanical connection between the ICE and the wheels, reducing the amount of power conversion from energy sources;
2. the downsized engine (and motor) due to its co-assisted capability in terms of propulsion power generation, resulting in enhanced fuel economy and reduced pollutant emissions.

1.5.3 Series-parallel and power-split hybrid architecture

The series-parallel hybrid is, as the name suggests, a combination of a series and parallel hybrid. In this type of hybrid, there are several possible ways to operate the vehicle - series, parallel, even some combination of both - for different loading conditions. This would utilize the advantages of both types of drivetrain. Depending on the driving situations, the most advantageous mode could be selected. This topology would, however, suffer from a more complicated structure and higher cost than either a series or a parallel does [25].

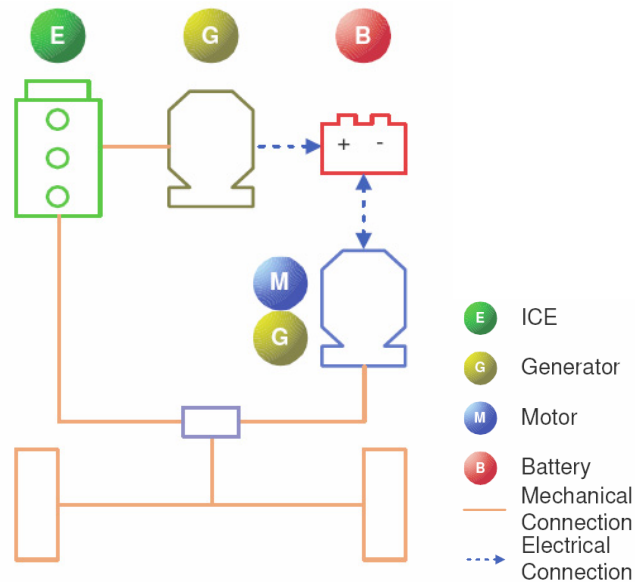


Fig. 1.12: series-parallel hybrid vehicle schema.

The system ensures high autonomy and reduced consumption in highway travels. In city travels, the reductions of fuel consumption and emissions is due to the regenerative braking system and the torque integration, which allows better management of engine.

All major automobile manufacturers are experimenting with this configuration, which is the one that is more compact and seems to be a natural evolution of traditional engines, because it is characterized from a best adaptability of the system to vehicles already in production.

A particular type of series / parallel configuration is the propulsion system of the Toyota Prius, which will be used as case-study in this dissertation for the optimization algorithm. The power split among electrical and thermal path is entrusted to a planetary gear set, assisted by appropriate electromagnetic clutches [17], [23]. This device is also called “power split”, and the schema is shown in Fig. 1.13.

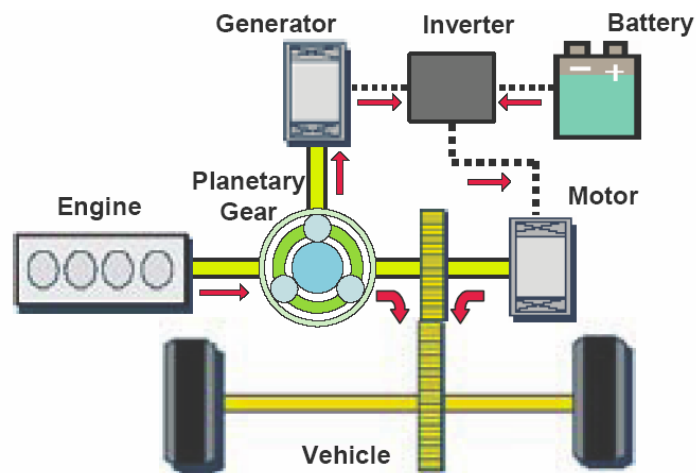


Fig. 1.13: power-split hybrid vehicle schema.

1.5.4 A commercial power-split hybrid vehicle: the Toyota Prius

The Prius is a parallel configuration hybrid, a vehicle that can run on just the combustion engine, just the electric motor, or a combination of both. Toyota's design goals are to reduce the amount of pollution and to maximise fuel efficiency. To do this, it uses a gasoline(petrol)/electric hybrid powertrain, incorporating large batteries that are charged by the gas (petrol) engine directly or by regenerative braking. Either the engine or the battery (or both) can power the vehicle, depending on conditions. This gives it the acceleration and power of a standard car having a much larger internal combustion engine.

The on-board computer ensures that the engine runs under the most efficient conditions. Typically, a petrol/gasoline engine runs inefficiently at half-throttle, creating a choking condition. This effect, called pumping loss, is a major reason for the inefficiency of gasoline engines compared to diesels. The Prius minimises pumping loss by running the gasoline engine at a high torque range with the throttle

fully open. Drive-by-wire throttle control technology and Toyota's *Hybrid Synergy Drive* (a torque combiner, electric drive, and computer control) are essential to this engine control [22], [24], [26].

2. State of the art of energy management strategies for automotive power systems

2.1 Introduction

The increase of on-board request of electric energy affects power train attributes but customers expect these new vehicle features will not have a negative impact on the performances of the vehicle and on fuel economy. At the same time, legal requirements force automotive manufacturers to comply with stringent exhaust gas emission levels. The expanding electrical system functions call for the introduction of high-level energy management control strategies that ensure electrical system robustness and optimum energy efficiency within various vehicle operative conditions.

Therefore, the target of any energy management strategy is to prioritize real-time power requests from the loads and allocate power resources available from the generation and storage devices in an optimized manner, in order to minimize fuel consumption and/or emissions.

To achieve these targets, several approaches have been investigated in the last years. These approaches can be distinguished in two classes: the first concerns real-time control strategies that can be used to control the vehicle; the second class of

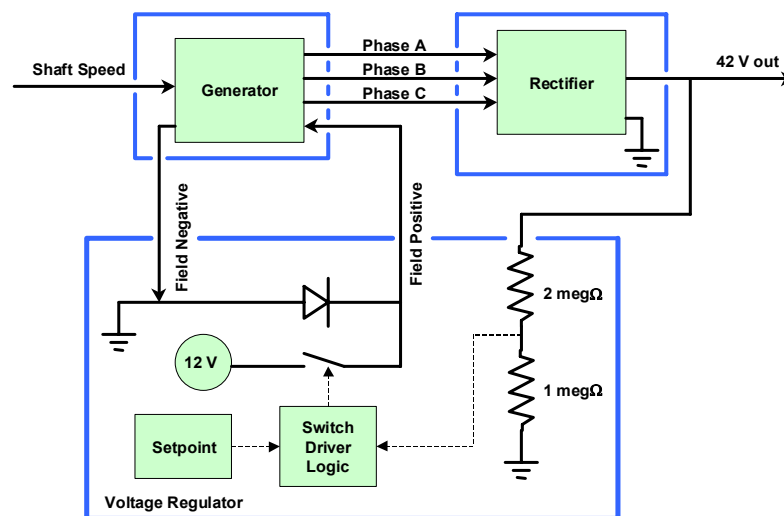
algorithms deals with the application of global optimization methods on the basis of the knowledge of the drive cycle and other information about the state of the vehicle. In this chapter, after the description of the actually implemented on-board energy management strategies for commercial conventional and hybrid electric vehicles, a review of the most researched innovative methods, known in scientific literature, for the management of the energy flows for the same categories of vehicles has been reported

2.2 Energy management strategy for conventional vehicles

In vehicles with conventional propulsion, the classical on-board energy management strategy is limited to the control of the bus voltage through the regulation of the alternator field voltage, when vehicle speed and power demand from the electric loads change, in order to have the bus voltage as much as possible constant and equal to 14 V. The alternator tries to maintain a fixed voltage level on the power bus. A traditional lead-acid battery is present for supplying key-off loads and for making the power bus more robust against peak-power demands.

This results in a continuous delivery of power from the alternator, a constantly recharging of the battery and an impulsive discharging of the battery, where the electrical power request exceeds the maximum deliverable alternator power, for that camshaft speed.

Below a schematic of a typical voltage regulator for a 14 V Lundell alternator.



Although the battery offers freedom to the alternator in deciding when to generate power, this freedom is generally not used.

The energy management problem of a conventional vehicle deals with controlling the amount of power exchange and other available input variables such that desired behavior of the vehicle is obtained. Desired behavior can be expressed by demands on, *e.g.*, fuel consumption, exhaust emissions, component wear, and comfort, while satisfying restrictions on operating points of components and energy storage levels.

The issue of reducing fuel consumption and pollutant emissions is dealt for conventional vehicles in different ways.

By making vehicles smaller, lighter, and more aerodynamic, the power necessary to propel the vehicle can be reduced, and thereby also the fuel consumption.

Another fitted way to meet these requirements is to maintain a conventional vehicle configuration, but improving the vehicle design and the performance of individual components of the drive train, especially the engine.

The working principle of internal combustion engines has been the same for over a century, but in the last 20 years, large improvements have been made. Although the improvement in fuel economy of modern engines is rather small, huge improvements have been made in lowering various exhaust emissions. This is done partly by replacing the traditional carburetor by a direct injection system in combination with a computer controlled motor management system that adjusts the amount of fuel, the air to fuel ratio, and the ignition timing, such that emissions are reduced. However, the largest improvement comes from using exhaust aftertreatment systems, especially the three-way catalytic converter [27].

About the research in this area, two approaches to the problem of optimal energy management have been followed: one related to real-time strategies, the second on the global optimization strategies, where the optimization occurs on the basis of knowledge of the drive cycle of the vehicle and the activation sequence of electrical loads [28].

In the first category are present methods that are based on fuzzy logic, predictive control or controllers based on the analysis of energy flows in the vehicle. In the second category are many algorithms based on linear programming, optimal control and dynamic programming.

2.3 Energy management strategies for hybrid electric vehicles

When designing a hybrid vehicle, the first challenge is choosing the component sizes (engine and motor) and the mechanical setup of the vehicle (parallel, series, or series-parallel). These decisions are made based on the target cost and performance of the vehicle. At the same time, the designer must think of the ways in which these components will interact. The vehicle must operate as a conventional vehicle where the performance of the vehicle corresponds to the actions of the driver.

A hybrid control strategy controls the flow of energy between the components of the HEV. Energy flow is designed so that the demands of the driver are met while reaching the objectives set for the control strategy. These objectives may be to:

1. Improve the fuel economy of the vehicle.
2. Reduce emissions.
3. Maintain or surpass the objectives set for the performance of the vehicle.

The objectives listed above are usually competing; therefore, improving one means hindering another objective. This is why most control strategies use a weighting function to define what objectives are more important than others. Usually, performance is the most important constraint.

Control strategy would differ for different types of vehicles. The types of vehicles can be broadly grouped by their mechanical setup (series, parallel, or series-parallel), intended use (sports car, SUV, city or inter-city driving), and by State Of Charge (SOC) control (charge depleting or sustaining).

The issue with designing a control strategy is that the problem is noncasual. This means that we cannot incorporate the driver's future action since there is no information on what the driver will do next. Therefore, a good control strategy is not optimized for only one drive cycle. For example, the driver can accelerate at any time for any period of time and the control strategy has to be defined so to be able to withstand this requirement. This is why charge sustaining control strategies are preferred. They provide for more power to be available at any given time since the control strategy keeps the battery SOC high. Again, the performance of the vehicle cannot be compromised. Control strategies determine the operating points of an

engine via the efficiency and emission maps of the engine, while maintaining the battery SOC.

In this section, we look at the differences between parallel and series control strategies as well as the differences between charge sustaining and charge depleting control strategies. Two practical examples has been considered, namely the control strategies of the Toyota Prius and Honda Insight [2].

2.3.1 Parallel and series-parallel hybrid vehicles

For parallel hybrids, the control strategy decides on the torque split between the engine and the motor. The speed is defined by the speed of the shaft.

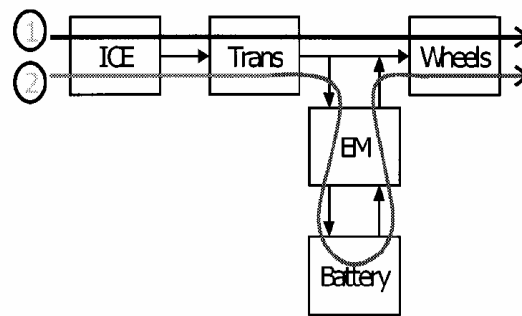


Fig. 2.1: series-parallel and parallel hybrid vehicle energy flow.

2.3.1.1 Charge sustaining parallel hybrids

For this control strategy, operation can be defined by the following constraints [29]:

- when the battery SOC is above a certain threshold, the motor is used to assist with the propulsion and to keep the motor out of the low efficiency region;
- once the battery SOC goes below a certain threshold, the control strategy changes to bring the SOC above the minimum by exerting extra torque from the ICE;
- battery recharging strategy can be overridden if the ICE alone cannot meet the power demand of the drivetrain;
- regenerative braking is always used.

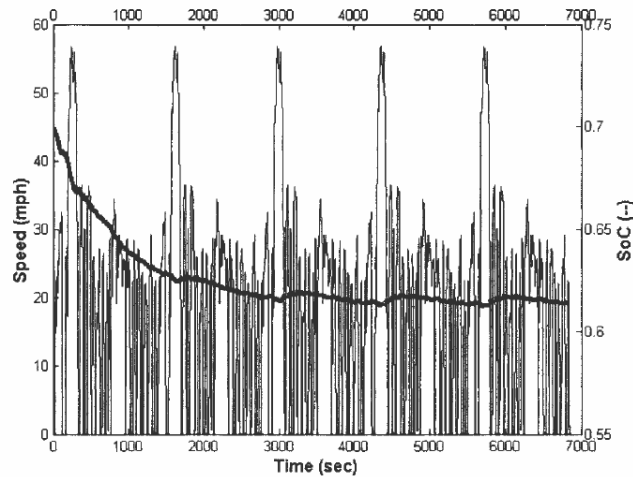


Fig. 2.2: SOC history over five UDDS cycles for charge sustaining parallel hybrids.

The advantage is that the vehicle has unlimited range since the batteries are never depleted. Also, the vehicle performance is not compromised since the batteries always have enough power to supply the motor. Fig. 2.2 shows a typical SOC history over five urban dynamometer driving schedule (UDDS) cycles for this control strategy.

2.3.1.2 Charge depleting parallel hybrids

For this control strategy, operation can be defined by the following constraints [30]:

- the motor is used for all propulsion below a certain threshold speed;
- when the threshold speed is reached, the control strategy switches into a mode where the ICE is used for propulsion, while the motor is used for propulsion assistance;
- as the battery gets depleted, the ICE kicks in at lower speeds.

This control strategy avoids using the ICE at low efficiency regions; it only allows the engine to operate at high power demands, where the engine is more efficient. However, the battery may get depleted to very low levels and the performance of the vehicle can be compromised if high accelerations are needed when the SOC is at its low. Fig. 2.3 shows a typical SOC history over five UDDS cycles for this control strategy.

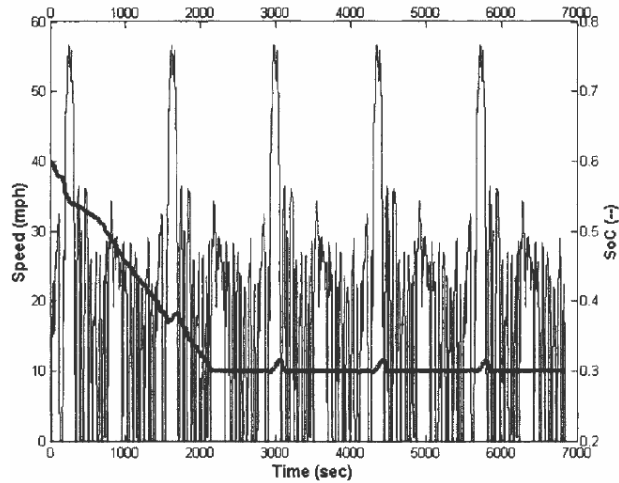


Fig. 2.3: SOC history over five UDSS cycles for charge depleting parallel hybrids.

2.3.2 Series hybrid vehicles

In parallel hybrids, all the torque that propels the vehicle comes from the electric motor. The ICE is only used to replenish the batteries via the generator. Series setups are usually used in larger vehicles that justify the use of two electric motors and that can fully utilize the capabilities of the small ICE that is on-board for energy generation.

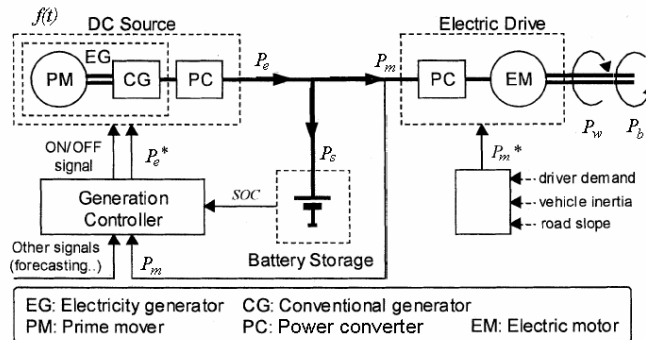


Fig. 2.4: series hybrid vehicle energy flow.

2.3.2.1 Charge sustaining series hybrids

In this control strategy [31], the load of the ICE would try to follow the load of the motor. Fig. 2.5 shows a typical SOC history over five UDSS cycles for charge sustaining series hybrids.

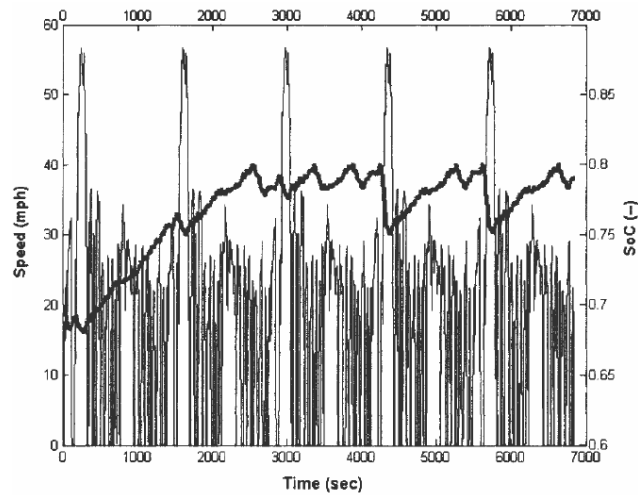


Fig. 2.5: SOC history over five UDDS cycles for charge sustaining series hybrids.

2.3.2.2 Charge depleting series hybrids

In this control strategy, the load of the ICE would be off until the battery reaches a low SOC [30]. Once the low SOC is reached, it will be on until a high state of charge is reached. The benefit of this control strategy is that the engine is allowed to operate at one single most efficient operating point. This greatly improves the efficiency of the ICE. However, the battery losses are increased dramatically due to high charge and discharge rates. In addition, battery life is shortened due to this aggressive use. Fig. 2.6 shows a typical SOC history over five UDDS cycles for charge depleting series hybrids.

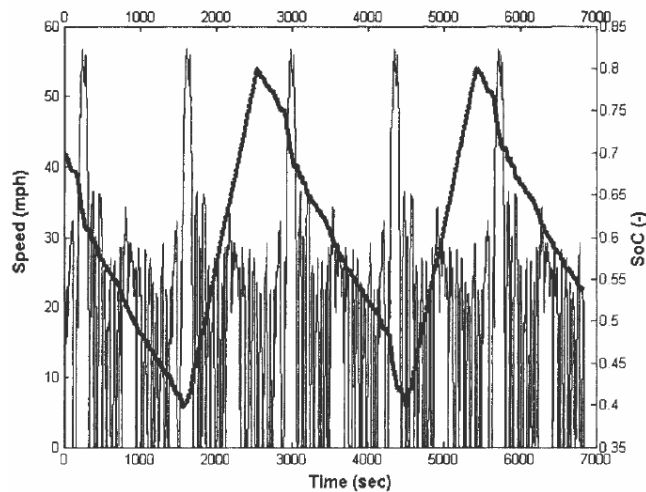


Fig. 2.6: SOC history over five UDDS cycles for charge depleting series hybrids.

2.3.3 Real control strategy of Toyota Prius

The Toyota Prius is a full size car similar to a Toyota Corolla. The engine uses a strategy similar to a parallel charge depleting strategy in the sense that the engine turns on only when the car is traveling above 12 mph [26]. However, the control strategy is charge sustaining, as can be seen from Fig. 2.7 [32]. In this sense, it is similar to the charge sustaining control strategy. If the battery SOC is below 50%, the engine is loaded so that the battery is replenished to this threshold value. Also, if the SOC is way above 50%, the electric motor is loaded more to bring this value down.

The Toyota Prius is optimized for low fuel consumption and extremely low emissions in the “around town” driving scenario. Still, the highway fuel economy is about 38 mpg.

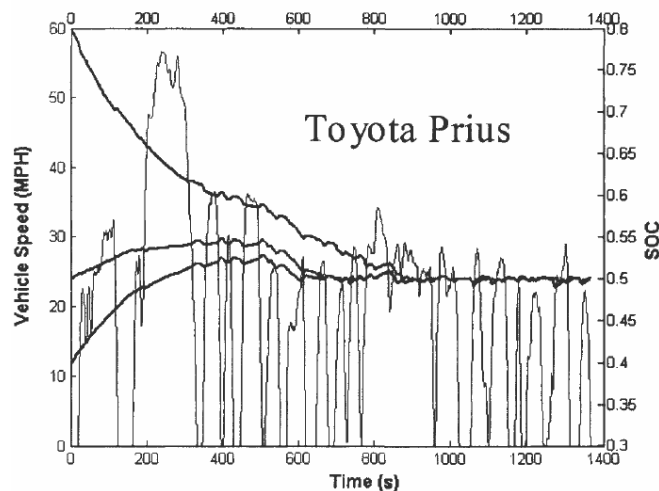


Fig. 2.7: SOC history over one UDDS cycle for Toyota Prius.

2.3.4 Real control strategy of Honda Insight

The Honda Insight is a 2-seat coupe that uses its 1L engine as the principal power source, with additional power provided by a 10kW electric motor. The control strategy does not allow the engine to idle, but the engine works at all speeds.

The Insight is capable of 100 mph speeds while averaging between 60 and 70 mpg overall. Such high fuel economy values are also attributed to the fact that the vehicle is very aerodynamic.

The control strategy is similar to a charge sustaining parallel vehicle in the sense that the electric motor is only used to start the engine and to assist the engine with propulsion. The ICE is only switched off when the vehicle is at a stop. The motor is designed so that it provides about 10 Nm of torque at any vehicle speed. This keeps the state of charge of the battery at a near constant value.

Fig. 2.8 shows the SOC history over one UDDS cycle for Honda Insight [32].

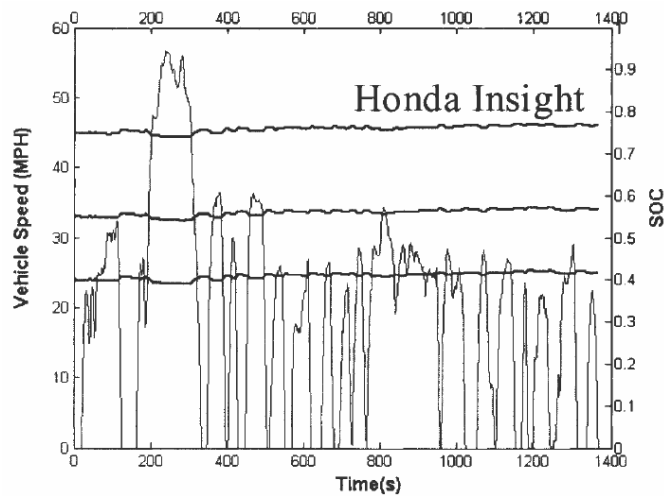


Fig. 2.8: SOC history over UDDS cycle for Honda Insight.

2.3.5 Choice of the suitable control strategy

In summary, the choice of control strategy greatly influences the performance, fuel economy, and emissions of a vehicle. In addition, as can be seen from the graphs, series control strategies allow for larger variations in the battery state of charge. This is intuitive since, in series hybrids, all torque is provided by the electric motor. Therefore, it is expected that the battery SOC varies more since the batteries are used more. It is important to notice that all control strategies that have been implemented in actual vehicles are charge sustaining. The reason is that the performance of the vehicle should never be compromised at the cost of better fuel economy.

2.3.6 Innovative energy management strategies

The gains in fuel economy associated with the introduction of HEVs is promising for the automotive industry. However, in order to realize these gains major challenges in

HEV design and operation, such as coordinating (managing) multiple energy sources, which is highly dependent on the configuration of drivetrain, components sizing, and other factors that affect the operation of HEVs, must be overcome.

The overall performance of an HEV with respect to fuel economy and emissions reduction is dependent not only on how the individual components are efficiently designed but also on how the operation of components is coordinated with each other.

That is, to maximize the advantages of hybrid drive, the following consideration should be made in parallel both in the design phase and in the operation phase of an HEV [33]: enhancement of powertrain components efficiency; optimal design of hybrid powertrain system; energy management control system design. Energy management strategy in HEV operation, especially, the coordination of energy flow in the powertrain, consists of two basic tasks:

- torque distribution (torque split) task;
- charge sustenance task.

The first task refers to the decision-making on the use of energy sources under a driving situation, while meeting driver's torque demand.

The second task reflects the extended driving capability of HEVs through controlling the operation of the battery. These two are the main issues in the development of energy management system coordinating the functioning of the energy sources and the energy flow in the hybrid powertrain.

In recent years, a lot of research is carried out in the field of hybrid electric vehicles. Especially the research activities on energy management strategies for parallel HEV's address many useful concepts. Although the electric power requirements in a parallel HEV are higher than in a conventional vehicle, both configurations can use the same concepts for controlling the amount of stored electric power. A number of control strategies to cope with these issues have been presented in literature. In the following, a short literature overview will be given on energy management strategies for HEV.

Classical and Fuzzy Logic Based Approach

Researches on classical and/or fuzzy logic based approach for energy management strategy of hybrid vehicles have been performed in the following literature.

Few strategies for logic based approach are available in literature [34]-[36].

In [34] has been designed a logic based switching control system for a parallel HEV with the objective of achieving acceptable vehicle performance and maximizing the state of charge of the battery throughout driving. To achieve this objective, control regions and control logic making pairs with each region are defined on the torque-speed plane. According to the driver torque demand, a control scheme under the control region is activated to meet driver torque demand while maximizing the battery state of charge.

In [35] has been presented a rule based control and energy management strategy for a series HEV. Their strategy aims at a power split (assignment) in a way that both power sources - engine and battery - are operated at high efficiency. The idea of power split was implemented under a rule-based frame that controls power assignment based on the status of the SOC, the power demand, and the acceleration command.

In [36] has been presented a logic based control strategy for a parallel HEV focusing on the best SOC (for acquiring maximum vehicle driving range.) For each vehicle modes - propelling and braking, engine and motor power are determined by the control logics which are set based on the operation modes of the engine and the motor given driver power demand.

Other fuzzy logic based control strategies for hybrid vehicles are available in literature [37]-[42]. In [37] and [38] is presented a fuzzy logic based power regulator to the control of power ow in a (series) hybrid HEV.

In [39] has been proposed a fuzzy logic torque controller for a parallel HEV with the control objectives of improving driveability, balancing of battery charge, and reducing NO_x (nitrogen oxide) emissions. To realize this, the construction of fuzzy rule bases was performed based on the dynamo test of parallel driving system. The proposed fuzzy controller has two units, each of which has its own fuzzy rule base, one is for driver's intention predictor (based on acceleration and its rate) and the other for power balance controller (based on the engine speed and vehicle speed.)

In [41] has been presented a vehicle operating mode-based fuzzy torque distribution control for a parallel HEV. The proposed controller is implemented in terms of a hierarchical architecture which incorporates the modes of operation of the vehicle as well as empirical knowledge of energy flow in each mode. Moreover, the rule set for each mode of operation of the vehicle is designed in view of an overall energy management strategy that ranges from maximum emphasis on battery charge sustenance to complete reliance on the electric power source.

In [42] and [43], the authors developed a power controller for a parallel HEV that will optimize the fuel economy by demanding all major power components – the engine, the motor, and the battery - to operate at each efficient region of operation of each component. The implementation was made via fuzzy logic control, which provides a method for realizing an optimal trade-off between the efficiencies of all components.

Similarly, in [40], authors designed fuzzy logic, rule-based controller to optimize the energy efficiency through the control of the power flows of a parallel HEV by commanding the engine to operate at its efficient operating region.

Optimization Based Approach

Some existing research works in the optimization based approach are available for scrutiny in [44]-[54]. In general, the solution to the optimal torque distribution (power split) problem is ultimately dependent on the objective (cost) defined. Fuel efficiency optimization problem with the energy-based cost function is shown in [49] and [53]. In [49], the aim of the control optimization is to minimize the energy-based objective function with torque split and gear ratio as the control variables. Especially in [53], a multi-objective nonlinear optimal torque distribution strategy is formulated and converted into a single-objective linear programming problem by linearization of the objective functions and by introducing an equivalent energy consumption rate for the fuel flow rate. In [52], by introducing the equivalent fuel flow rate for the use of the electric machine, an instantaneous optimization problem with the objective of equivalent fuel flow rate for power split is formulated and solved. Again the same formulation is extended to enforce emission reduction with the appropriate weighting coefficients which penalize equivalent fuel flow rates in the objective function.

Authors in [50] introduced an effective specific fuel consumption that is used as equivalent fuel consumption in the electric drive in which battery output power is transformed into an equivalent amount of fuel for finding optimal torque distribution solution in the parallel HEV operation. The application of convex optimization to the problem of finding optimal engine operation in a series hybrid vehicle over a fixed drive cycle is addressed in [51].

Dynamic programming approach for the development of hybrid vehicle control strategy can also be found in the literature. In [46] and [47], aim was to optimizing the energy transfer and conversion in the hybrid powertrain by dynamic programming using criterion of minimization of fuel consumption within a given drive cycle. Also, in [48] has been formulated the optimal power split problem for series hybrids and solved the problem using a dynamic programming approach.

Optimization technique with driving pattern recognition is also addressed in [54]. In particular, the authors of [54] considered six representative drive cycles and found optimal control parameters being used in the objective function to find optimal powersplit ratio. During the operation of the vehicle, the study proposed to find optimal power split ratio using control parameters that forms a pair with the recognized drive cycle. However, optimized control action, due to its dependency on a specific drive cycle used in optimization process, may not be an optimal one for a misclassified drive cycle, or an arbitrary drive cycle segment which seems not to be a part of drive cycles used in the generation of optimal control action.

Real-time Optimization Methods

A real-time control strategy based on an instantaneous optimization needs a definition of the cost function to be minimized at each instant. Such a function has to depend only upon the system variables at the current time. Since the main control goal is the minimization of the fuel consumption, it is clear that this quantity has to be included in the cost function. However, based on the requirements of electrical self-sustainability, the variations in the stored electrical energy (or state-of-charge, SOC) have to be taken into account as well.

To deal with such aspects, various approaches have been proposed in the literature. In some cases, a tuning parameter, which is adjusted according to the current SOC

deviation by means of a PID controller, is introduced into the cost function minimization [55]. In other cases, the cost function is the sum of all losses in the electrical and thermal paths [56].

Another, more promising approach was used in [52] and [57]-[59]. It consists of evaluating the instantaneous cost function as a sum of the fuel consumption and an equivalent fuel consumption related to the SOC variation equivalent consumption minimization strategy (ECMS). In this case, it is clearly recognized that the electrical energy and the fuel energy are not directly comparable, but an equivalence factor is needed. The equivalence between electrical energy and fuel energy is basically evaluated by considering average energy paths leading from the fuel to the storage of electrical energy. If the overall efficiencies of the electrical and thermal paths were rigorously constant, such an equivalence would be theoretically exact. Since efficiencies vary with the operating point, this approach only allows the use of average values.

In the real-time control strategy proposed in [60], the equivalent fuel consumption is evaluated under the assumption that every variation in the SOC will be compensated in the future by the engine running at the current operating point. The equivalent fuel consumption therefore changes both with the operation point and with the power split control, and its evaluation requires an additional, inner loop in the instantaneous optimization procedure, or the prior storage of the results in a look-up table.

A model based predictive control concept for hybrid drive trains is presented in [61], [62] and [63]; in this last, a fuzzy logic controller (FLC) is proposed to predict the future state of the vehicle.

3. Comparative evaluation of automotive power bus architectures

3.1 Introduction

In this chapter we expose methods and results of the research about the comparative evaluation of automotive electrical power system (power bus in the following) architectures for conventional and hybrid propulsion vehicles, oriented to the choice of innovative solutions with higher performances, in terms of reliability, quality of electric service, for a specific automotive application.

The first step has been to realize an overview on existing and more researched automotive power bus architectures. Then, the mathematical model for several loads have been deduced, implemented in MAST language and in MATLAB framework, in way to be simulated as templates in SABER® DESIGNER environment and in MATLAB environment.

Next step has been the implementation of a decision support technique, the software tool *Evaluator*, in order to compare different power bus architectures and to identify which of them has higher performances and is more economically competitive.

This software is based on a stochastic approach and has required the application of the Montecarlo method and the multicriteria analysis.

Different families of architectures can be compared in terms of cost, weight, efficiency, reliability of every components and of the whole system, electric service quality. The multicriteria analysis is the approach adopted to perform the comparison rules among the different architectures. To evaluate the electric service quality, a further multicriteria analysis is adopted, which take in account several electrical indexes. To calculate the value of some of multicriteria analysis indexes (S.O.C., supply continuity, etc.) it is necessary to simulate the whole power bus behavior when it's forced from a well defined vehicle drive cycle and from an opportune activation sequence of loads in the same cycle. Therefore the tool *Evaluator* interacts with three independents routines: the powernet simulator, the critical drive cycles maker and the critical loads activation sequence maker.

3.2 State of the art of automotive power bus architectures

Since the adaptability of the conventional electrical system to the needs of near future and actual electrical loads is very little, as remarked in chapter 1, alternative architectures of power bus are required, particularly in applications x-by-wire based, where it is important to improve some of characteristics of power supply, such as reliability, uninterruptible power feed, fault-tolerant components, autonomous control [13]-[16]. For these reasons, different architectures have been presented in literature, in order to overcome the problems of the traditional power bus [2]-[3], [5], [7]-[8], [12], [64]-[71].

Although a large number of alternative architectures have been suggested, they have not been rigorously evaluated. Hence, it isn't still comprehensible how to detect the best architecture for a fixed automotive application.

As well known, existing automotive power bus comprise six main components [2]-[3], [71]: generator, battery, electrical loads, starting motor, supercaps, dc/dc converters.

The battery, generator and starter form a distinct group of components with special wiring requirements positioned around the engine (electrical power source system). How the electric power is topologically distributed determine the particular architecture of the power bus [66].

The architectures more quoted in literature are the following:

- 12 V point-to point architecture;
- multiplexed architecture;
- closed-ring architecture;
- AC distribution architecture;
- dual-voltage architecture for conventional vehicles;
- dual-voltage architecture for hybrid vehicles.

Actually, most of power bus architectures for conventional vehicles has a single voltage level 12V DC, with the loads being controlled by manual or electronically actuated switches and relays. These configurations are *point-to-point* topologies in which all the electrical wiring are distributed from the single main bus to different loads through relays and switches of the dashboard control (Fig. 3.1).

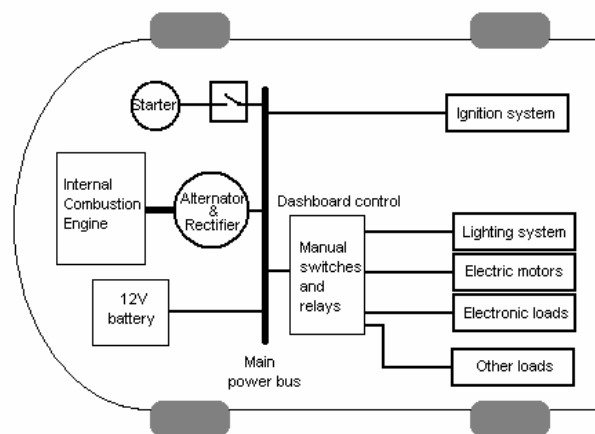


Fig. 3.1: point-to-point 12V DC architecture.

As known, this kind of architecture leads to expensive, complicated and heavy wiring circuits. In this conventional electrical system, bus voltage is comprised between 9V (overall loaded system) and 16V (no-load system), with results in overrating the loads at nominal system voltage. Other disadvantages are related to the load dump transient, where a voltage spike is caused by sudden load loss on a fully loaded alternator, and considering that DC motors at 12V produce high losses in brushes, connectors have high rate of failure. Moreover, with the increase in electrical/electronic components in vehicles, the on-board electric power requirement

is rapidly growing towards 5 kW for non-propulsion loads. Since the adaptability of the conventional architecture to the needs of near future and actual electrical loads is very little, new conceptions of electrical power bus architecture in automotive sector are required, particularly in applications x-by-wire based, where it is important to improve some of characteristics of power supply such as reliability, uninterruptible power feed, fault-tolerant components, autonomous control.

The actual power bus architecture can be improved using multiplexed architecture (Fig. 3.2) with separated power and communication buses.

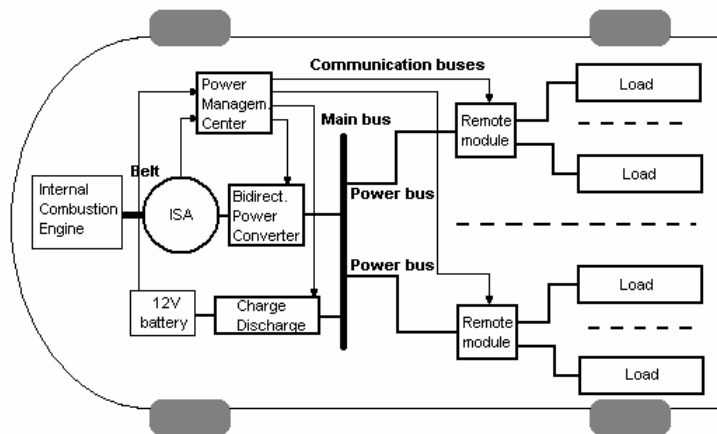


Fig. 3.2: Advanced multiplexed power system architecture with separated power and communication buses.

The loads are controlled by intelligent remote modules, so number and length of wires in the harness are reduced. Then, interconnections between remote modules with communication buses determine possibility to have a power management system on-board, which can comprise battery and charging management, load management (strategies of load-activation sequence), management of alternator and regulator too, control of a high integrity supply system.

The passage from a conventional point-to-point towards a multiplexed power bus architecture with separated power and communication buses can simplify vehicle design and assembly process and offers additional benefits such as the following:

- all the loads are under intelligent control, this mean the possibility to integrate power management into existing control;
- power management strategy can help to optimize the size of the batteries and alternator;

- vehicle economy can be improved using the knowledge of battery SOC in a networked system.

Other innovative architectures proposed in last few years [3], [8], [64], are depicted in following figures.

In Fig. 3.3 a closed-ring power bus based on distributed and multiplexing architecture is shown [8], [66]. The load boxes include the interface circuits, load selector switches, load drivers and loads.

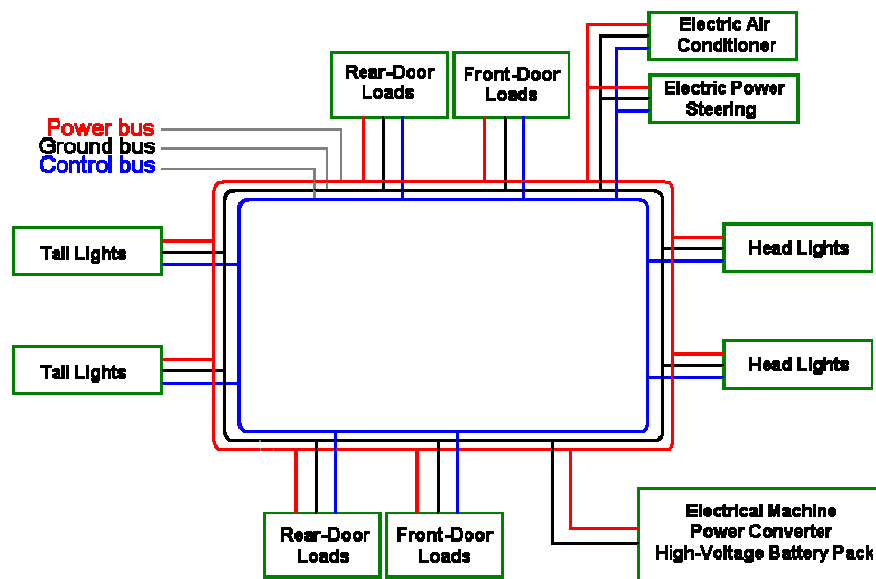


Fig.3.3: A closed-ring power system topology with separated power and control buses.

This type of architecture comprises a single power bus, a single control bus and a single ground bus for the whole vehicle, therefore it simplifies and minimizes harness complexity, cost and weight. The power bus is distributed around the vehicle and electrical loads are connected directly to this bus at load points.

Main advantage related to the use of these distribution systems is that this type of architecture simplifies and minimizes harness complexity, cost and weight increasing the reliability of the whole system.

On the other hand:

- only one voltage level is available for loads;
- the faults monitoring is more complicated than the previous topologies.

Fig. 3.4 shows an AC power bus distribution system [8], [65]-[68].

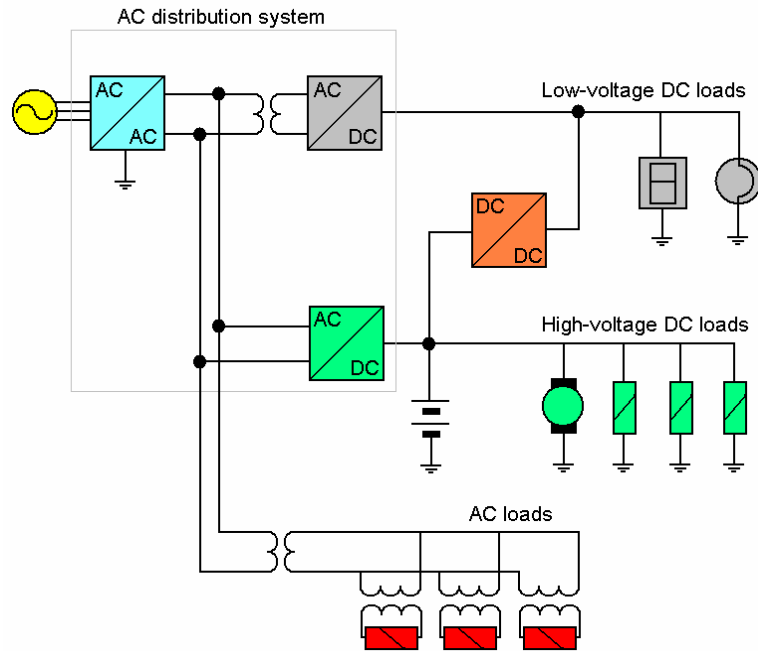


Fig. 3.4: AC automotive power bus distribution system.

This architectures can be classified into low-frequency (25-500 Hz) and high-frequency (20-200 kHz) AC systems. The regulated constant-voltage, constant frequency single-phase AC power, obtained from a three- phase to single-phase AC converter, is distributed around the vehicle. Several power converters are used at various load points to convert AC power in DC power needed from loads.

Benefits of these distribution systems are the following:

- easy conversion to different voltage levels by transformers;
- easy isolation of critical AC loads with transformers;
- availability of different levels of voltage;
- AC machine can be also used.

Disadvantages of these distribution systems are the following:

- necessity to use expensive low-inductance and capacitance cables in high-frequency harnesses;
- the vehicle chassis cannot be used as the return conductor in high-frequency systems (EMI problems, potential high inductance);

- skin effect increases the resistance of cables;
- presence on AC bus of harmonics produced by DC loads;
- possible disruptive short-circuits between DC bus and AC bus, at different voltage levels.

At last, Fig. 3.5 shows a wholly power system architecture which comprises at least two buses at different level of voltage and power (42 V/14 V), communication connections between every component, Power Control Units (PCU), DC/DC and AC/DC converters, redundancy battery units at every level of bus voltages, an Integrated Starter Alternator (ISA) and various alternative sources of electrical energy [65].

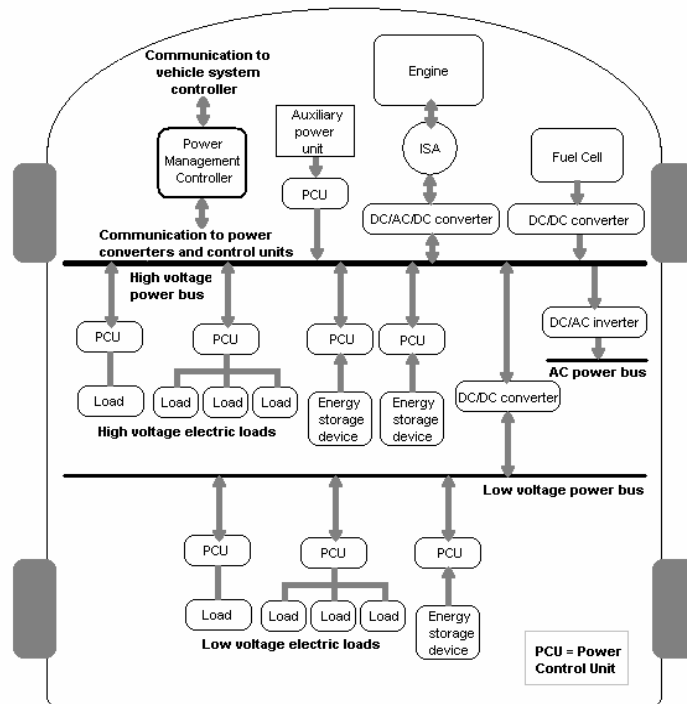


Fig. 3.5: Generic automotive power/energy management and distribution system

A higher voltage level such as the recently proposed 42 V will reduce the weight and volume of wiring harness, among several other vantages.

Because automobile engineers are currently introducing many new electronic developments such as electric power steering, braking, suspension, accelerator, electronically actuated engine valves etc., in some large cars the 12 V charging systems are already struggling to cope, as they are compromised by bulky wiring

harnesses, heavy motors, and electronics that are subject to voltage irregularities. These new electronic developments require the higher system voltage provided by the 42 V PowerNet [12], [69], [72].

This development is expected to proceed in 2 stages with a dual voltage system initially [6], [73]-[77] (42 V/14 V), followed after a few years by a single 42 V system in which lower voltages e.g. for lighting, are achieved by a low cost dc-dc converter [75]-[77].

For first, increasing voltage level consent to cope with increasing electrical power request on board. The most important advantages that can be reached using a 42 V powernet architecture are the following [12], [71]-[72], [74]:

- lower currents;
- reduction of power semiconductor costs;
- cable cross section reduction;
- more and optimized power sources (all power sources and generators have their own optimal operating ranges in terms of power output and efficiency);
- the use of two or more power buses at different voltages in a vehicle can simultaneously address power and safety requirements;
- efficiency increase (particularly for alternator, distribution system, switching devices);
- cost reduction due to new specifications (overvoltage, reverse battery load dump, jump start);
- new power application can be realized on board (e.g. x-by-wire);
- enables reduction of fuel and emission;
- enables electrification of accessory drives;
- power electronics components, including all power converters and PCUs, consent to implement an on-board optimized power/energy management system strategy.

On the other hand, in a system such this, some loads need for source at lowest level of voltage (such as lamps and electronic equipments) so a dual voltage system is actually necessary (Fig. 3.6). Besides, the following disadvantages are related:

- complexity of the overall system;
- possible short-circuits between buses at different voltage levels;

- polarity reversal protection required;
- presence of arcing phenomenon;
- typical problems of AC distribution architectures on ac bus of the system.

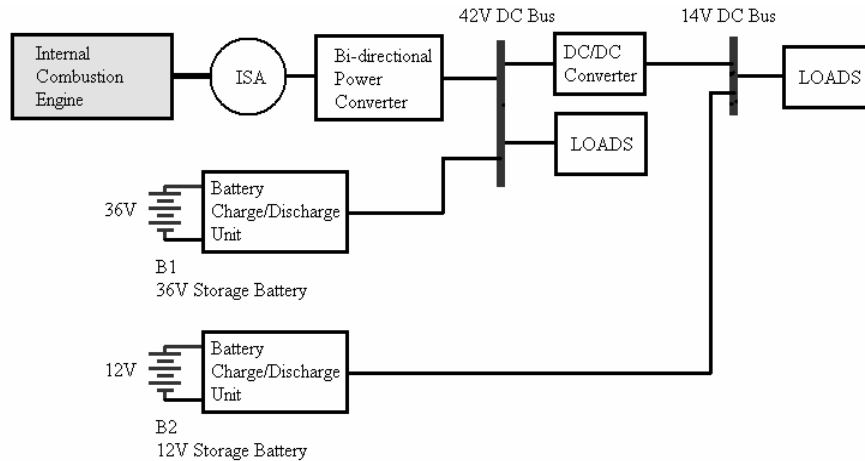


Fig. 3.6: dual-voltage (42/14V) architecture of power bus for conventional vehicles.

Fig. 3.7 depicts the conventional electrical power distribution system architecture for hybrid electric vehicles [2].

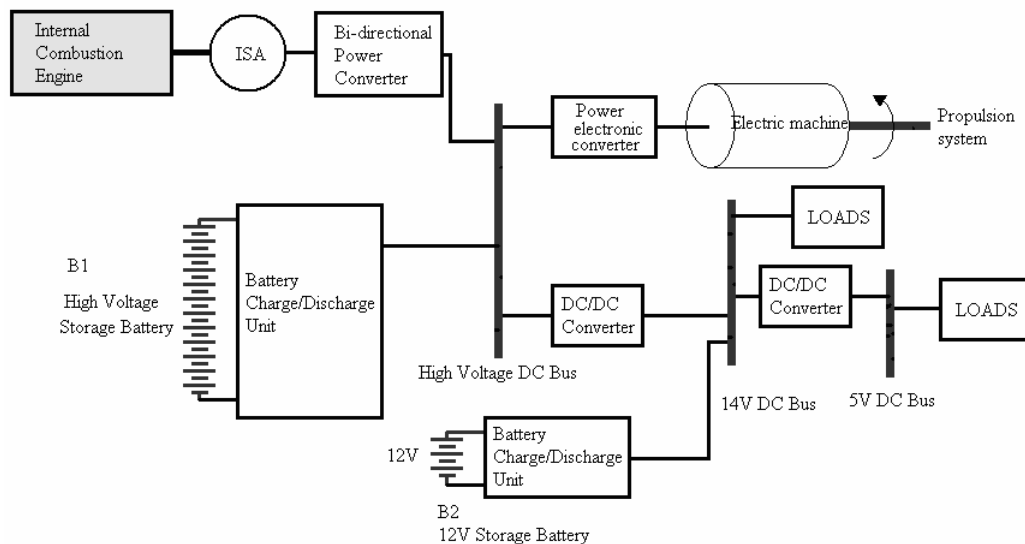


Fig. 3.7: Conventional electrical power distribution system architecture for hybrid electric vehicles.

It is a DC system with main high voltage bus, e.g., 300V or 140V. A high voltage storage system is connected to the main bus via the battery charge/discharge unit.

This unit discharges and charges the batteries in motoring and generating modes of the electric machine operation, respectively. There are also two other charging systems, which are on-board and off-board. The off-board charger has three phase or single phase AC/DC rectifiers to charge the batteries when the vehicle is parked at a charging station. The on-board charger, as is shown in Fig. 3.7, consists of a starter/generator and a bi-directional power converter. In the generating mode, an internal combustion engine provides mechanical input power to the electric generator. Therefore, the electric generator supplies electric power to the bidirectional power converter, providing high voltage DC to the main bus.

Moreover, in the motoring mode, i.e., cranking the engine, a high voltage DC system via the bi-directional power converter provides input electric power to the electric machine, which is a starter to the vehicle engine.

In Fig. 3.7, electric propulsion system is feeding from the main high voltage bus. Furthermore, conventional low power 14V and 5V DC loads are connected to the 14V bus. A low voltage 14V bus is connected to the main bus with a step-down DC/DC converter. A 12V storage system via the battery charge/discharge unit is also connected to the low voltage bus. It should be mentioned that Fig. 3.7, without internal combustion engine, starter/generator, and bi-directional power converter, shows the electrical power distribution system architecture of electric vehicles.

As described, demand for higher fuel economy, performance, and reliability as well as reduced emissions will push the automotive industry to seek electrification of ancillaries and engine augmentations. This is the same concept of more electric vehicles (MEV) described in chapter 1 for conventional vehicles.

Expansion of the MEV concept to HEV leads to more electric hybrid vehicles (MEHV). In future MEV and MEHV, throttle actuation, power steering, anti-lock braking, rear-wheel steering, airconditioning, ride-height adjustment, active suspension, and electrically heated catalyst will all benefit from electrical power systems.

Fig. 3.8 shows the architecture of the MEHV electrical power system [2].

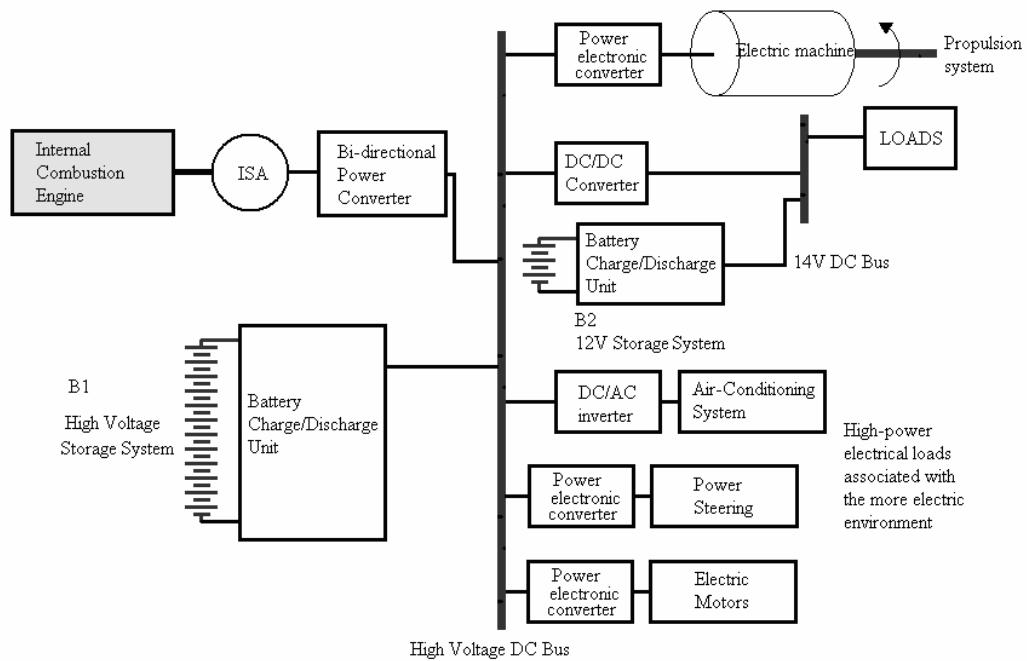


Fig. 3.8: MEHV electrical power distribution system architecture.

It is a multi-voltage hybrid (DC and AC) electrical power distribution system with a main high voltage (e.g., 300V or 140V) DC bus providing power for all loads. Conventional loads as well as new electrical ancillary and luxury loads associated with the more electric environment are feeding from the main bus via different DC/DC and DC/AC power electronic converters.

3.3 Modelling of classical on-board loads

Mathematical models of the following automotive electrical drives have been deduced:

- electric window winder;
- air-conditioned's electric fan;
- radiator's electric fan;
- electric windscreen wiper;
- rear window wiper.

The effectiveness, accuracy and performances of the models have been tested and validated, with comparisons between theoretical and experimental data.

Models have been finally implemented in MAST language (for SABER templates) and in MATLAB language, for the simulations in steady-state and transient conditions.

3.3.1 Subspace methods for the parameter identification of linear systems

A common way of describing linear systems is to use the *state-space* discrete-time form:

$$\begin{aligned} x(k+1) &= Ax(k) + Bu(k) + Ke(k) \\ y(k) &= Cx(k) + Du(k) + e(k) \end{aligned} \quad (3.1)$$

where:

$u(k)$ - input signal

$y(k)$ - output signal

$e(k)$ – noise signal

$x(k)$ – state vector

Every device which has been considered for the modelling, in no-load conditions, can be represented from the following equations (DC brushed PM motor without mechanical load):

$$\begin{cases} V_a = R_a i_a(t) + L_a \frac{di_a(t)}{dt} + k_\phi \omega_r(t) \\ J \frac{d\omega_r(t)}{dt} = k_\phi i_a(t) - k_{aM} \omega_r \end{cases} \quad (3.2)$$

In other form:

$$\begin{cases} \frac{di_a(t)}{dt} = -\frac{R_a}{L_a} i_a(t) - \frac{k_\phi}{L_a} \omega_r(t) + \frac{1}{L_a} v_a(t) \\ \frac{d\omega_r(t)}{dt} = \frac{k_\phi}{J} i_a(t) - \frac{k_a}{J} \omega_r + 0v_a(t) \end{cases} \quad (3.3)$$

where:

- $v_a(t)$: armature voltage;
- $i_a(t)$: armature current;
- ω_r : rotor speed;
- R_a, L_a : armature resistance and inductance;
- k_ϕ, k_a : motor constants.

If we introduce the following matrices:

$$X = \begin{pmatrix} i_a \\ \omega_r \end{pmatrix}, \dot{X} = \begin{pmatrix} \frac{di_a}{dt} \\ \frac{d\omega_r}{dt} \end{pmatrix}, U = (v_a \ 0)$$

$$E = \begin{pmatrix} -\frac{R_a}{L_a} & -\frac{k_\phi}{L_a} \\ \frac{k_\phi}{J_M} & -\frac{k_{aM}}{J_M} \end{pmatrix}, F = \begin{pmatrix} 1 \\ L_a \\ 0 \end{pmatrix}, G = \begin{pmatrix} 1 & 0 \\ 0 & 1 \end{pmatrix}, H = \begin{pmatrix} 0 \\ 0 \end{pmatrix}$$

the system (3.3) can be rewritten as:

$$\begin{cases} \dot{X} = EX + FU \\ Y = GX + HU \end{cases} \quad (3.4)$$

The matrix equations (3.4) represents the mathematical model of the linear system “dc motor” at no-load conditions in the state-space representation.

In these equations we have:

- X : state vector;
- U : input vector;
- Y : output vector.

Now the problem is to estimate matrices E, F, G, H . This problem can be solved with one of the methods known from literature, as the *subspace* method [78], following depicted.

Starting from discrete-time space-state representation of the model, it has been deduced the relationships between A , B , C , D matrices in discrete-time and E , F , G , H matrices in continuous-time:

$$A = I + ET_s, B = FT_s, C = G, D = H \quad (3.5)$$

with:

$$A = \begin{pmatrix} 1 - \frac{R_a T_s}{L_a} & -\frac{k_\phi T_s}{L_a} \\ \frac{k_\phi T_s}{J} & 1 - \frac{k_a T_s}{J} \end{pmatrix}, B = \begin{pmatrix} \frac{1}{L_a} T_s \\ 0 \end{pmatrix}, C = \begin{pmatrix} 1 & 0 \\ 0 & 1 \end{pmatrix}, \quad (3.6)$$

$$D = \begin{pmatrix} 0 \\ 0 \end{pmatrix}, I = \begin{pmatrix} 1 & 0 \\ 0 & 1 \end{pmatrix}$$

The state-space matrices A , B , C , D , and K in (3.1) can be estimated directly, without first specifying any particular parameterization, by efficient subspace methods. The idea behind this can be explained as follows: if the sequence of state vectors $x(k)$ were known, together with $y(k)$ and $u(k)$, equation (3.1) would be a linear regression, and C and D could be estimated by the least squares method. Then $e(t)$ could be determined, and treated as a known signal in equation (3.1), which then would be another linear regression model for A , B , and K .

Thus, once the states are known, the estimation of the state-space matrices is easy. How to find the states $x(t)$?

All states in representations like equation (3.1) can be formed as linear combinations of the k -step ahead predicted outputs ($k = 1, 2, \dots, n$). It is thus a matter of finding these predictors, and then selecting a basis among them. The subspace methods form an efficient and numerically reliable way of determining the predictors by projections directly on the observed data sequences.

3.3.2 Torque estimation for the considered models

The load torque estimation is a numerical method which consents to take into account every complex physical phenomena that is not negligible for the electro mechanical device operation. This method starts from experimental data, like voltage, current and speed samples and from motor constants (resistance, inductance, inertia of the motor and the equivalent inertia of the load, etc.) that have been previously identified.

If we know everyone of these parameters, we can introduce the inverse d'Alembert equation:

$$T_L(nT_s) = k_\phi I_a(nT_s) - k_{aM} \omega_r(nT_s) - (J_M + J_L) \frac{\omega_r(nT_s) - \omega_r((n-1)T_s)}{T_s} \quad (3.7)$$

where T_s is the sampling period and n goes from 1 to the observation period length.

3.3.3 Definition of the model's parameters

The models' parametrization method has obtained the identification of a set of specific parameters for the modelled drives. These parameters are defined and reported in the following. They can be classified as they are related to the experimental-theoretical method adopted for the evaluation.

3.3.3.1 Electric window winder model's parameters

Fig. 3.9 shows an exploded view of the electric window winder's motor. Fig. 3.10 shows a simplified representation of the transmission of movement in the window winder and Table 3.1 reports the parameters' set for the electric window winder.

Model's parameters for the electric window winder are the following:

- motor's armature resistance;
- motor's armature inductance;
- motor's friction torque coefficient;
- motor's back-emf/torque coefficient;

- total motor/load inertia.

Moreover, for this model, it is necessary to know the load torque profile, respect to the motor shaft, in rising and falling mode, as function of the linear position of the glass or the angular position of the rotor.

Model's outputs could be:

- motor current in several operative conditions (rising, falling, block);
- glass and motor speed and memory of the position status of the glass/rotor.



Fig. 3.9: exploded view of the window winder's motor.

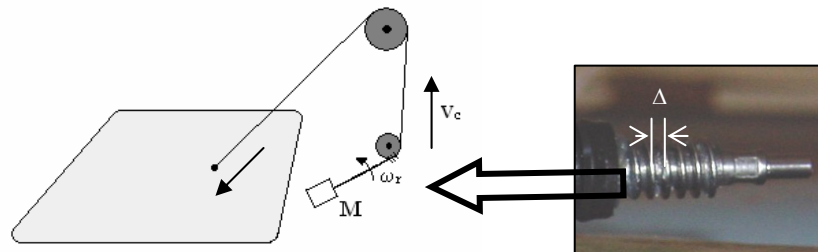


Fig. 3.10: simplified representation of the transmission of movement in the window winder.

Motor parameters	θ	R_s	R_i	$R_a = R_s + R_i$	L_a	$k_{a,M}$	k_ϕ	J_M
Load parameters	$m, \Delta \Rightarrow J_L$				T_L			

Tab. 3.1: parameters' set for the electric window winder.

3.3.3.2 Electric fans model's parameters

Figs. 3.11 and 3.12 show an exploded view of the radiator fan's motor and the air-conditioner fan's motor, respectively. Table 3.2 reports the parameters' set for both the electric fans.

Model's parameters for for both the electric fans are the following:

- motor's armature resistance;
- motor's armature inductance;
- motor's friction torque coefficient;
- motor's back-emf/torque coefficient;
- total motor/load inertia.

Moreover, for this model, it is necessary to know the load torque profile, respect to the motor shaft, as a quadratic function of the rotor speed.

Model's outputs could be:

- motor current;
- motor speed.

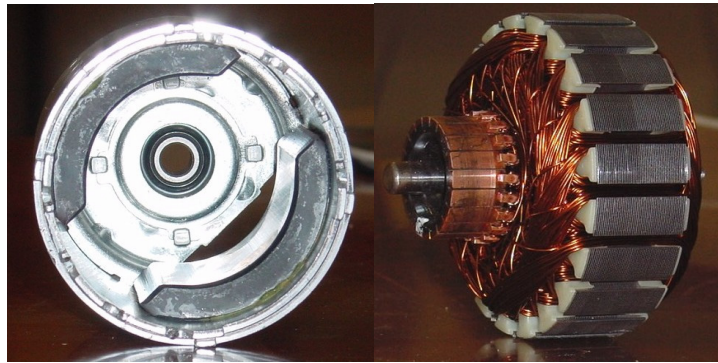


Fig. 3.11: exploded view of the radiator fan's motor.



Fig. 3.12: exploded of the air-conditioner fan's motor.

Motor's parameters	θ	R_s	R_i	$R_a = R_s + R_i$	L_a	$k_{a,M}$	k_ϕ	J_M
Load's parameters	J_L			$T_L = k'_L \omega_r^2$				

Tab. 3.2: parameters set for both the electric fans.

3.3.3.3 Front electric windscreen wiper model's parameters

Fig. 3.13 shows the modelled front electric windscreen wiper. Fig. 3.14 shows the front electric windscreen wiper modelled as an articulated quadrilateral and Table 3.3 reports the parameters' set for the front electric windscreen wiper.

Model's parameters for the front electric windscreen wiper are the following:

- motor's armature resistance;
- motor's armature inductance;
- motor's friction torque coefficient;
- motor's back-emf/torque coefficient;
- total motor/transmission/brushes/load inertia as function of the brushes position.

Moreover, for this model, it is necessary to know the load torque profile, respect to the motor shaft, in direct and inverse direction, in dry and wetted glass, in slow and fast mode, as function of the angular position of the brushes on the glass.

Model's outputs could be:

- motor current profile in several operative conditions;
- brushes and motor speed and angular position profiles.

in several operative modes (dry and wetted glass, slow and fast mode).

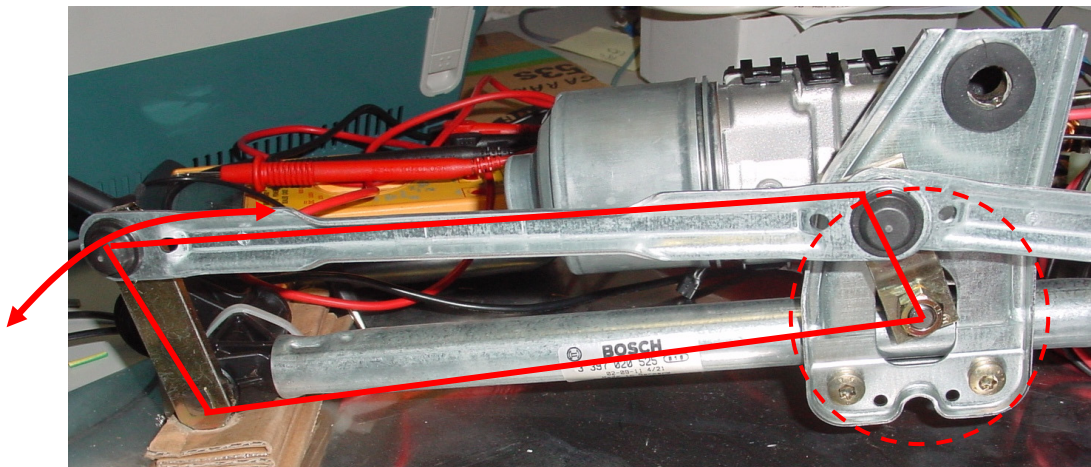


Fig. 3.13: the modelled front electric windscreen wiper.

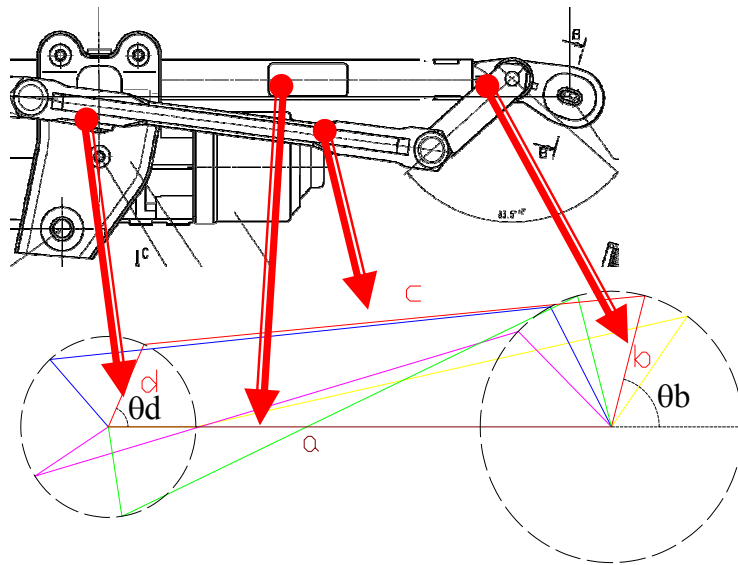


Fig. 3.14: the front electric windscreen wiper as an articulated quadrilateral.

Motor's parameters	θ	R_s	R_i	$R_a = R_s + R_i$	L_a	$k_{a,M}$	k_ϕ	J_M
Transmission's parameters	a, b, c, d, D_c, Δ							
Load's parameters	$L, m \Rightarrow J_L$					T_L		

Tab. 3.3: parameters set for the front electric windscreen wiper.

3.3.3.4 Rear electric windscreen wiper model's parameters

Fig. 3.15 shows the modelled rear electric windscreen wiper. Fig. 3.16 shows the the rear electric windscreen wiper as a particular articulated quadrilateral and Table 3.4 reports the parameters' set for the rear electric windscreen wiper.

Model's parameters for the rear electric windscreen wiper are the following:

- motor's armature resistance;
- motor's armature inductance;
- motor's friction torque coefficient;
- motor's back-emf/torque coefficient;
- total motor/transmission/brushes/load inertia as function of the brushes position.

Moreover, for this model, it is necessary to know the load torque profile, respect to the motor shaft, in direct and inverse direction, in dry and wetted glass, as function of the angular position of the brush on the glass.

Model's outputs could be:

- motor current profile in several operative conditions;

- brush and motor speed and angular position profiles.
in several operative modes (dry and wetted glass).

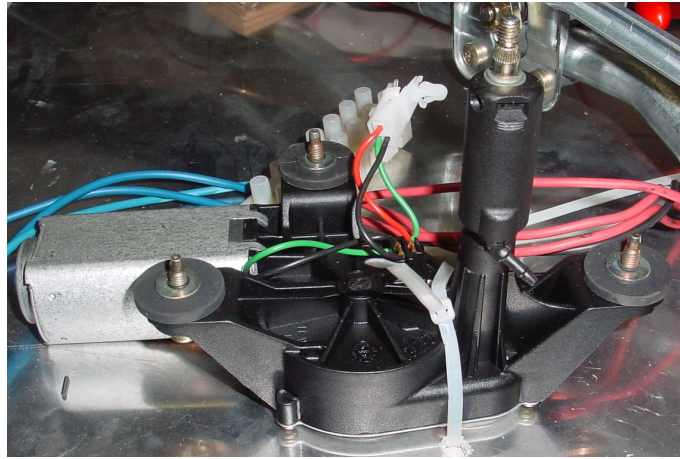


Fig. 3.15: the modelled rear electric windscreen wiper.

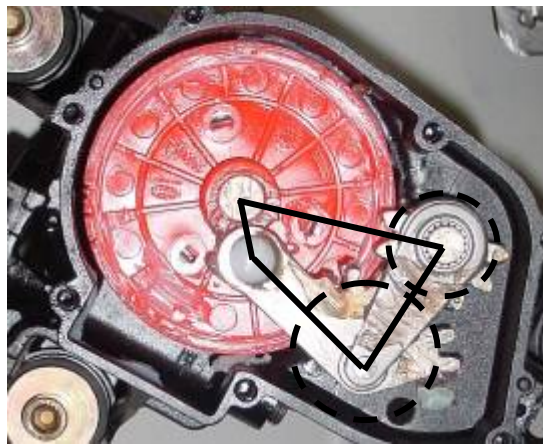


Fig. 3.16: the modelled rear electric windscreen wiper as a particular articulated quadrilateral.

Motor's parameters	θ	R_s	R_i	$R_a = R_s + R_i$	L_a	$k_{a,M}$	k_ϕ	J_M
Transmission's parameters	$a, b, c, d, D_c, \Delta, D_{R1}/D_{R2}$							
Load's parameters	$L, m \Rightarrow J_L$					T_L		

Tab. 3.4: parameters set for the rear electric windscreen wiper.

3.3.4 Electric window winder model validation

Figs. 3.17 and 3.18 report the load torque profile estimated as indicated in paragraph 3.3.2 for the electric window winder respectively in rising and falling operative mode.

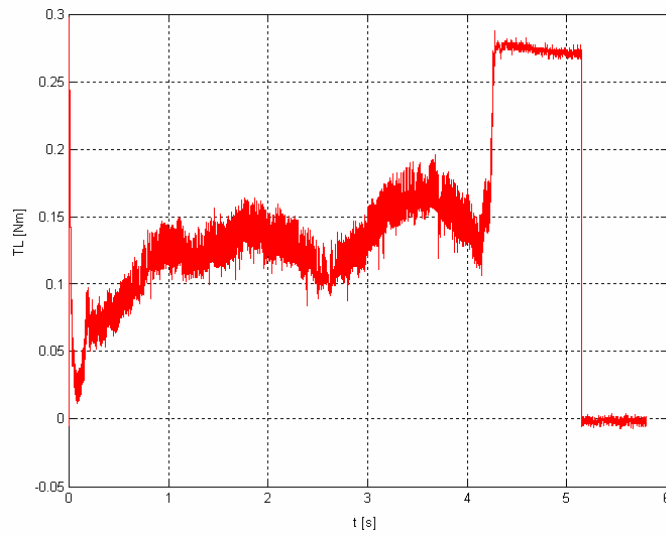


Fig. 3.17: the estimated load torque profile for the window winder in rising mode.

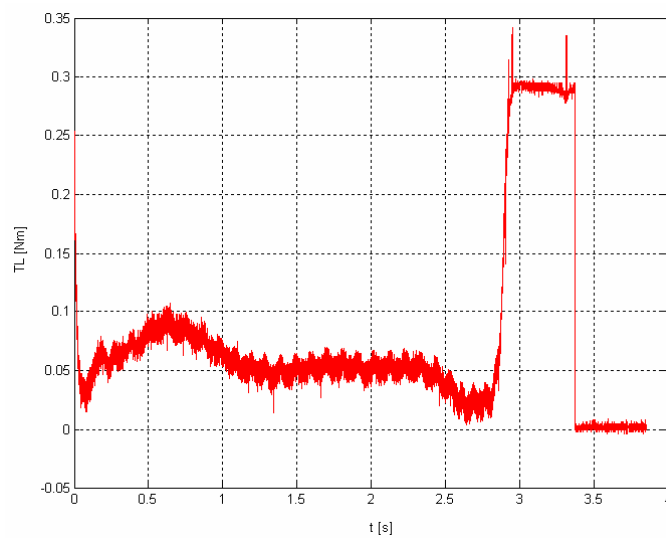


Fig. 3.18: the estimated load torque profile for the window winder in falling mode.

This profile has been applied, together with parameters previously identified and measured, to validate the model. Results are those shown in Fig. 3.19, for the armature current, and in Fig. 3.20, for the rotor speed, in rising mode.

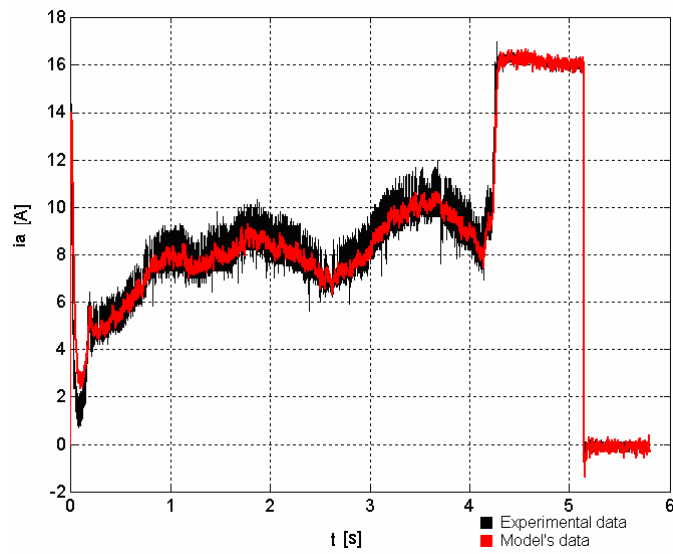


Fig. 3.19: comparison between experimental and modelled armature current for the window winder in rising mode.

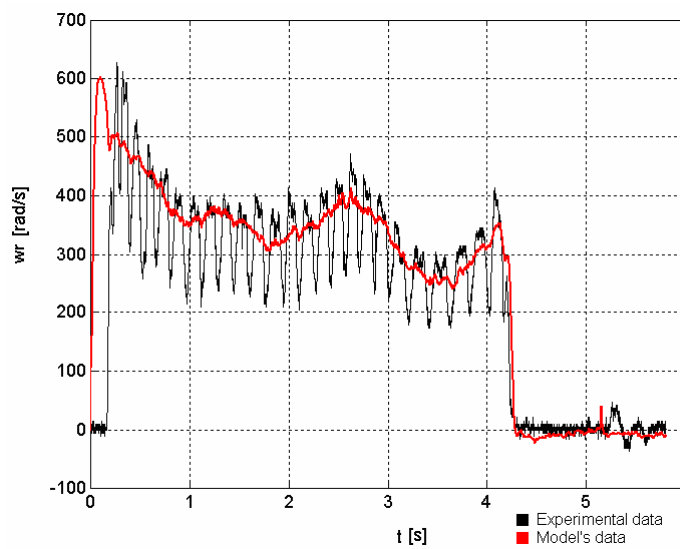


Fig. 3.20: comparison between experimental and modelled rotor speed for the window winder in rising mode.

3.3.5 Air conditioner's electric fan model validation

Fig. 3.21 reports the load torque profile estimated (compared with a quadratic profile) as indicated in paragraph 3.3.2 for the air conditioner's electric fan.

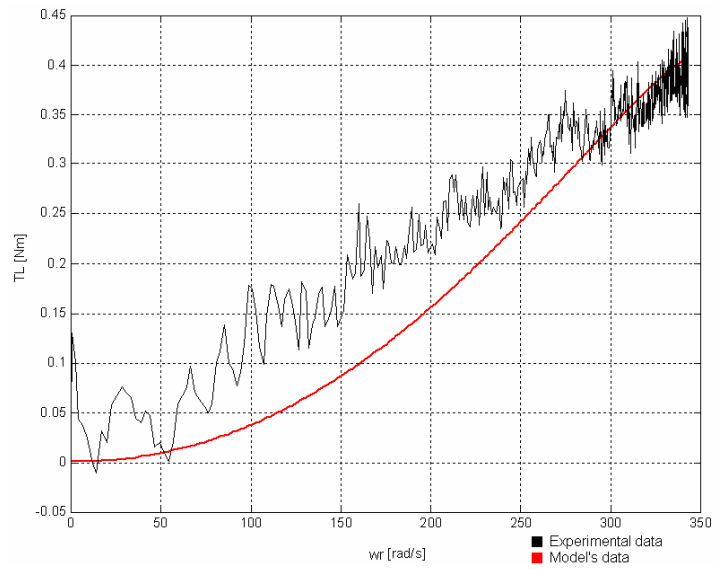


Fig. 3.21: the estimated (and modelled) load torque profile for the air conditioner's electric fan.

The quadratic profile has been applied, together with parameters previously identified and measured, to validate the model. Results are those shown in Fig. 3.22, for the armature current, and in Fig. 3.23, for the rotor speed.

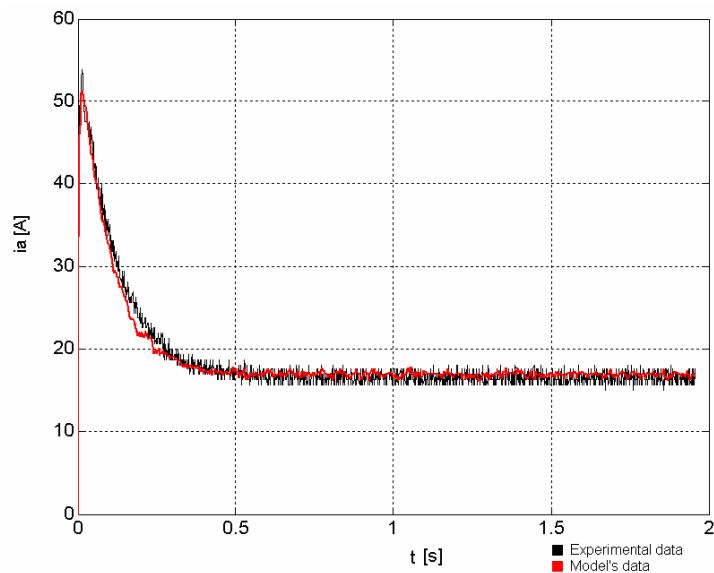


Fig. 3.22: comparison between experimental and modelled armature current for the air conditioner's electric fan.

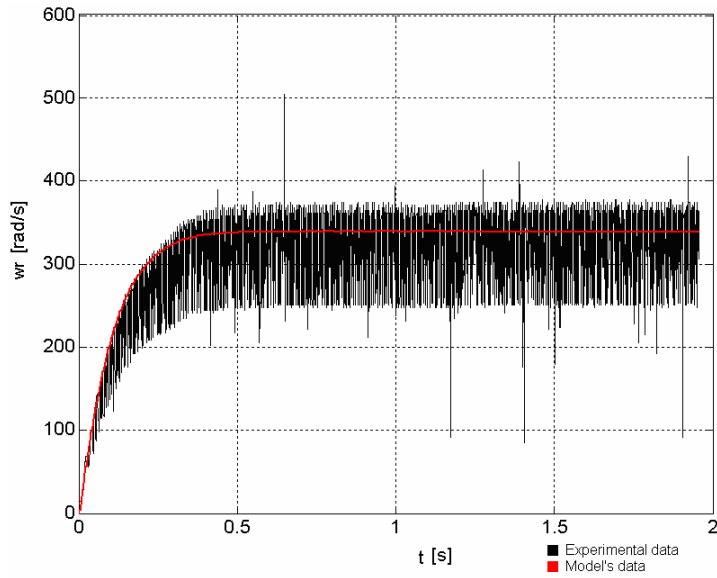


Fig. 3.23: comparison between experimental and modelled rotor speed for the air conditioner's electric fan.

3.3.6 Radiator's electric fan model validation

Fig. 3.24 reports the load torque profile estimated (compared with a quadratic profile) as indicated in paragraph 3.3.2 for the radiator's electric fan.

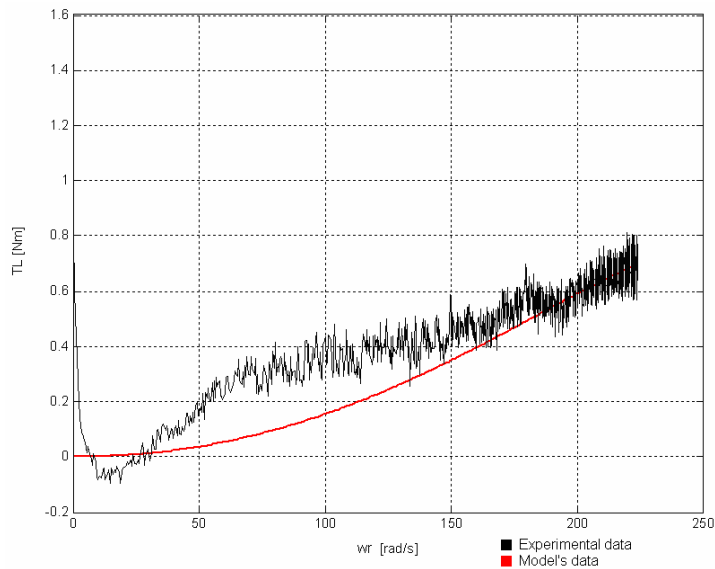


Fig. 3.24: the estimated (and modelled) load torque profile for the radiator's electric fan.

The quadratic profile has been applied, together with parameters previously identified and measured, to validate the model. Results are those shown in Fig. 3.25, for the armature current, and in Fig. 3.26, for the rotor speed.

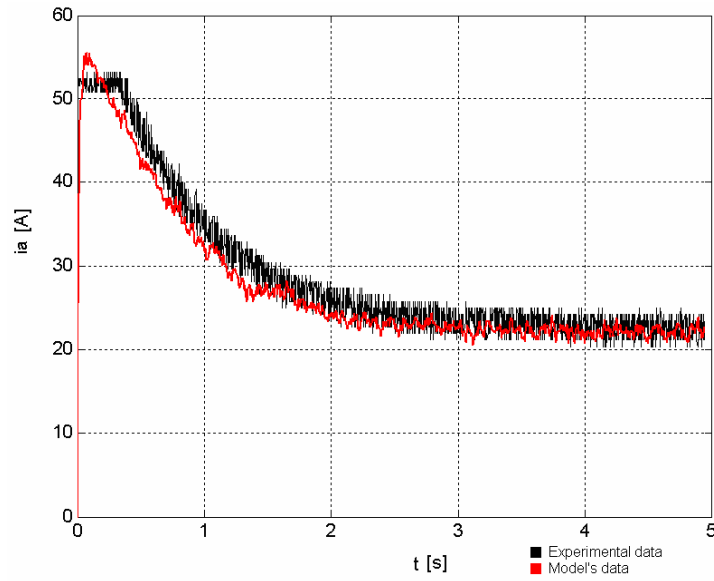


Fig. 3.25: comparison between experimental and modelled armature current for the radiator's electric fan.

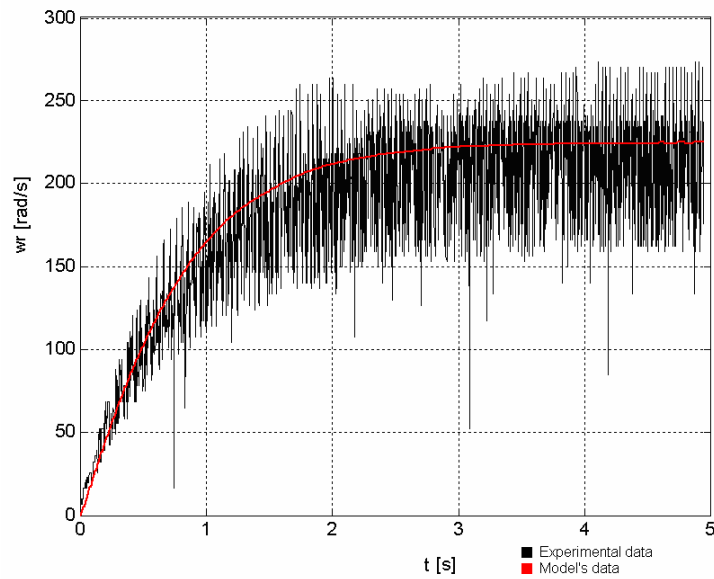


Fig. 3.26: comparison between experimental and modelled rotor speed for the radiator's electric fan.

3.3.7 Front electric windscreen wiper model validation

Fig. 3.27 reports the load torque profile estimated (compared with an interpolated curve used for the simulations) as indicated in paragraph 3.3.2 for the front electric windscreen wiper, in slow mode, direct and inverse direction of the brushes, dry glass.

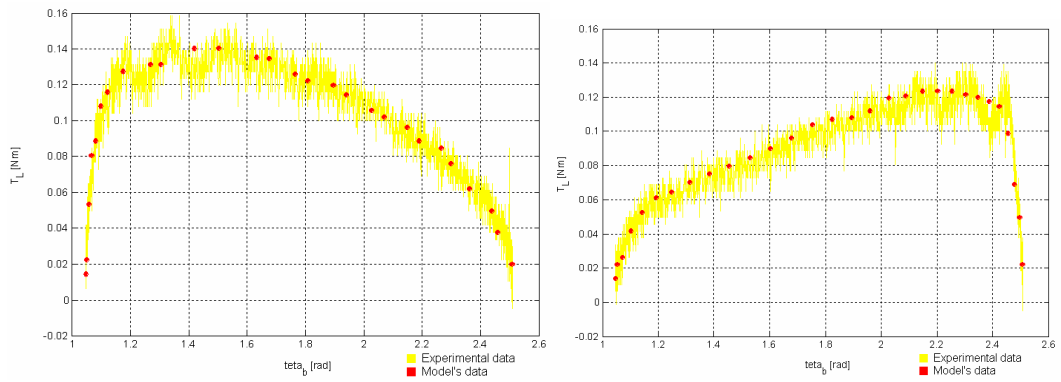


Fig. 3.27: the estimated (and interpolated) load torque profile for the front electric windscreen wiper, in a fixed operative mode.

The interpolated profile has been applied, together with parameters previously identified and measured, to validate the model. Results are those shown in Fig. 3.28, for the armature current, and in Fig. 3.29, for the brushes speed, in the same operative conditions.

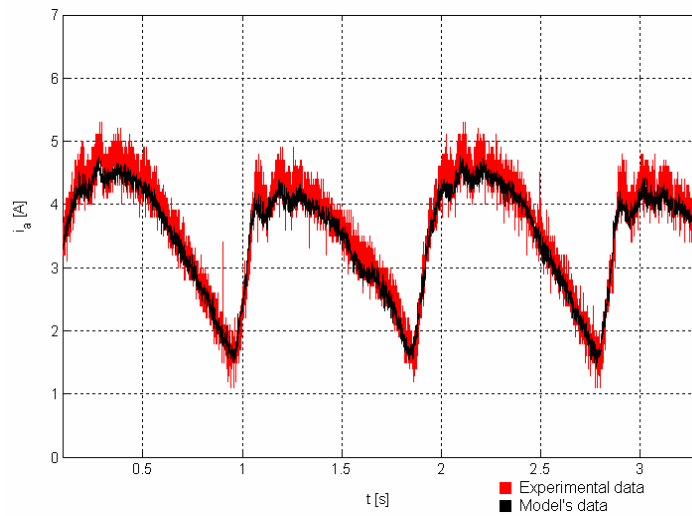


Fig. 3.28: comparison between experimental and modelled armature current for the front electric windscreen wiper, in a fixed operative mode.

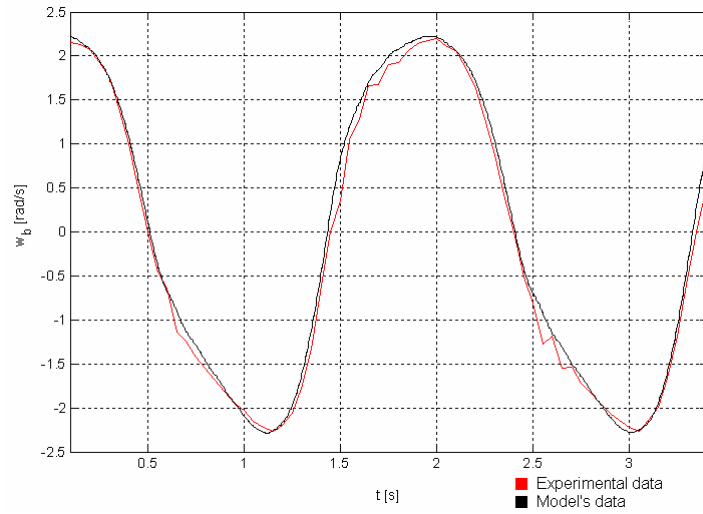


Fig. 3.29: comparison between experimental and modelled brushes speed for the front electric windscreen wiper, in a fixed operative mode.

3.3.8 Rear electric windscreen wiper model validation

Fig. 3.30 reports the load torque profile estimated (compared with an interpolated curve used for the simulations) as indicated in paragraph 3.3.2 for the rear electric windscreen wiper, in direct and inverse direction of the brushes, dry glass.

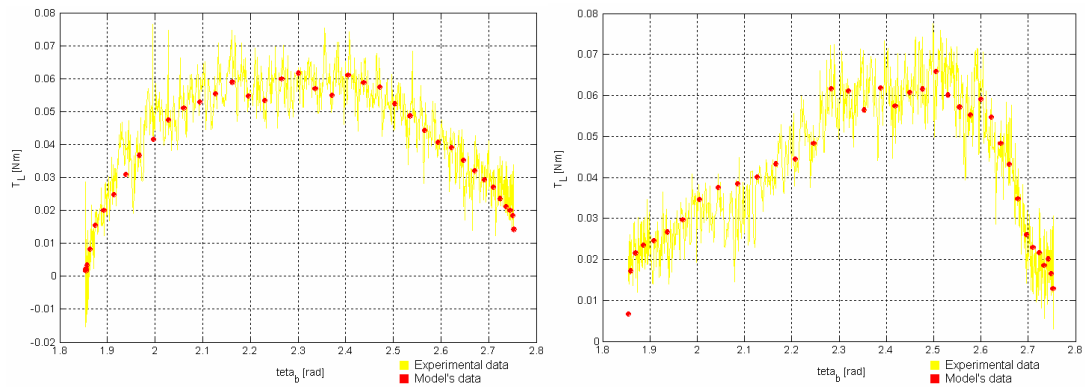


Fig. 3.30: the estimated (and interpolated) load torque profile for the rear electric windscreen wiper, in a fixed operative mode.

The interpolated profile has been applied, together with parameters previously identified and measured, to validate the model. Results are those shown in Fig. 3.31, for the armature current, and in Fig. 3.32, for the brushes speed, in the same operative conditions.

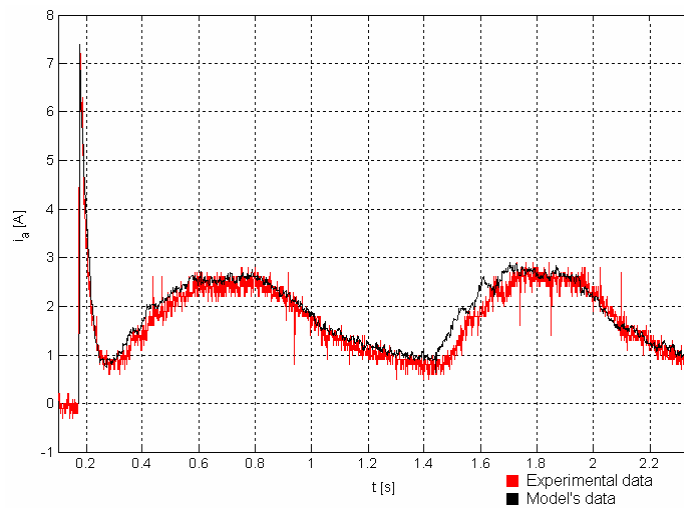


Fig. 3.31: comparison between experimental and modelled armature current for the rear electric windscreen wiper, in a fixed operative mode.

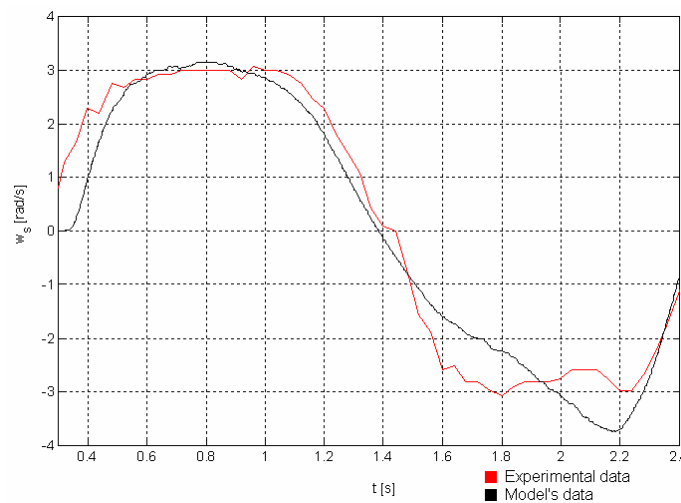


Fig. 3.32: comparison between experimental and modelled brushes speed for the rear electric windscreen wiper, in a fixed operative mode.

3.4 Modelling of innovative on-board electric loads

3.4.1 EPAS (*Electrical Power Assisted Steering*)

Electric type of power steering system completely does away with all hydraulic components. It provides steering assistance with an electric motor that directly assists steering maneuvers only when turning is desired. The electric motor may be mounted to assist lateral motion, or to assist circular motion. The control system for the electric motor consists of the typical components for an electric motor drive. The

controller uses torque commands and current/voltage feedback to control the power electronic converter. The converter then outputs the voltage needed to carry out the desired steering operation.



Fig. 3.33: double pinion rack EPAS.

Since the simulations for the evaluation of automotive architectures doesn't take into account the direction on the road of the vehicle, we have considered a virtual behavior of a real EPAS system into the electrical system, deduced from simulations realized in AMESIM simulator [79].

The simulation schema in AMESIM is reported in Fig. 3.34.

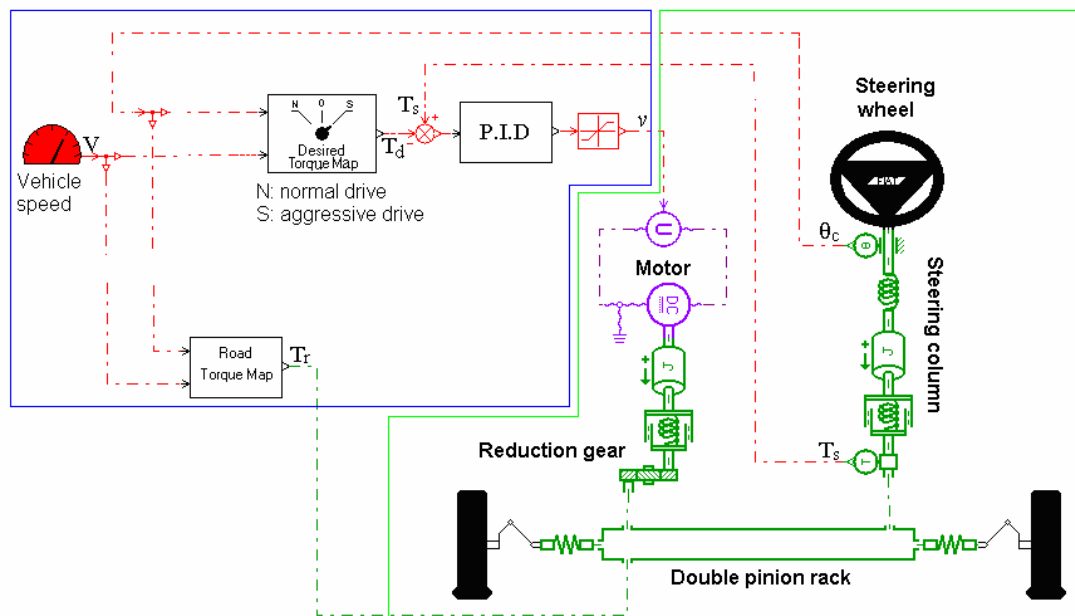


Fig. 3.34: simulation schema in AMESIM of a EPAS double pinion rack system, with innovative control system.

Fig. 3.36 shows the current and voltage profiles of the dc motor, that assists the driver's steering, when the steering profile reported in Fig. 3.35 is realized.

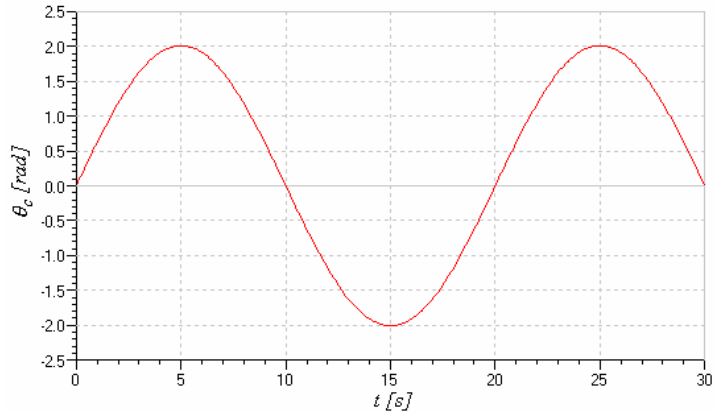


Fig. 3.35: steering wheel angle profile.

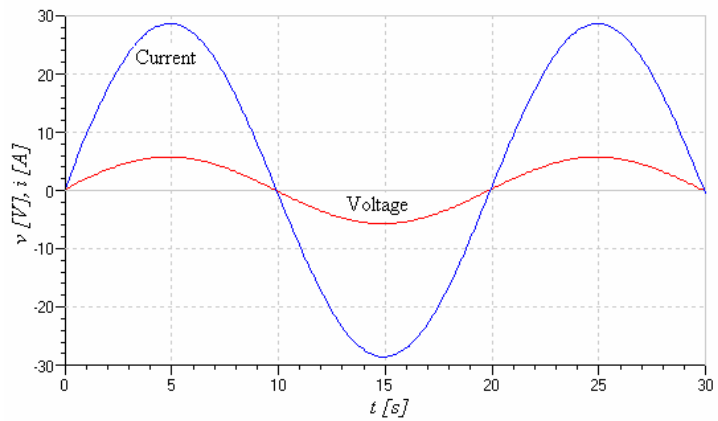
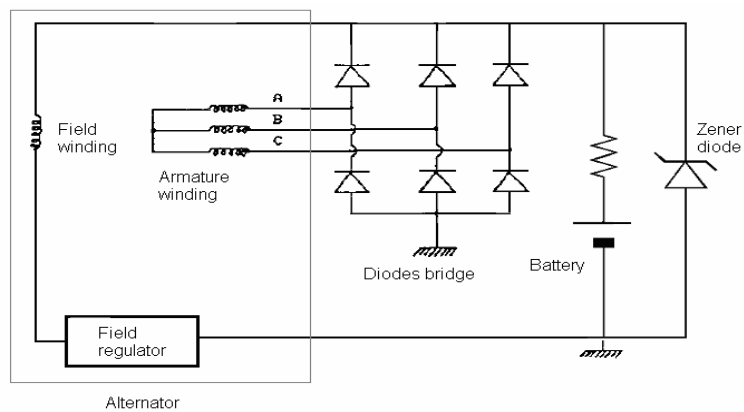


Fig. 3.36: voltage and current profile results from AMESIM simulations.

3.5 Modelling of the power supply system for conventional vehicles



3.5.1 Lead-acid batteries

A simple behavioral model for the lead acid batteries has been adopted. The simplicity consents to simulate the battery behaviour belonging to any kind of plant without complicating too much the electric study of the same plant. For this reason the equivalent model has to be represented with simple mathematical expressions and independent of time variable [80]. There are different equivalent models representing batteries behaviour, but these models are specialized for discharge operations and are dependent on time. The adopted model is not connected with chemical phenomena taking place in the batteries but originates from the study of batteries like a black box. However because battery behaviour is dependent on previous history, it's necessary to use integral quantities in the model:

$$Q(t) = Q_o + \int_0^t i_b(\tau) d\tau \quad (3.8)$$



Fig. 3.37: equivalent model of a lead acid battery.

The model (Fig. 3.37) is realized with a series of a controlled voltage source and a non-linear resistor, both depending from State Of Charge of the battery as polynomial functions.

3.5.2 Lundell alternator

The generation system in an automotive electrical system is usually realized with a three-phases synchronous machine (Lundell type), with a rectifier (diode bridge) that gives the DC voltage in output (Fig. 3.38).

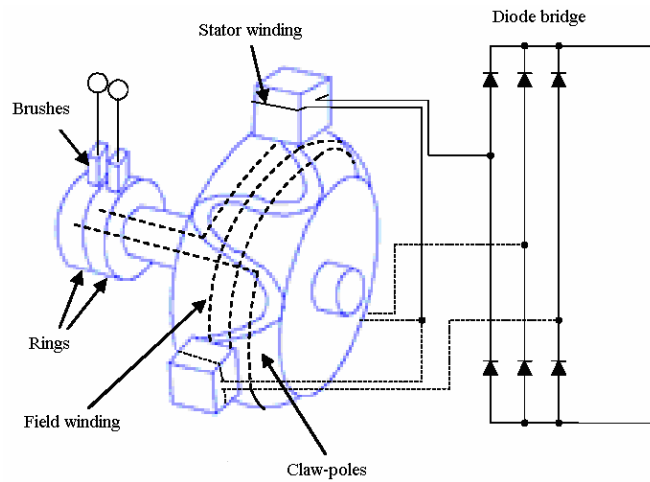


Fig. 3.38: a Lundell alternator with diode bridge.

An equivalent model of a Lundell alternator must relate the output voltage with the rotor speed, in other words with the vehicle speed in a specific drive cycle [81].

An ideal three-phase voltage source connected with a diode bridge (Fig. 3.39) has the following behavior.

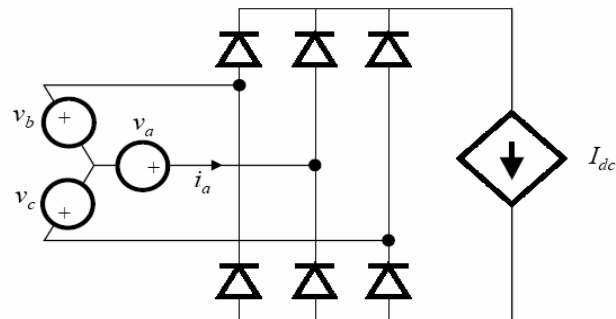


Fig. 3.39: an ideal voltage source with a diode bridge.

Fig. 3.40 show the qualitative profiles of the phase voltage and current for an ideal voltage generator with a diode bridge. The phase current has a square shape.

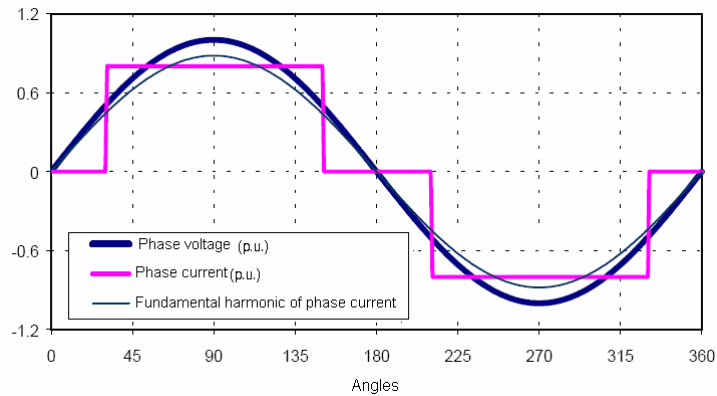


Fig. 3.40: voltage and current profiles for an ideal alternator with a diode bridge.

A real alternator is quite different from the ideal model in Fig. 3.39.

The voltage source has a resistance and an inductance connected in series. Fig. 3.41 depicts the equivalent circuit of the alternator.

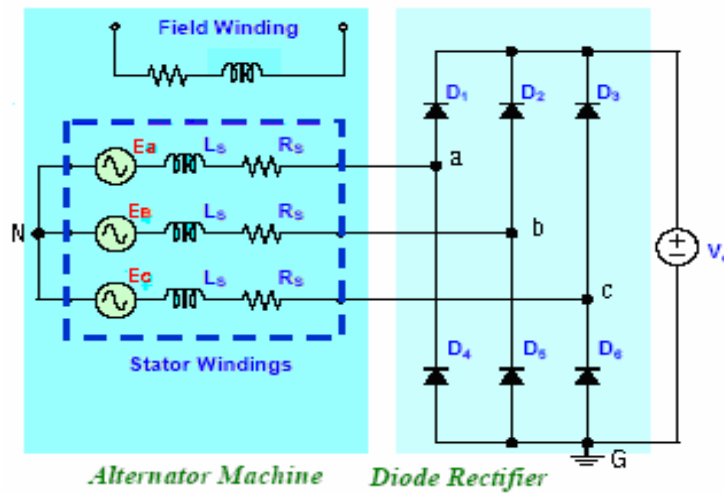


Fig. 3.41: a real alternator equivalent circuit with a diode bridge.

Maximum value of the e.m.f. is $E_{Max} = K_M \omega_s i_f$, where i_f is the field current, ω_s is the electric frequency of the alternator, K_M is a machine constant, while the d.c. voltage can be considered constant because of the presence of the battery that fixes the voltage value. The diodes commutations are not ideal for the presence of the inductances; the commutation angle depends on L_s , I_{dc} and I_f .

$$\mu = \cos^{-1} \left(1 - \frac{2\omega L_s I_{dc}}{\sqrt{3} E_M} \right) = \cos^{-1} \left(1 - \frac{2\omega L_s I_{dc}}{\sqrt{3} K_M \omega i_f} \right) \quad (3.9)$$

The non-istantaneous diodes commutations causes a distortion in the phase voltage profile, while current is filtered by L_s .

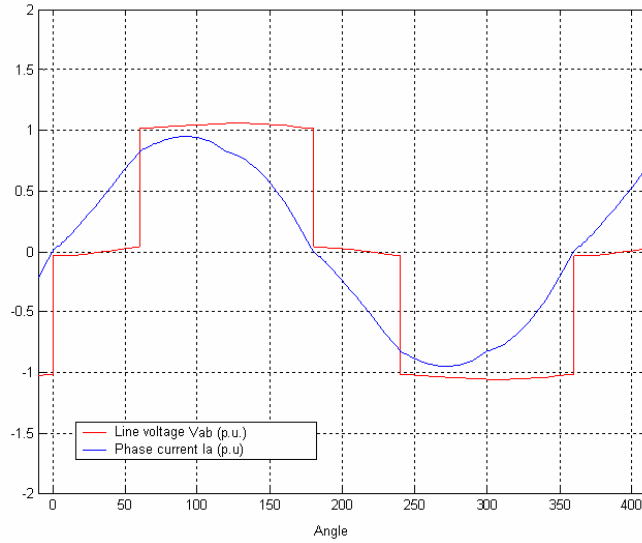


Fig. 3.42: real alternator voltage and current profiles.

The phase equivalent circuit of the alternator is reported in Fig. 3.43.

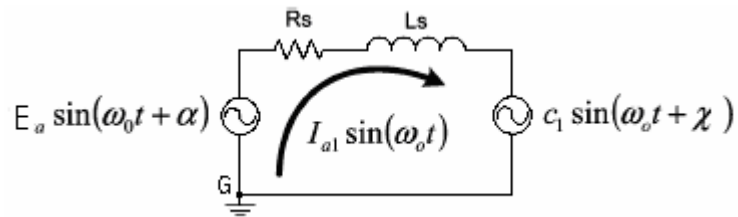


Fig. 3.43: phase equivalent circuit of a real alternator respect to the fundamental of current.

where $c_1 = \sqrt{a_1^2 + b_1^2} = b_1$ and $\chi = \tan^{-1}(a_1/b_1) = 0$, $a_1 = 0$ and $b_1 = \frac{2}{\pi} V_o$.

The alternator phase impedance, for the fundamental of current, can be expressed as $\dot{Z}_{RL} = R_s + j(\omega_o L_s)$. Solving the equivalent circuit in Fig. 3.43 we have (projecting on the real and imaginary axes):

$$|I_{a1}| = \left[\frac{E_a}{|Z_{RL}|} \cos(\alpha - \theta_{Z_{RL}}) - \frac{c_1}{|Z_{RL}|} \cos(\chi - \theta_{Z_{RL}}) \right] \quad (3.10)$$

$$0 = \left[\frac{E_a}{|Z_{RL}|} \sin(\alpha - \theta_{Z_{RL}}) - \frac{c_1}{|Z_{RL}|} \sin(\chi - \theta) \right] \quad (3.11)$$

From equation (3.11) we have:

$$\alpha = \theta_{Z_{RL}} + \sin^{-1} \left[\frac{c_1}{E_a} \sin(\chi - \theta_{Z_{RL}}) \right] \quad (3.12)$$

Equation (3.10) with (3.12) provides the fundamental phase current amplitude.

The load power characteristics of the alternator can be traced (output bridge current-alternator speed, for a fixed field voltage and dc bus voltage), taking into account the influence of the winding armature temperature, which depends from several factors.

The model adopted for a Lundell alternator has been validated comparing simulations results with numerical data available from commercial alternators. This comparison has been realized for three different machines, whose rating values are reported in Table 3.5.

	Alternator 1	Alternator 2	Alternator 3
$R_s @ 25^\circ\text{C}$ [m Ω]	58	28	25
L_s [μH]	160	140	120
$R_e @ 25^\circ\text{C}$ [Ω]	3.1	2.83	2.75
Pole pairs	6	6	6
Nominal voltage [V]	14	14	14
Power @ 10.000 rpm and full field voltage [W]	2.000	2.500	3.000

Tab. 3.5: rating values for three commercial alternators.

In Figs. 3.44, 3.45, 3.46 the results of the comparisons among numerical and experimental data for the three commercial alternators have been reported, at full excitation voltage and 14 V bus voltage.

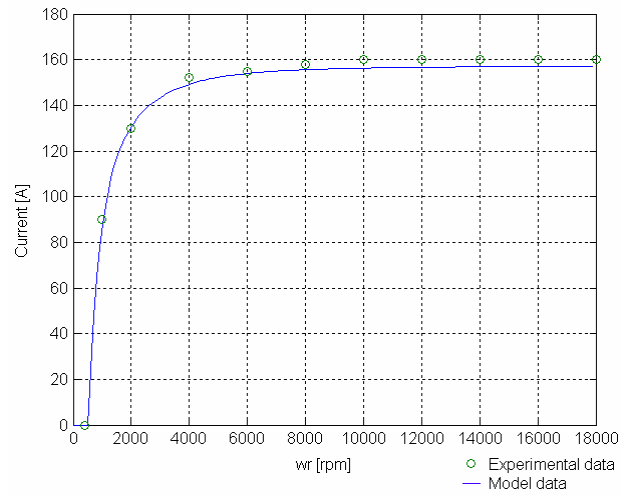


Fig. 3.44: loading curve for alternator 1, at full excitation voltage and 14 V bus voltage.

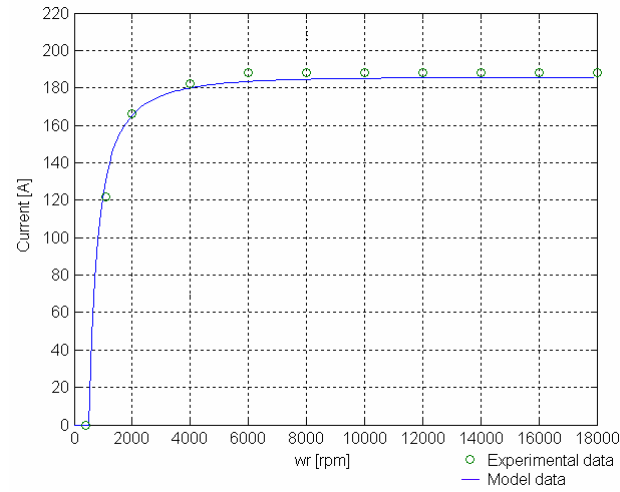


Fig. 3.45: loading curve for alternator 2, at full excitation voltage and 14 V bus voltage.

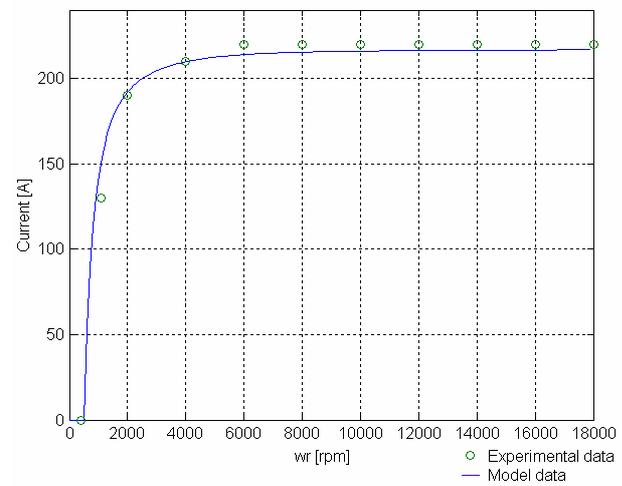


Fig. 3.46: loading curve for alternator 3, at full excitation voltage and 14 V bus voltage.

3.6 A tool for the comparative analysis of power bus architectures

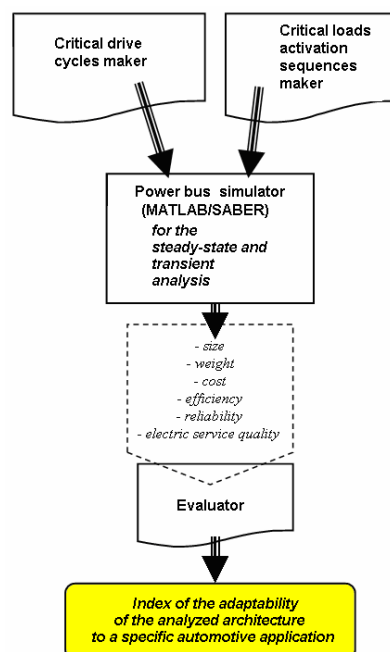
The comparative analysis is formulated by means of stochastic and expert system approaches, and is specifically oriented for the analysis of automotive electrical systems. Since it automates two critical functions: system analysis and comparative evaluation, it can be used to quantitatively compare a large number of architectural alternatives in a relatively short time [82].

The software that implements these functionality is a suite composed from four tools:

- *critical drive cycles maker*;
- *critical loads activation sequences maker*;
- *power bus simulator* (system analysis);
- *evaluator* (comparative evaluation)

The proposed technique, starting from the following system indexes: size, weight, cost, efficiency and reliability of every components and of the whole system, electric service quality, gives a global index that defines the adaptability of analyzed architecture to the specific automotive application.

Below, a flow-chart of the suggested technique is reported.



The *evaluator* module compares different architectures adopting a multicriteria analysis [83], [84]. To find some of these multicriteria analysis indexes (S.O.C., supply continuity, etc.) it is necessary to simulate the power bus configuration running under a well defined vehicle drive cycle and an adequate activation sequence of loads (at this scope the tools *critical loads activation sequences maker* and *critical drive cycles maker* have been implemented, see paragraphs 3.6.1 and 3.6.2).

For these reasons, the tool *power bus simulator* has been developed (see paragraph 3.6.3).

3.6.1 Critical drive cycles maker

This tool starts from a set of data (i.e. limit of speed for every gear change or compatibility condition for every change) and generates, by means of a stochastic approach, different possible drive cycles and gives as results, by means of the Montecarlo technique, the probability distribution of the average speed values of the drive cycles and the related drive cycles.

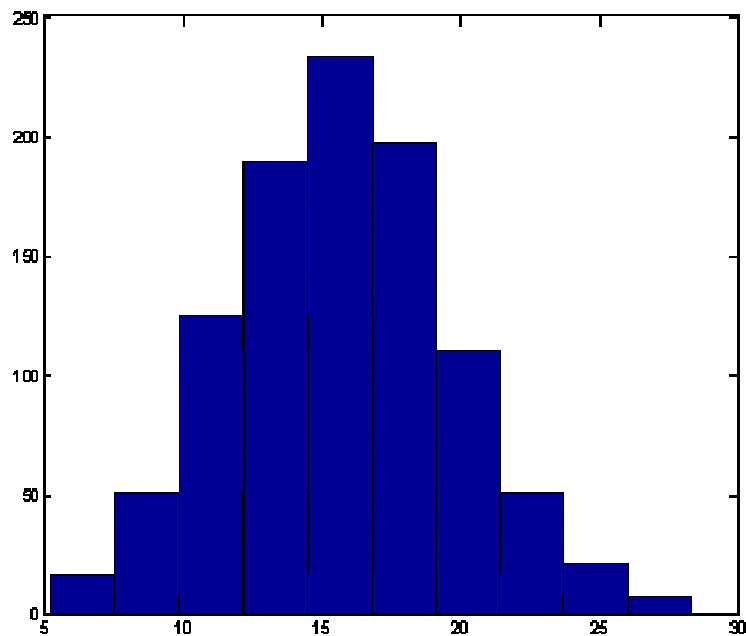


Fig. 3.47: histogram of the average vehicle speeds in a Montecarlo simulation (occurrences as function of average velocity, in km/h).

3.6.2 Critical loads activation sequences maker

This module gives information about electrical stress of power bus. The critical operative conditions are evaluated respect to the power bus and respect to the power source system.

The inputs for the software are some known data such as minimum and maximum load activation duration for every load, activation rates on a whole drive cycle, the on-board loads currents and so on.

The software tool generates, by means of a stochastic approach, different sequences of loads activation and gives, by means of Montecarlo technique, the probability distribution of the maximum values of bus current I_{max} and the probability distribution of the maximum values of product $I_{max} \times T$ (T is the time while I_{max} is greater then the rated alternator current in a drive cycle) for each sequence. This tool considers only sequences which give I_{max} value greater than the rated alternator current value.

The outputs represent a set of critical operative conditions suitable for testing the power source system while the second output is a set of critical operative conditions suitable for testing the power bus.

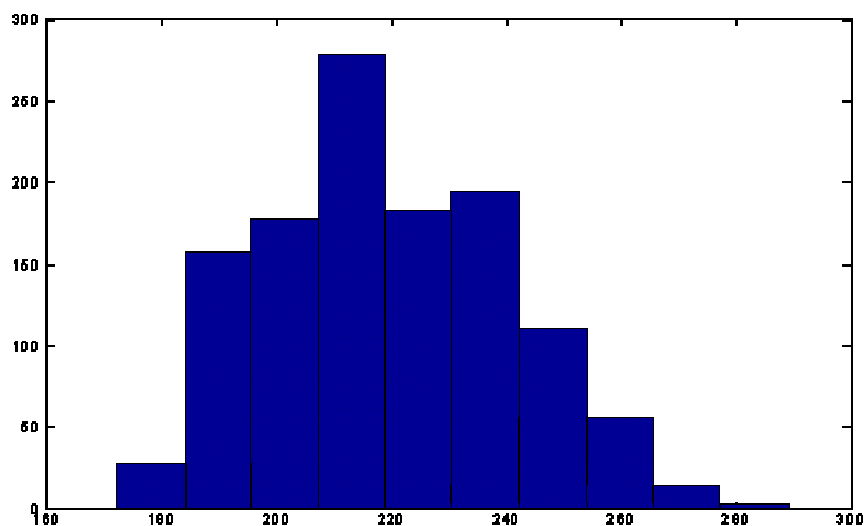


Fig. 3.48: histogram of the maximum values of the bus current in a Montecarlo simulation (occurrences as function of I_{max} , in A).

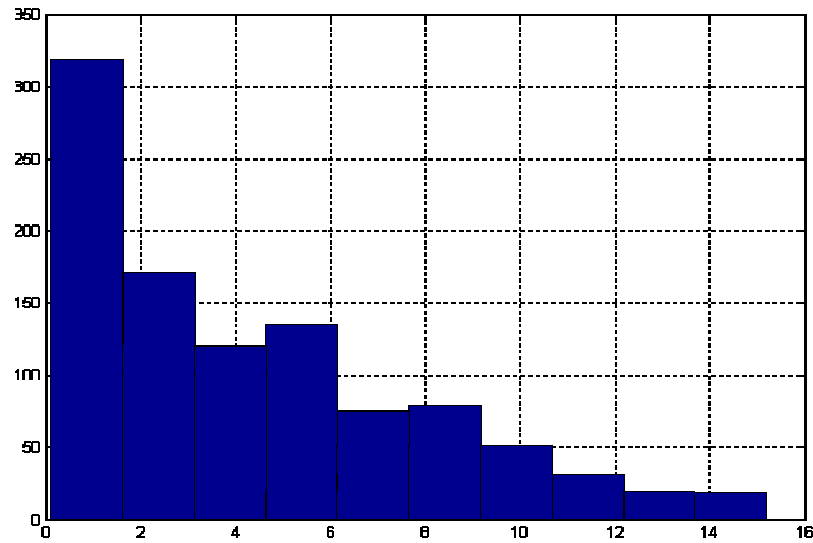


Fig. 3.49: histogram of the maximum values of $I \times t$ in a Monte Carlo simulation (occurrences as function of $I \times t$, in Ah).

Among the simulated activation sequences where the bus current is over the alternator's rated current, the tool chooses those sequences where $I \times T$ is over a critical value. This critical value is represented by the $X\%$ percentiles of $I \times T$ of the simulated sequences (percentiles = higher limit of the ordered values of the distribution which occurs in 90% of cases).

3.6.3 Power bus simulator

This tool gives the steady-state and the transient analysis of the overall on-board electrical system. Inputs are: topology of chosen architecture for power bus; models of all the loads in the automotive electrical system; critical loads activation sequence (found with the *critical loads activation sequences maker* tool) and critical drive cycle (found with the *critical drive cycles maker* tool).

As reported in paragraphs 3.3, 3.4 and 3.5, several models have been developed for the devices which compose the power bus. Appropriate algorithms for each model have been realized, implemented in MAST language [85], in way to be simulated as templates in SABER[®] DESIGNER environment [86]; particularly, battery, alternator, electrical window winders, radiator and air conditioner fans, electrical windscreen wipers templates have been realized.

Once a system has been characterized, the *power bus simulator* tool calculates the indexes that are of interest for the multicriteria analysis: cost, weight, efficiency, reliability, etc. Cost is broken down into parts cost and assembly cost; efficiency is measured in terms of the average mechanical power consumption of the electrical system as measured at the crank-shaft of the engine. These indexes are generally calculated from the data available in a specific database. However, if an appropriate part was not found in the database and a virtual component was created, *power bus simulator* calculates the component indexes using physically based component properties models.

Power bus reliability depends on the topology of power system, so it can be evaluated with classical schemes (series, parallel, etc.). Electric service quality is evaluated employing a further multicriteria analysis, which take in account the following indexes: continuity of supply, state of charge of the batteries in a drive cycle, bus voltage profile and consequently voltage sags and dips.

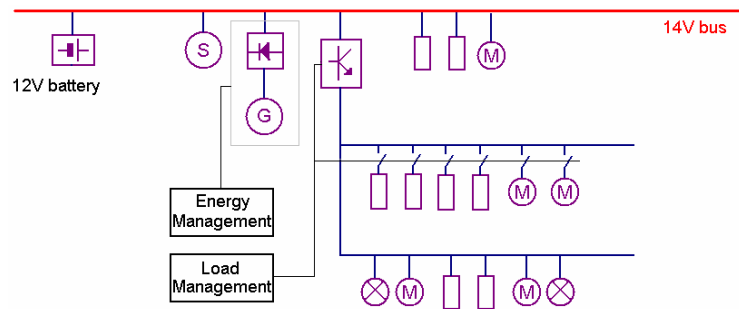
The indexes employed for the evaluation of service quality have been obtained simulating the selected architecture in a full SABER schema.

Drive cycle and loads activation sequence are the output of the other two tools (paragraphs 3.6.1 and 3.6.2), that are of fundamental importance because they identify the opportune operative conditions on which the power bus must be tested.

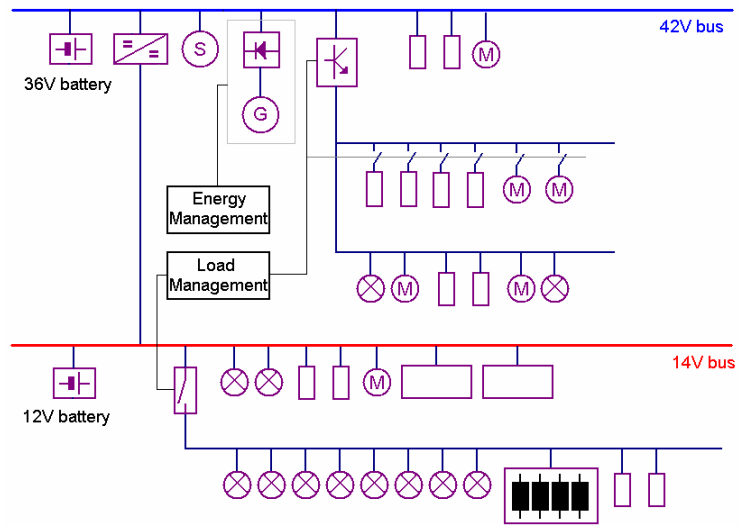
3.7 Case-study for the testing of Evaluator

Since the software *Evaluator* automates two important activities: the system analysis and the comparative evaluation, it can be used for a quantitative analysis of a large number of architectural alternatives in a relatively short time.

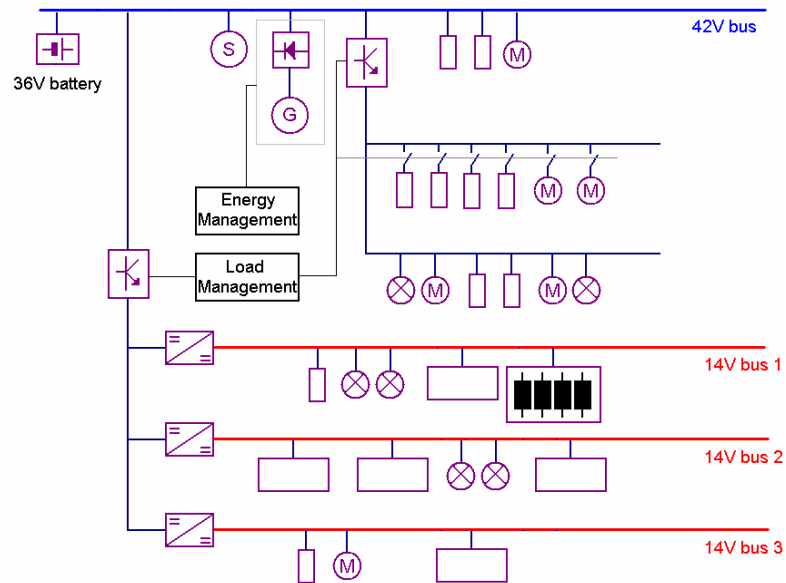
Two families of power bus architectures (conventional and dual voltage) have been analyzed under different aspects: energetic, systemic and of reliability [7], [64] (Figs. 3.50 (a)-(c)).



(a) - 14V DC supply concentrated architecture



(b) - 42-14V DC dual voltage supply concentrated architecture



(c) - 42-14V DC dual voltage supply distributed architecture

Fig. 3.50: considered power bus architectures for the analysis

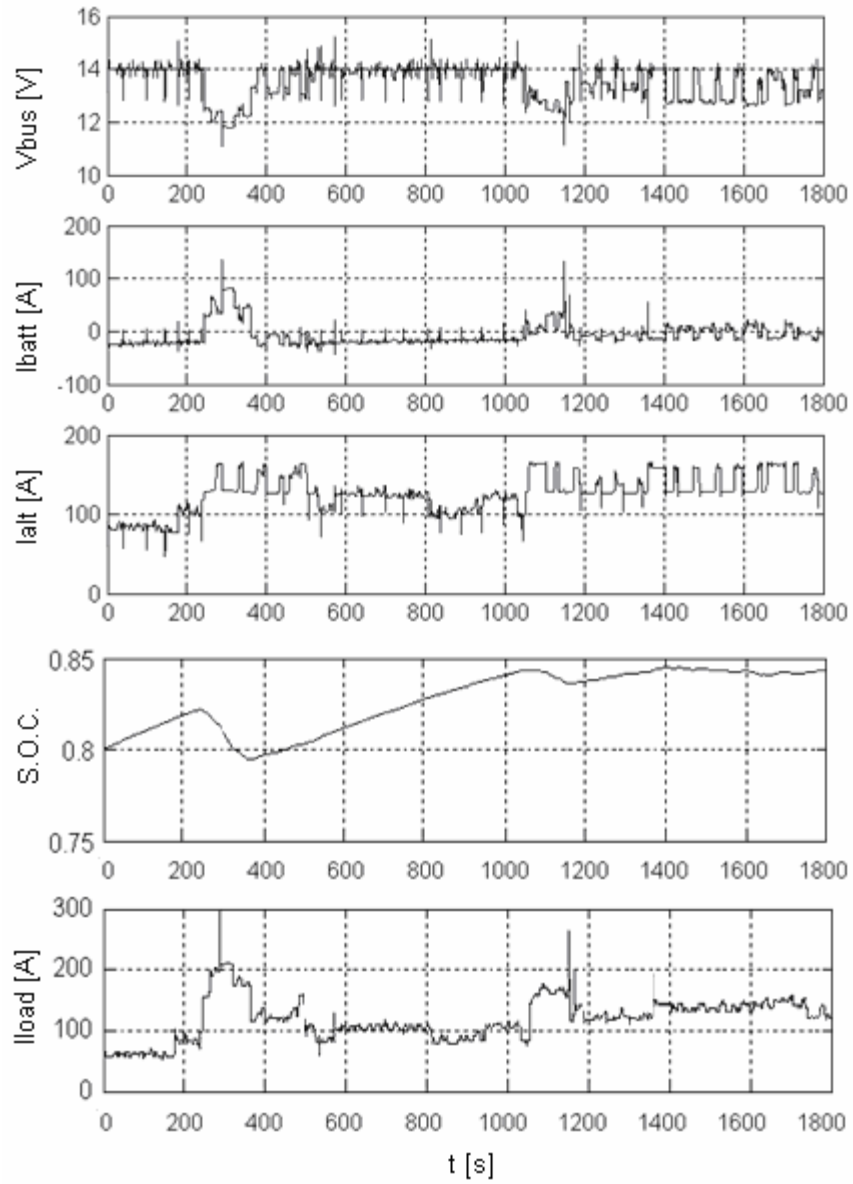


Fig. 3.51: bus voltage, battery current, alternator current, S.O.C., total load current vs. time, for a critical loads activation sequence applied to the arch. (a).

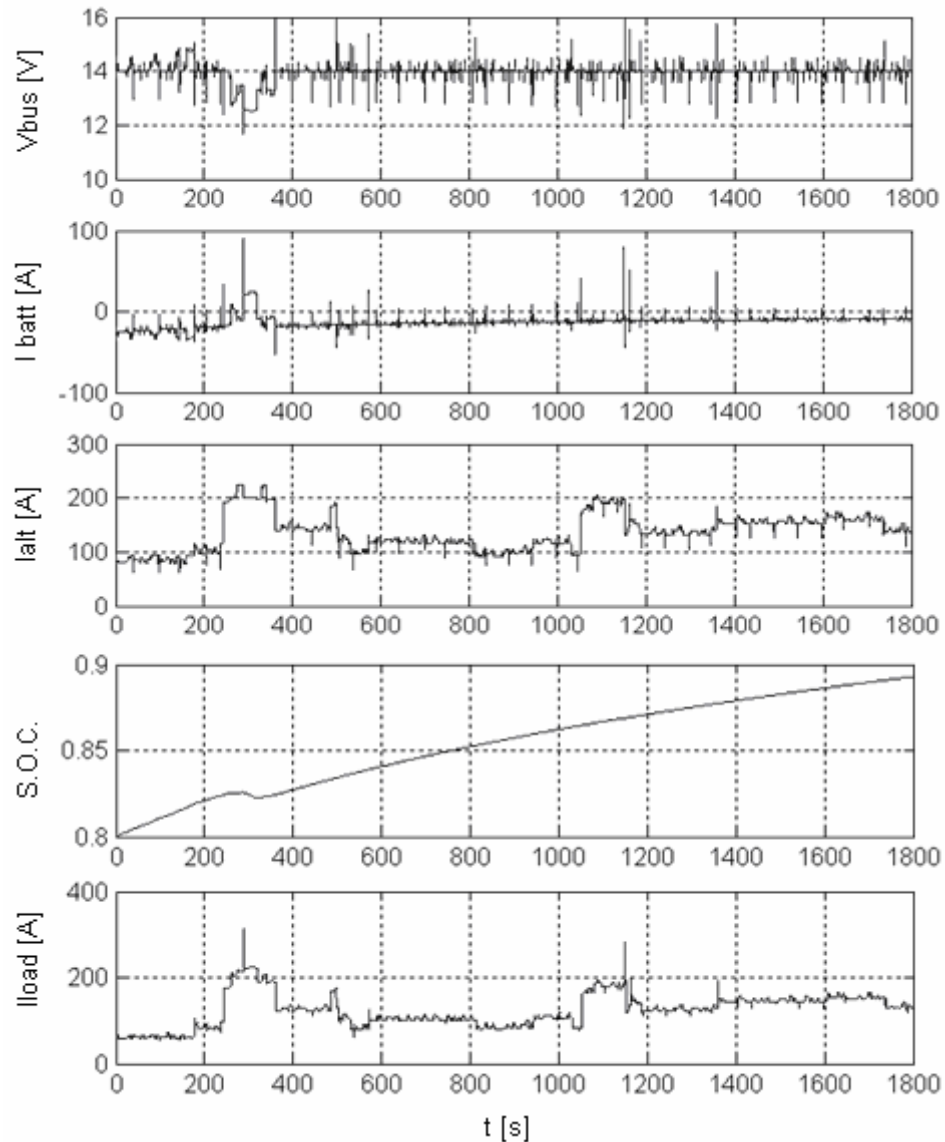


Fig. 3.51: Bus voltage, battery current, alternator current, S.O.C., total load current vs. time, for a critical loads activation sequence applied to the arch. (b).

Table 3.7 reports the power bus indexes computed from the *power bus simulator* and the global index result given from the multicriteria analysis.

As can be noted, the best performances have been obtained with the solution (c) (42-14 V DC dual voltage supply distributed architecture). Naturally, the result significantly depends on the values assumed for the indexes weight. Therefore it's very important to define adequately these values.

Table 3.8 reports as example the same results when different values are fixed for the indexes weight. In both the tables it has been fixed as maximum of indexes weight a value of 5.

Results reported in both the tables confirm that good performances in terms of $\Delta S.O.C.$ and ΔV are obtained with power bus architectures (b) and (c), even if the choice of the weight fixed for the “cost” item significantly influences the result.

POWERNET INDEX	Arch. (a)	Arch. (b)	Arch. (c)	Index weight
V_{avg} [V]	13.52	13.97	13.99	3
ΔV [V]	3.44	3.61	2.59	4
$\Delta S.O.C.$	0.05	0.09	0.1	5
Weight [kg]	82	100	93	2
Powernet size [dm ³]	12	32	38	4
Cost [€]	1525	1626	2050	3
Powernet efficiency	0.53	0.60	0.60	3
Powernet reliability	0.850	0.890	0.910	5
Global index result	0.5128	0.5052	0.5169	

Tab. 3.7: comparison among three different simulated architectures: case (a).

POWERNET INDEX	Arch. (a)	Arch. (b)	Arch. (c)	Index weight
V_{avg} [V]	13.52	13.97	13.99	2
ΔV [V]	3.44	3.61	2.59	0
$\Delta S.O.C.$	0.05	0.09	0.1	5
Weight [kg]	82	100	93	0
Powernet size [dm ³]	12	32	38	1
Cost [€]	1525	1626	2050	5
Powernet efficiency	0.53	0.60	0.60	2
Powernet reliability	0.850	0.890	0.910	5
Global index result	0.4977	0.5549	0.5348	

Tab. 3.8: comparison among three different simulated architectures: case (b).

4. The proposed energy management strategy for conventional vehicles

4.1 Introduction

As before mentioned, the target of any energy management strategy is to prioritize real-time power requests from the loads and allocate power resources available from the generation and storage devices in an optimized manner, in order to minimize fuel consumption and/or emissions.

To achieve these targets, several approaches have been investigated in the last years, as reported in paragraph 2.2. In general, the relative algorithms do not offer a real-time solution because they assume that the drive cycle is entirely known. In addition they require a lot of computational time and a fine tuning of their parameters therefore their use is restricted to single experiments and for a fixed drive cycle. Nevertheless, their results can be used as a benchmark for the performance of other strategies, or to derive rules for rule-based strategies.

To outperform these algorithms, another efficient approach based on the optimal control theory is here proposed.

The proposed solution for the optimal energy management implementation in vehicles with thermal engine is based on the use of the battery as an energy flywheel,

this is possible with a suitable control of the alternator output power.

The battery stores the electrical energy from the alternator in chemical form, this power is a part of the engine mechanical power; the battery provides electric power required from loads when the alternator is overloaded.

The proposed energy management strategy fixes, at every control step, the modulus operandi of battery and alternator that leads the engine to operate at maximum efficiency.

This strategy requires an innovative control technique method of the alternator, which must be activated for the generation only at the operative points of engine with less fuel consumption; these operative points are evaluated from the control algorithm.

In this chapter, the problem of optimizing fuel consumption will be formulated as a nonlinear convex optimization problem.

This formulation asks for the energetic modelling of every components of the vehicle.

4.2 Energetic model of the vehicle

Fig. 4.1 shows a power flow diagram of a conventional vehicle.

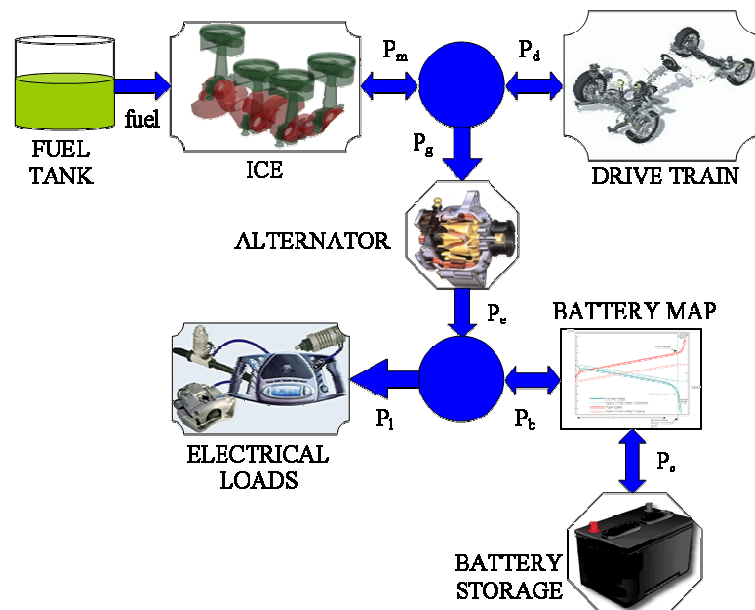


Fig. 4.1: Power flow diagram of a conventional vehicle.

The Internal Combustion Engine (ICE) gives mechanical power to the drive train of the vehicle for the propulsion (P_d) and at the same time activates the alternator for the power bus and to recharge the battery.

4.2.1 Basic assumptions

There are many vehicle architectures that could be considered for the proposed strategy. In the next, a conventional vehicle with a manual transmission and a traditional drive train will be considered.

The following assumptions are made:

- The drive cycle is known;
- The sampling interval of the control strategy is sufficiently large (1 s or larger) so that to neglect the dynamic behavior of the engine and of the alternator: their characteristics can be represented by static maps;
- The control strategy guarantees that the drivability of the vehicle remains unaffected, therefore at each time instant the drive train power, as well as the mechanical speed, the gear number and the power request from the electric loads are known;
- The voltage on the electrical bus is constant;
- The battery losses are not depending on the temperature and on the level of the energy stored in the battery.

According to the previous assumptions, the modeling of each component reported in Fig. 4.1, can be formulated.

4.2.2 Engine model

The fuel consumption is denoted $f(P_m, \omega)$ and is related to the engine power (P_m) and to the engine speed (ω) by a nonlinear, memoryless function f (static map). The equation (4.1) gives a polynomial approximation of this relationship:

$$f(P_m, \omega) = a(\omega)P_m^2 + b(\omega)P_m + c(\omega) \quad (4.1)$$

where a , b and c are coefficients depending of the engine speed.

Fig. 4.2 shows the fuel map of a fixed spark ignition engine as function of engine mechanical power, for different engine speeds.

The CO₂ and CO maps of an SI engine are shown in Fig. 4.3, while Fig. 4.4 shows the maps of HC and NO_x.

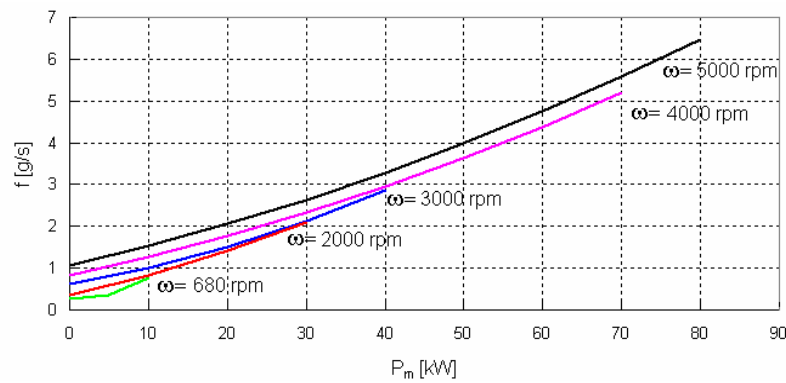


Fig. 4.2: fuel map of a 100kW spark ignition engine, for various engine speeds.

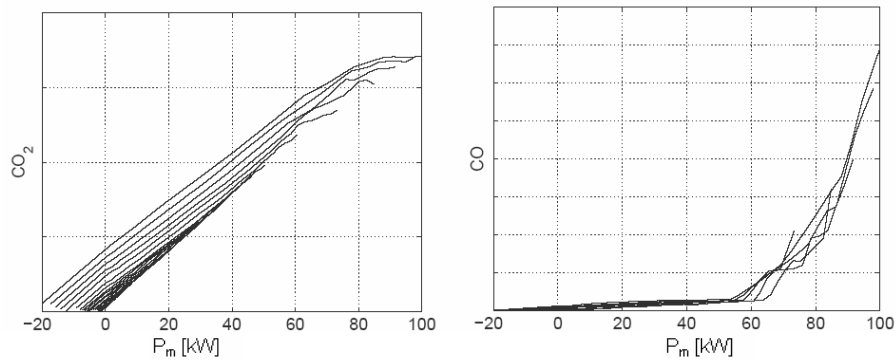


Fig. 4.3: CO₂ and CO map of a 100kW spark ignition engine, for various engine speeds.

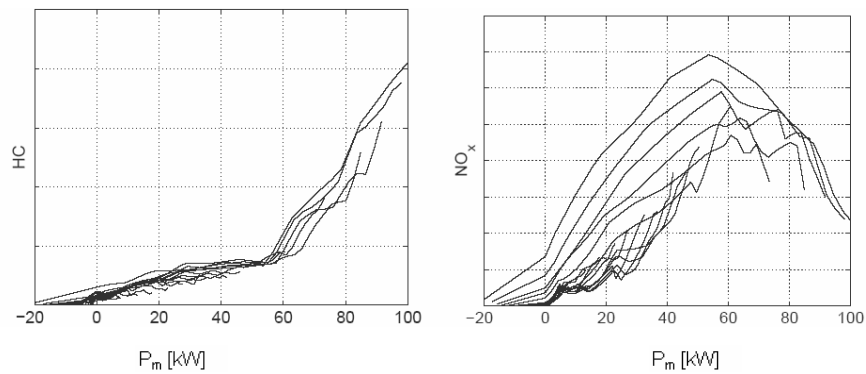


Fig. 4.4: HC and NO_x map of a 100kW spark ignition engine, for various engine speeds.

4.2.3 Power train model

The power P_m given from the engine is divided in a part needed for the propulsion and in a part needed for the electric loads. The part P_d needed for propulsion is related to vehicle velocity v , acceleration \dot{v} and road slop h as in equation (4.2):

$$P_d(t) = f_d[v(t), \dot{v}(t), h(t)] \quad (4.2)$$

The function f_d includes aerodynamic and rolling losses, acceleration power and the power related to changing the vehicle's altitude. This relationship is typically expressed as follows:

$$f_d(v, \dot{v}, h) = \left[m\dot{v} + \frac{1}{2} \rho C_d A v^2 + mg \left(C_r + \frac{\dot{v}}{g} + \frac{h}{100} \right) \right] v \quad (4.3)$$

where:

- m – Vehicle mass [kg];
- A_d – Vehicle frontal area [m²];
- C_d – Air drag coefficient;
- C_r – Rolling resistance;
- ρ – Air density [kg/m³];
- g – Gravity [m/s²].

For a given speed profile and selected gears, the engine speed is related to the vehicle speed by means of the following relation:

$$\omega(t) = \frac{F_r}{R} G_r(t) v(t) \quad (4.4)$$

where:

- R – wheel radius [m];
- G_r – gear ratio;

- F_r – Final drive ratio.

4.2.4 Alternator model

Alternators as used in vehicles are equipped with a voltage regulator that tries to maintain a constant power bus voltage. The alternator considered in this application is equipped with a voltage regulator of which the voltage set-point can be adjusted, thereby also affecting the resulting current to the battery and the loads. An outer control loop is applied that controls the delivered electric power by measuring the current and manipulating the voltage.

Because of the adopted sampling time, the alternator modeling reduces, as the engine model, to a static nonlinear map. This function relates the mechanical power in input P_g to the alternator with the electric power P_e in output from the alternator. It represents the inverse function of the efficiency of the alternator for different engine speed:

$$P_g(t) = f_g(P_e, \omega) \quad (4.5)$$

The measured map of a 42 V 5 kW alternator is shown for various engine speeds in Fig. 4.5.

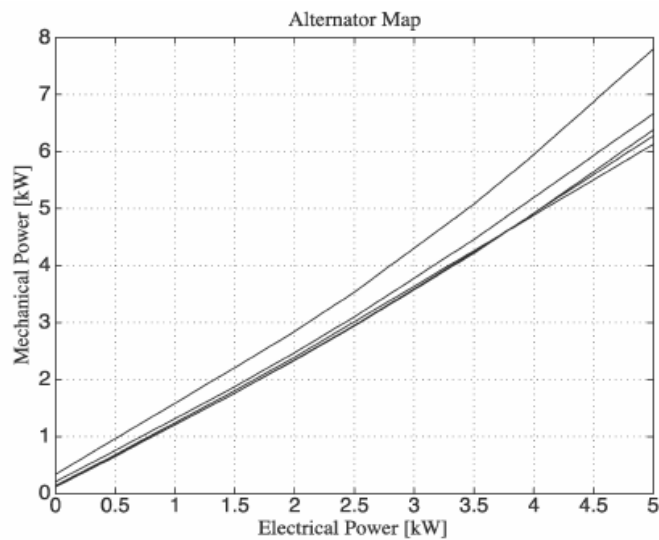


Fig. 4.5: static model of a 42V 5kW alternator.

The alternator can be approximated by a linear relation between electrical power P_e and mechanical power P_g with a constant slope k_g :

$$P_g = k_0(\omega) + k_g P_e(\omega) \quad (4.6)$$

where the term $k_0(\omega)$ is caused by mechanical friction and increases with the speed.

4.2.5 Battery model

Battery is an electrochemical energy source whose output voltage is almost constant during its discharge and therefore it is often modeling using ideal voltage source. In the following, battery behaviour will be represented by means of an equivalent electrical model, in which the battery has been considered as a voltage source controlled by current and state of charge (S.O.C.), with one resistance in series R_b . In particular, the voltage is given by a polynomial expression of current and state of charge [80]. It has to be taken into account that coefficients for charge and discharge operations are different.

It can be written as:

$$V_b = \sum_{k=1}^4 Q^{k-1} \sum_{h=1}^2 a_{hk} i_b^{h-1} \quad (4.7)$$

$$R_b = \sum_{h=1}^2 b_h Q^h \quad (4.8)$$

where V_b , i_b and Q are respectively the battery voltage, current and S.O.C.; a_{ij} are the coefficients of two 2×4 matrixes, one for charge and one for discharge operations; these are dependent on the type of the used battery.

The power P_b in input or in output from the battery is the algebraic addition of the power P_s (positive or negative quantity) actually stored in the battery and the battery losses P_{loss} that are function of P_s (according with the assumptions in paragraph

4.2.1), and are positive for both charging and discharging conditions:

$$P_b = P_s + P_{loss}(P_s) \quad (4.9)$$

where:

$$P_{loss} = \beta P_s^2, \text{ with } \beta = \frac{R_b}{E_b^2} \quad (4.10)$$

The battery energy level E_s is given by:

$$E_s(t) = E_s(0) + \int_0^t P_s(\tau) d\tau \quad (4.11)$$

The state of charge is defined as:

$$Q(t) = \frac{E_s(t)}{E_{cap}} \quad (4.12)$$

where E_{cap} is the energy capacity of the battery.

4.2.6 Schematic of the power bus

Fig. 4.6 shows a schematic of a dual-voltage concentrated power bus architecture, adopted for the simulations.

The power bus is comprehensive of a main dc-dc converter that realizes two subsystems at different voltage levels (14 V and 42 V), some 14 V electric loads connected to the 14 V bus, and some 42 V loads connected to the 42 V bus, with some of them (electromechanical loads) fed with local 42 V/14 V converters.

The power bus adopted for the conventional vehicle comprises two batteries, at 36 V for the 42 V bus and 12 V for the 14 V bus.

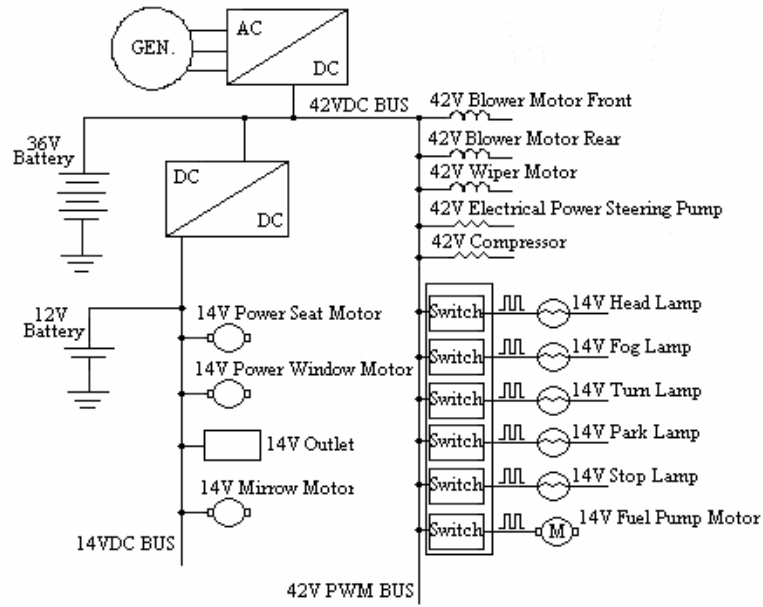


Fig. 4.6: dual-voltage concentrated power bus architecture.

4.3 Analytic formulation of the proposed optimal control strategy

The target of the proposed control strategy is to minimize the fuel consumption and the exhaust emissions unaffacting the drivability of the vehicle. This can be achieved shifting the ICE operating point versus regions with maximum efficiency. Nevertheless, in order to unaffacting the drivability of the vehicle, only the alternator power P_e can be controlled. The alternator is coupled to the engine therefore, controlling its output power, the operating power of the combustion engine will be influenced. The power in output of the alternator can be regulated only if the power required from the electric loads is given from the contribution of the energy stored in the battery. Such control action implicates that the power P_b is not used, as in a conventional vehicle, only to supply key-off loads and to assist the alternator against peak-power demands, but is instead used with the alternator's power P_e to satisfy the requests of the electric loads. The power P_b flows in output or in input of the battery depending on the necessity of the control strategy to shift the engine operating point versus regions with maximum efficiency. To yield a positive effect on the total fuel consumption the energy losses in the battery must be smaller than the benefit obtained in the fuel saving. Obviously, the conventional alternator must be replaced with a power controlled alternator [28].

Indicating with T_f the length of the considered drive cycle, the total fuel consumption is given by:

$$F = \int_0^{T_f} f(\tau) d\tau \quad (4.13)$$

The goal of the control strategy is to minimize the total fuel F . Because the range of the different quantities involved in the power diagram are limited by physics constraints or by engineering reasons, the control strategy can be formulated as a nonlinear optimization problem subject to constraints. In particular the following inequality constraints must be imposed:

$$\begin{aligned} P_{m,min} &\leq P_m \leq P_{m,max} \\ P_{e,min} &\leq P_e \leq P_{e,max} \\ P_{b,min} &\leq P_b \leq P_{b,max} \end{aligned} \quad (4.14)$$

The battery is constrained to have the same amount of energy at the start of the drive cycle and at the end:

$$E_s(T_f) = E_s(0) \quad (4.15)$$

Indicating with T_s the sampling time of the control strategy and indicating with k the k -th sampling time, the modeling of the vehicle, in discrete time, is given by the following equations (the generic quantity $f(k) \equiv f(kT_s)$):

$$\begin{aligned} P_e(k) &= P_b(k) + P_L(k) \\ P_g(k) &= g(P_e(k), \omega(k)) \\ P_d(k) &= f_d(v(k), \dot{v}(k), h(k)) \\ P_m(k) &= P_d(k) + P_g(k) \\ f_r(k) &= f_r(P_m(k), \omega(k)) \\ \omega(k) &= \frac{F_r}{R} G_r(k) v(k) \end{aligned} \quad (4.16)$$

By means of these equations, considering the basic assumptions and the equations (4.7)-(4.12), the fuel rate can be expressed, for a fixed k -step, as a function of the battery storage power only:

$$f_r(P_m, \omega) = f(P_d, P_L, P_s, \omega) = f(P_s) \quad (4.17)$$

with P_L , P_d assigned for every k , and the constraints (4.14) can be translated to constraint on P_s only:

$$P_{s, \min}(k) \leq P_s(k) \leq P_{s, \max}(k) \quad (4.18)$$

In this way, the optimization problem statement is expressed with the following equations (N is integer and is the ratio between the length of the drive cycle T_f and the sampling time T_s):

$$\min_{\substack{P_s(k) \\ k=1, \dots, N}} J = \min_{\substack{P_s(k) \\ k=1, \dots, N}} \sum_{k=1}^N \gamma(P_s(k)) = \min_{\substack{P_s(k) \\ k=1, \dots, N}} \sum_{k=1}^N \left[\omega_1 f_r(P_s(k)) + \sum_i \omega_i \text{emiss}_i(P_s(k)) \right] \quad (4.19)$$

subject to:

$$f_r(k) = \varphi_2^2(k) P_s^2(k) + \varphi_1(k) P_s(k) + \varphi_0(k) \quad (4.20)$$

$$P_{s, \min}(k) \leq P_s(k) \leq P_{s, \max}(k) \quad (4.21)$$

$$\Delta SOC = 0 \Leftrightarrow \sum_{k=1}^N P_s(k) = 0 \quad (4.22)$$

$$P_{s, \min}(k) \geq -P_L(k) - P_{\text{loss}}(k) \quad (4.23)$$

where φ_1 , φ_2 , φ_3 are functions resulting from the equations (4.16) and from the

approximation:

$$f_r(\omega, P_m) = a(\omega)P_m^2 + b(\omega)P_m + c(\omega)$$

ω_i are weight factors of the cost function J . $P_{s,max}$ represents the maximum power that the battery can absorb in charging mode; $|P_{s,min}|$ represents the maximum power that the battery can provide in discharging mode and is limited by the alternator constraint $P \geq 0$.

From now to the end of this chapter, the term of the emissions has been suppressed, for reducing the order of the analytical problem, but the method is easily extendable if emissions are considered for the minimization.

The problem is now formulated as a finite dimensional nonlinear optimization problem. Because every function involved in the problem is convex functions, the formulated problem is a nonlinear convex problem with inequality and equality constraints [87].

The solution of this problem is given from the Kuhn-Tucker (KT) conditions (KKT) [87]: consider the problem of minimizing a function $f(\mathbf{x})$ subjected to m equality constraints $\mathbf{a}(\mathbf{x}) = \mathbf{b}$, and p inequality constraints $\mathbf{c}(\mathbf{x}) \leq \mathbf{d}$ ($\mathbf{a}(\mathbf{x})$ and \mathbf{b} are vectors of m components, and $\mathbf{c}(\mathbf{x})$ and \mathbf{d} are vectors of p components). If \mathbf{x}_0 is a local minimum for the constrained problem and if it is a regular point, there is a vector $\boldsymbol{\lambda}$ with p components and a vector $\boldsymbol{\mu}$, with m components, such that:

$$\nabla_x L(\mathbf{x}_0, \boldsymbol{\lambda}, \boldsymbol{\mu}) = 0 \quad (4.24)$$

$$\boldsymbol{\lambda}^T (\mathbf{c}(\mathbf{x}_0) - \mathbf{d}) = 0 \quad (4.25)$$

$$\mathbf{c}(\mathbf{x}_0) \leq \mathbf{d} \quad (4.26)$$

$$\mathbf{a}(\mathbf{x}_0) = \mathbf{b} \quad (4.27)$$

$$\boldsymbol{\lambda} \geq \mathbf{0} \quad (4.28)$$

where:

$$L(\mathbf{x}, \boldsymbol{\lambda}, \boldsymbol{\mu}) = f(\mathbf{x}) + \boldsymbol{\lambda}^T (\mathbf{c}(\mathbf{x}) - \mathbf{d}) + \boldsymbol{\mu}^T (\mathbf{a}(\mathbf{x}) - \mathbf{b}) \quad (4.29)$$

is the Lagrange function and ∇ is the linear operator nabla.

The eqs. (4.24)-(4.28) are also sufficient if the problem is convex. In our case we have:

$$\begin{cases} \min_{\substack{P_s(k) \\ k=1, \dots, N}} \sum_{k=1}^N f_r(P_s(k)) \\ P_s(k) - P_{s,\min}(k) \leq 0 \quad \forall k \in [1, N] \\ -P_s(k) + P_{s,\max}(k) \leq 0 \quad \forall k \in [1, N] \\ \sum_{k=1}^N P_s(k) = 0 \end{cases} \quad (4.30)$$

with:

$$\mathbf{x} = [P_s(1) \cdots P_s(k) \cdots P_s(N)]_{1 \times N} \quad (4.31)$$

$\boldsymbol{\lambda}$ is a vector of $2N \times 1$ components, $\boldsymbol{\mu}$ and \mathbf{b} in our case are scalar.

The Lagrange function is:

$$\begin{aligned} L(P_s, \boldsymbol{\lambda}, \boldsymbol{\mu}) = & \sum_{k=1}^N f_r(P_s(k)) + \\ & \boldsymbol{\mu} \left(\sum_{k=1}^N P_s(k) \right) + \sum_{k=1}^N \lambda_k (P_s(k) - P_{s,\max}(k)) - \sum_{k=1}^N \lambda_{T_c+k} (P_s(k) - P_{s,\min}(k)) \end{aligned} \quad (4.32)$$

Condition (4.24) becomes:

$$\frac{\partial f(P_s(k))}{\partial P_s(k)} + \mu + \lambda_k - \lambda_{N+k} = 0 \quad \forall k \in [1, N] \quad (4.33)$$

Condition (4.25) becomes:

$$\begin{cases} \lambda_k [P_s(k) - P_{s,max}(k)] = 0 \\ \lambda_{N+k} [P_s(k) - P_{s,min}(k)] = 0 \end{cases} \quad \forall k \in [1, N] \quad (4.34)$$

Now the problem is to solve numerically the system of equations (4.21), (4.22), (4.33), (4.34).

The solution of the KT equations forms the basis for many nonlinear programming algorithms [88]. These algorithms attempt to compute the Lagrange multipliers directly. These methods are commonly referred to as Sequential Quadratic Programming (SQP) methods, since a QP subproblem is solved at each major iteration. In particular, for the simulations, the Schittkowski method has been adopted [89]. The method allows to closely mimic Newton's method for constrained optimization just as is done for unconstrained optimization. At each major iteration, an approximation is made of the Hessian of the Lagrangian function using a quasi-Newton updating method. This is then used to generate a QP subproblem whose solution is used to form a search direction for a line search procedure [90].

4.4 Case-study: an application to a real vehicle

In order to test the suggested control strategy, several simulations have been developed. The parameters of the considered vehicle are reported in Tab. 4.1 [28].

The considered vehicle is equipped with a 100 kW engine, a manual transmission with five gears, a 36 V lead-acid main battery and a 12 V lead-acid battery, a 42 V 5 kW alternator. The main battery has an energy capacity of 4×10^6 J and operates around 70 % of SOC.

Symbol	Quantity	Value	Unit
m	Vehicle mass	1400	kg
A	Vehicle frontal area	2	m ²
C_d	Air drag coefficient	0.3	
C_r	Rolling resistance	0.015	
ρ	Air density	1.2	kg/m ³
g	Gravity	9.81	m/s ²
R	Vehicle wheel radius	0.3	m
F_r	Final drive ratio	4.0	
G_r	Gear ratio	[3.4-2.1-1.4-1.0-0.77]	
V_b	Main battery voltage	36	V
C_b	Battery capacity	30	Ah
$S.O.C._0$	Battery initial S.O.C.	70%	
$P_{m,n}$	ICE nominal power	100	kW

Table 4.1: vehicle main attributes.

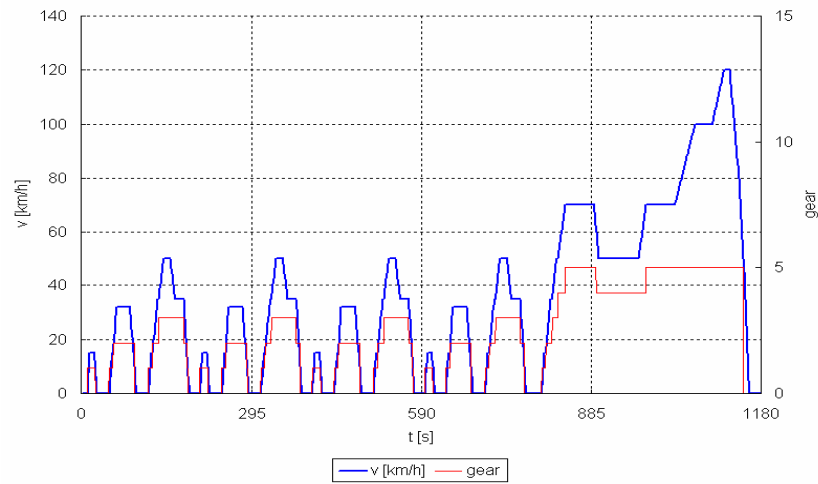


Fig. 4.7: New European drive cycle (NEDC).

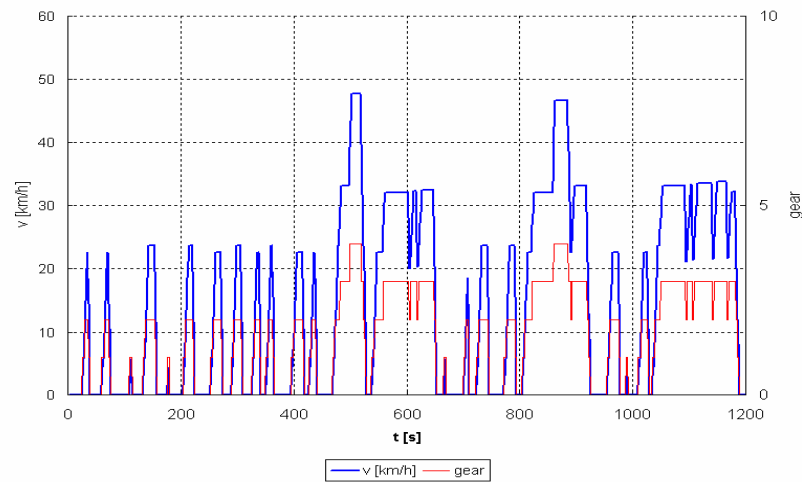


Fig. 4.8: critical drive cycle.

Two different drive cycles have been adopted for the simulations.

Fig. 4.7 shows the new European driving cycle (NEDC) [91], Fig. 4.8 shows a drive cycle critical for the generation system. This drive cycle has been computed with the software *Evaluator* (see chapter 3) [82].

Fig. 4.9 shows the electrical loads power profile, adopted for both the drive cycle. Also this profile has been computed with *Evaluator*. It is critical for the generation system and for the power bus.

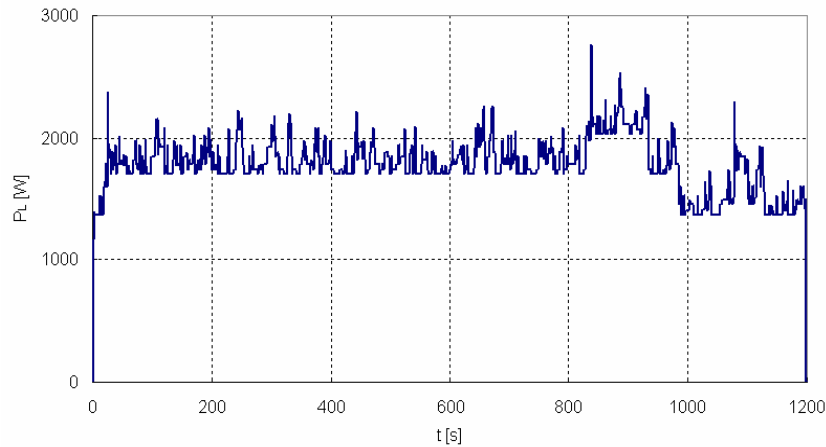


Fig. 4.9: Critical electrical loads power profile used for both drive cycles.

The considered engine fuel consumption map and the alternator map are those reported in Figs. 4.2 and 4.5.

4.4.1 Simulations and results

Figs. 4.10-4.13 show respectively the drive train power and the battery storage power, the SOC and the fuel rate, resulting from the optimization strategy, when the drive cycle reported in Fig. 4.7 is considered (NEDC).

Figs. 4.14-4.17 show respectively the drive train power and the battery storage power, the SOC and the fuel rate, resulting from the optimization strategy, when the drive cycle reported in Fig. 4.8 is considered (critical drive cycle).

As can be noted from the Figs. 4.12 and 4.16, the variation of the SOC between the start and the end of the cycle is zero, according to the constraint (4.22). The power stored in the battery, according to the eq. (4.21) is always less than of the limits $P_{s, min}$ and $P_{s, max}$, (Figs. 4.11 and 4.15).

Figs. 4.18-4.19 show respectively the SOC and the fuel rate when the critical drive cycle and the electrical loads power profile reported in Fig. 4.9 are considered. They are related to a strategy of energy management traditionally adopted in vehicles. As can be noted, in this case the SOC starting from the value of 70%, reaches the value of 47% at end of cycle. The invariance of the SOC therefore has not been guaranteed.

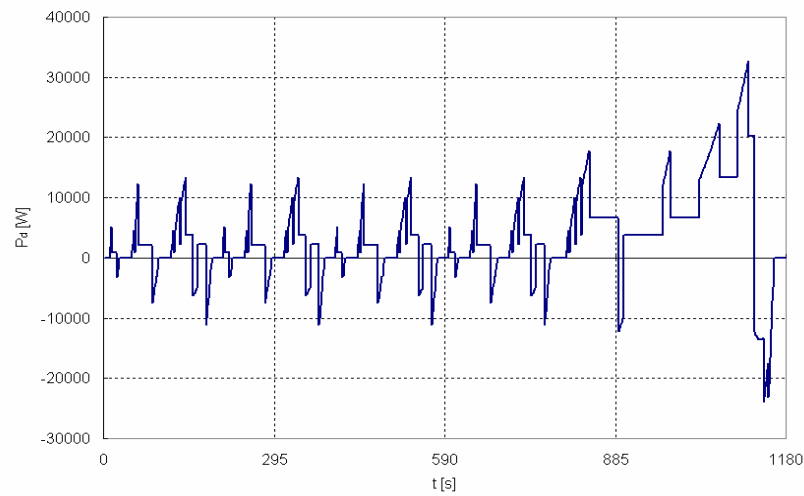


Fig. 4.10: Drive train power profile for NEDC.

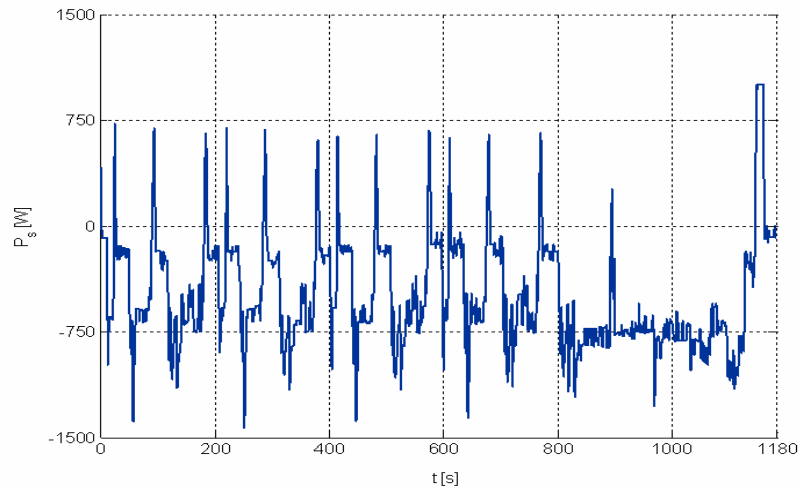


Fig. 4.11: Battery storage power profile for NEDC, resulting from the proposed optimization strategy.

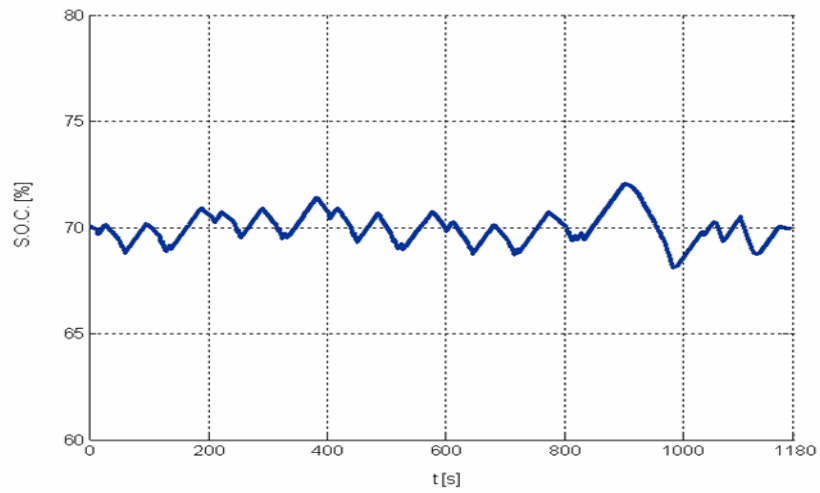


Fig. 4.12: Battery S.O.C. profile for NEDC, resulting from the proposed optimization strategy.

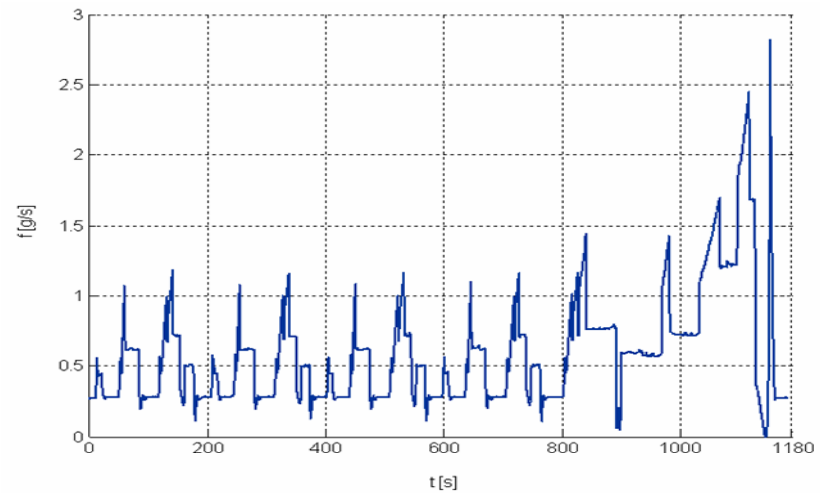


Fig. 4.13: Fuel rate profile for NEDC, resulting from the proposed optimization strategy.

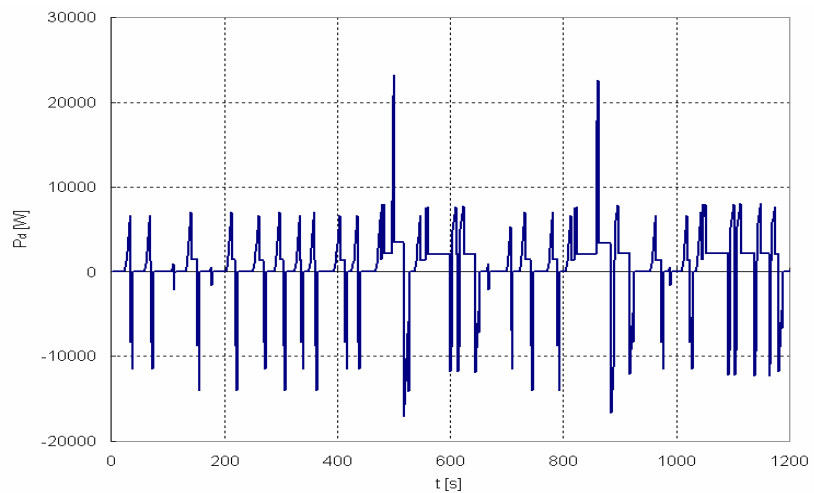


Fig. 4.14: Drive train power profile for critical drive train.

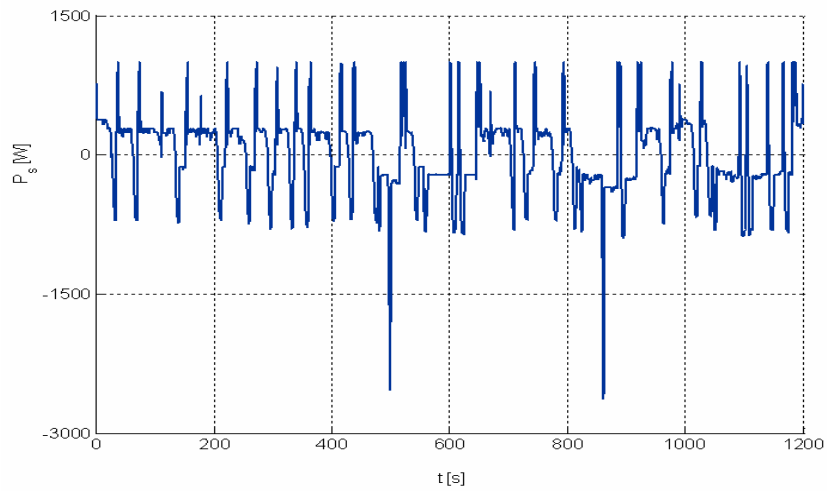


Fig. 4.15: Battery storage power profile for critical drive cycle, resulting from the proposed optimization strategy.

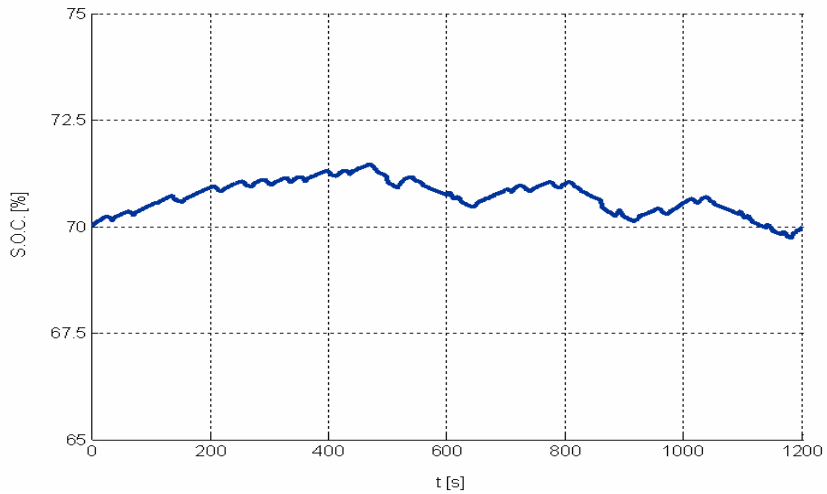


Fig. 4.16: Battery S.O.C. profile for critical drive cycle, resulting from the proposed optimization strategy.

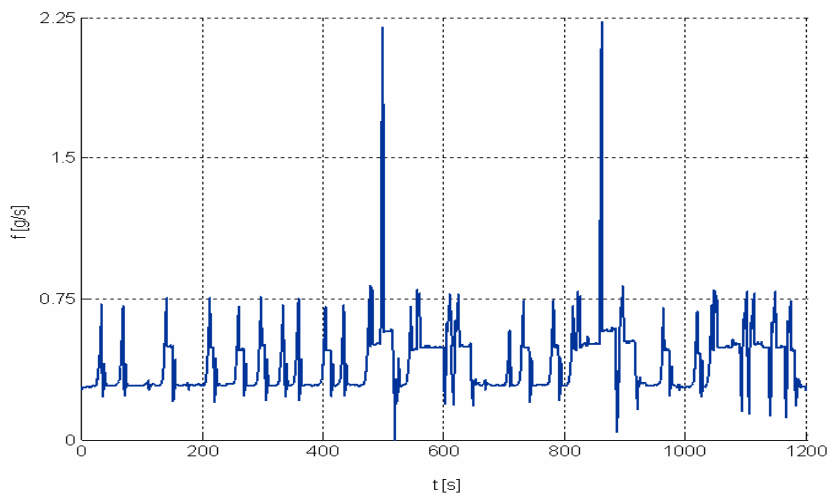


Fig. 4.17: Fuel rate profile for critical drive cycle, resulting from the proposed optimization strategy.

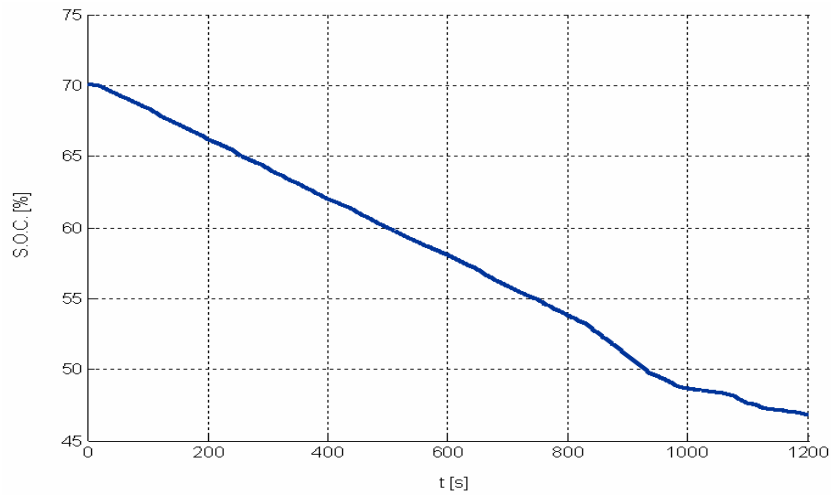


Fig. 4.18: Battery S.O.C. profile for critical drive cycle, resulting from the conventional strategy.

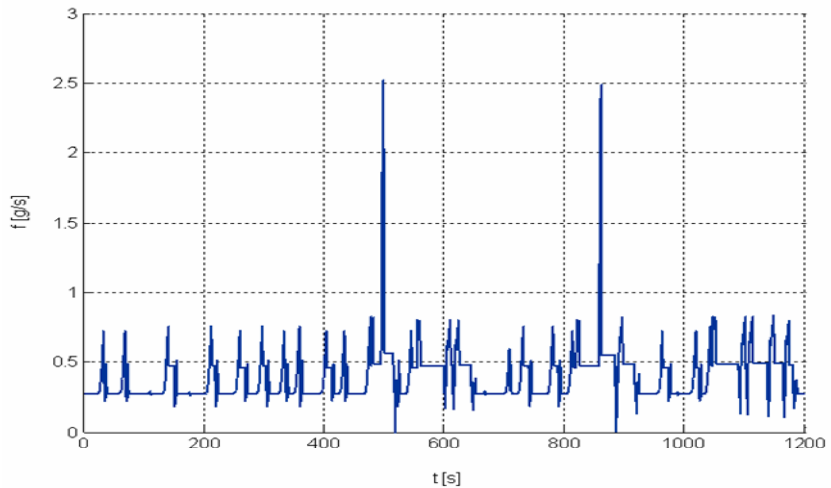


Fig. 4.19: Fuel rate profile for critical drive cycle, resulting from the conventional strategy.

Respect to the conventional strategy the fuel reduction have been computed. When NEDC drive cycle has been adopted, the proposed strategy provides a fuel reduction of 2.06 %, whereas a reduction of 1.46 % has been obtained with the proposed strategy when the critical drive cycle has been adopted [28].

The same logic of the proposed strategy for conventional vehicles has been extended to hybrid vehicles.

5. The proposed energy management strategy for hybrid power-split vehicles

5.1 Introduction

As depicted in chapter 2, the aim of any energy management strategy for a parallel hybrid electric vehicle, as for a power-split architecture, is to split the power for the propulsion between the thermal and electric path, redistributing power through the battery and the generator, in order to reduce the fuel consumption and the engine emissions, unaffected the drivability of the vehicle and the on-board electrical loads supplies and keeping as constant as possible the SOC of the battery.

To achieve these targets, several approaches have been investigated in the last years, as reported in paragraph 2.3.6.

However, many of these techniques have not been tested on commercial vehicles. Their results are obtained on theoretical architectures of hybrid vehicles (series, parallel, parallel-series) or prototype realizations. To outperform these algorithms, a particular approach based on the optimal control theory is proposed in this thesis and a concrete case-study, with relative solution, has been reported for a validation of the strategy.

Specifically, the Toyota Prius NHW10 model (1997) has been considered for the simulations and the related data given from the manufacturer and present in literature have been adopted.

The proposed control algorithm is able to split the power for the propulsion between the thermal and electric path, redistributing power of the battery and the generator, in order to reduce the fuel consumption and the engine emissions, unaffacting the drivability of the vehicle, the comfort of the driver and the on-board electrical loads supplies, keeping as constant as possible the SOC of the battery.

This target can be achieved shifting the operating points of engine, electric motor, generator and battery versus regions with the maximum efficiency, realizing an optimal power split between thermal and electric path for the drive train.

Nevertheless, in order to unaffacting the drivability of the vehicle, both the generator power and the electric motor power must be adequately controlled, since the electric motor and the generator are coupled to the engine.

The battery can be recharged even by means of re-generative braking; this is possible by controlling the electric motor as a generator during the braking mode.

The problem of off-line optimization of fuel consumption and pollutant emissions has been formulated as a nonlinear convex optimization problem. It has been theoretically formulated directly for the case-study of Toyota Prius and the numerical solution has been computed, as for conventional vehicles, adopting the Sequential Quadratic Programming (SQP) theory and the Schittkowski method.

5.2 Energetic model of the vehicle

5.2.1 The considered hybrid architecture

There are several hybrid vehicle architectures that could be considered for the application of the proposed optimization strategy. In the next, the Toyota[®] Prius NHW10 model (1997) will be considered; it is a full-hybrid vehicle with a Continuously Variable Transmission (CVT) device.

The proposed method can be easily extended to other hybrid architectures.

The Prius NHW10 model (Fig. 5.1) is a full hybrid vehicle, also known as Hybrid Synergy Drive [26].



Fig. 5.1: The NHW10 model of TOYOTA PRIUS (1997)

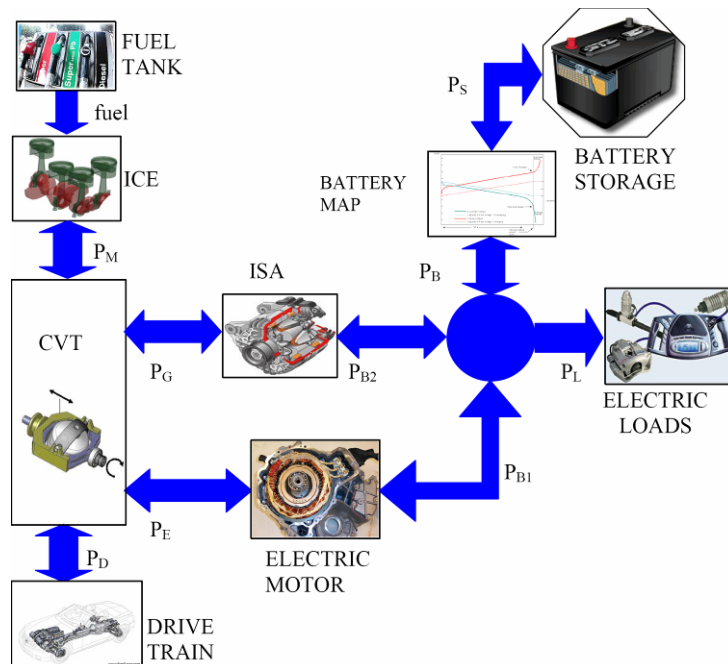


Fig. 5.2: Power flow diagram of a power-split hybrid vehicle [92].

The Prius incorporates the following [26], [93]:

1. The ICE uses the more efficient Atkinson cycle instead of the more common Otto cycle; it provides 43 kW (58 hp) @ 4000 rpm and 102 Nm @ 4000 rpm;
2. An electric motor (500 V PM brushless), providing 30 kW (40 hp) @ 940 rpm and 305 Nm torque @ zero speed;
3. An electric generator (500 V PM brushless) which provides 15 kW @ 6000 rpm;
4. An IGBT inverter controlled by a 32-bit microprocessor, which efficiently converts power between the batteries and the motor/generators;

5. The regenerative braking, a process for recovering the kinetic energy when braking or traveling down a slope and storing it as the electrical energy in the traction battery for later use while reducing the wear and the tear on the brake pads;
6. The sealed 240-cell nickel metal hydride (NiMH) battery providing 288 volts, 6 Ah/cell, 6.2 MJ rated capacity, 25 kW max. output power;
7. The CVT — the Prius does not use a typical CVT; Toyota calls it the Power Split Device. The electric machines and gasoline engine are connected to a planetary gear set which is always engaged, and there is no shifting.

5.2.2 Basic assumptions

The following assumptions are made (they are almost the same introduced for the conventional vehicles application):

- The drive cycle is known;
- The sampling interval of the control strategy is sufficiently large (1 s or larger) so that to neglect the dynamic behavior of the engine, of the electric motor and of the generator: their characteristics can be represented by static models;
- The control strategy guarantees that the drivability of the vehicle remains unaffected, therefore at each time instant the drive train power, as well as the vehicle speed, are known;
- The power required from the electric loads is assigned;
- The voltage on the electrical bus is constant;
- The battery losses don't depend on the temperature.

Fig. 5.2 shows a power flow diagram of the vehicle.

According to the previous assumptions, the modeling of each effective component of the considered Toyota Prius (see Fig. 5.2) has been formulated as reported in the following. The data used for modelling the components of the vehicle are available in [94], [95].

5.2.3 Engine model

Fig. 5.3 shows a view of the Toyota Prius ICE. It implements an Atkinson's cycle. For this component, a static model of the fuel consumptions and the pollutant emissions has been adopted.

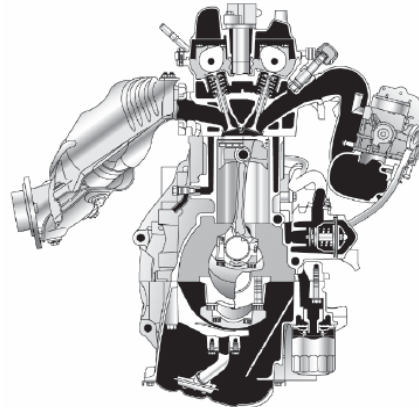


Fig. 5.3: The Toyota Prius internal combustion engine (with Atkinson's cycle).

Fuel consumption model.

It is assumed that the fuel rate consumption $\dot{m}_f(P_M, n)$ depends on the engine power (P_M) and the engine speed (n) by means of a nonlinear, memoryless function (static map). Fig. 5.4 shows the fuel map of the 1.5L Prius engine with Atkinson cycle, as a function of the engine mechanical power, for different engine speeds.

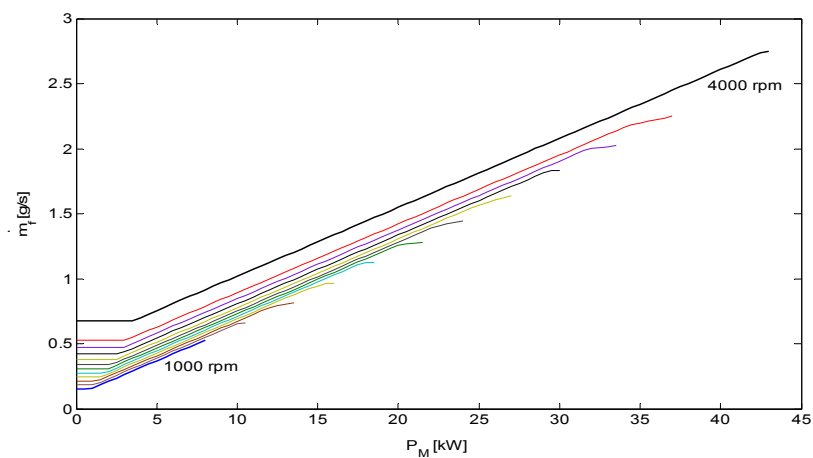
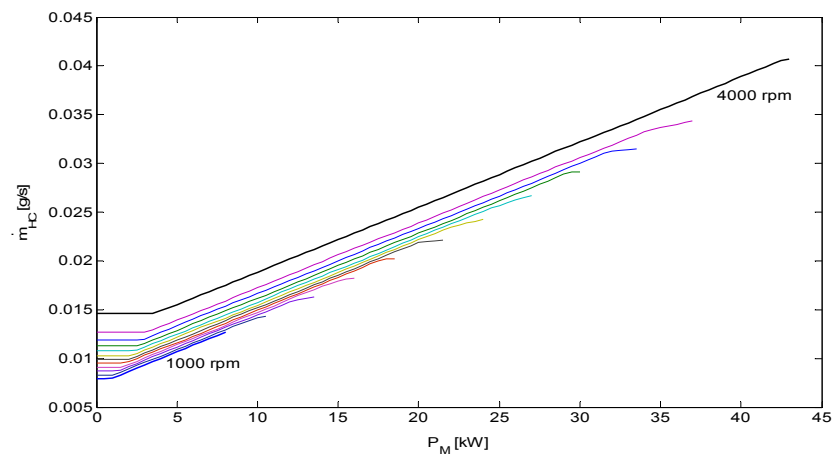


Fig. 5.4: Fuel map of a 1.5L Toyota Prius engine (Atkinson's cycle).

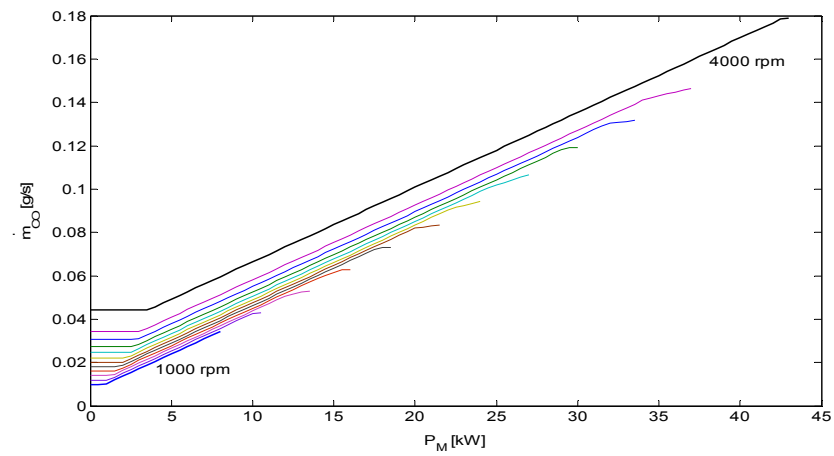
Emissions model.

The pollutant emissions rate (HC, CO, NO_x) are denoted with $\dot{m}_{HC}(P_M, n)$, $\dot{m}_{CO}(P_M, n)$ and $\dot{m}_{NO_x}(P_M, n)$ and, as the fuel rate, depend on the engine power (P_M) and the engine speed (n) by means of a nonlinear, memoryless function (static map).

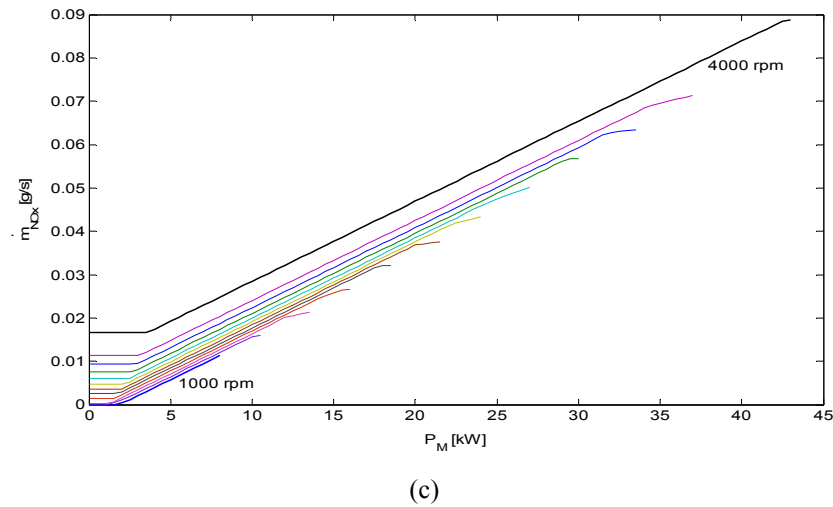
Figs. 5.5 show the emissions maps of the 1.5L Prius engine, as a function of the engine mechanical power, for different engine speeds.



(a)



(b)



Figs. 5.5: Emissions maps of a 1.5L Prius (Atkinson cycle) engine:
 (a) HC rate map, (b) CO rate map, (c) NO_x rate map.

5.2.4 Electric motor model

The electric propulsion motor of the considered Toyota Prius (NHW10 model), derived from results of the research of Toyota in the electric vehicles field, is a 500 V PM brushless motor, 8 poles, providing 30 kW at 940 rpm and 305 Nm torque at zero speed (Fig. 5.6); its permanent magnets are Neodymium type and the efficiency is very high at low speed and high torque.

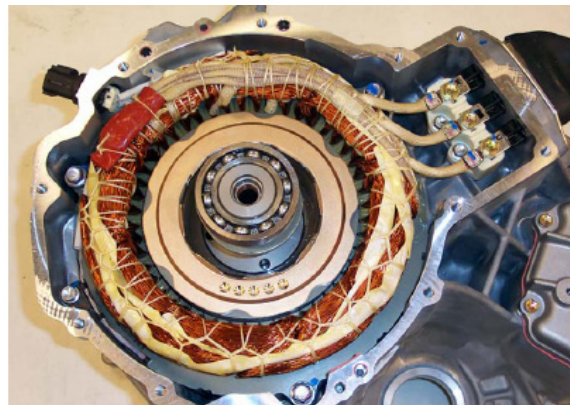


Fig. 5.6: The Toyota Prius brushless motor.

It has been hypothesized that the efficiency of the electric motor is related to the electric power (P_{Bl}) and to the motor speed (n_e) by a nonlinear, memoryless function (static map):

$$\begin{cases} \eta_e = f_e(P_{B1}, n_e) \\ P_E = P_{B1} \eta_e^{\text{sign}(P_{B1})} \end{cases} \quad (5.1)$$

Fig. 5.7 shows the efficiency map of the brushless motor, as a function of the input electric power and of the motor speed.

Fig. 5.8 shows the maximum mechanical power and the torque developed by the electric motor, over the whole range of speed.

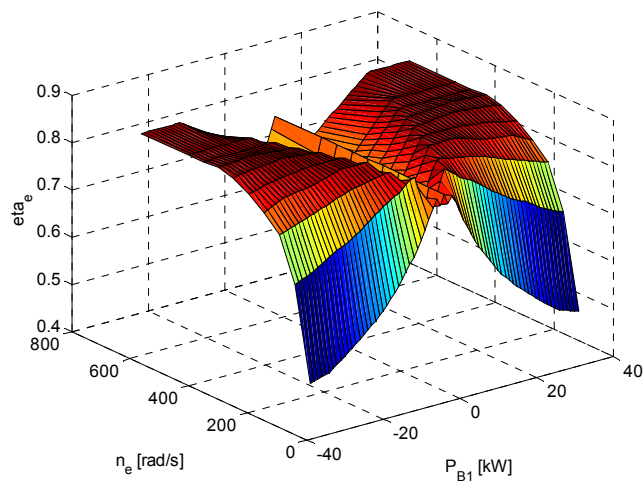


Fig. 5.7: The two-quadrant efficiency map of the electric motor.

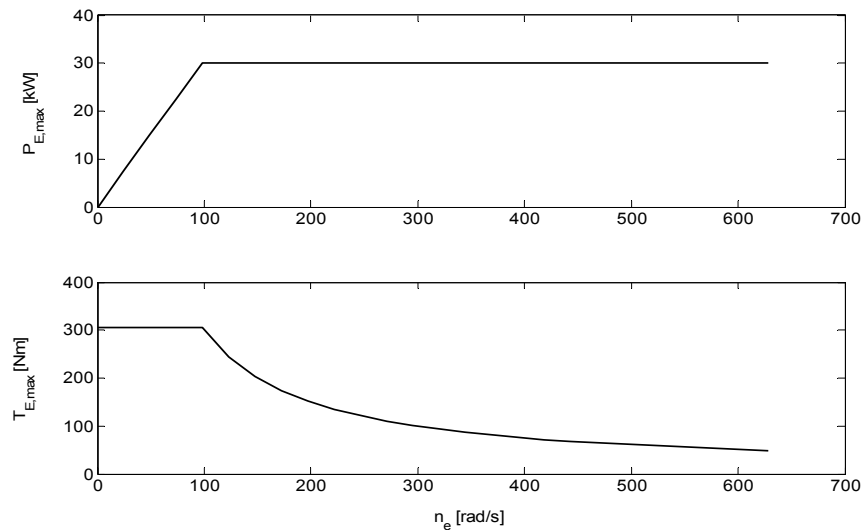


Fig. 5.8: Maximum mechanical power and torque of the electric motor.

5.2.5 Power train model

As similarly obtained in chapter 4, the power P_M given from the engine is splitted into a part needed for the propulsion and a part that will be converted in electric power from the generator, for the electric loads and the battery recharging. The power P_D needed for propulsion is related to the vehicle velocity v , acceleration \dot{v} and road slope h as follows:

$$P_D(t) = f_d[v(t), \dot{v}(t), h(t)] \quad (5.2)$$

The function f_d includes the aerodynamic and rolling losses, the acceleration power and the power related to the changes of the vehicle's altitude. This relationship is typically expressed as follows:

$$f_d(v, \dot{v}, h) = \left[m\dot{v} + \frac{1}{2} \rho C_d A v^2 + mg \left(C_r + \frac{h}{100} \right) \right] v \quad (5.3)$$

5.2.6 CVT model

A fundamental component of the Prius transmission is an epicyclic gear defined "Power Split Device" (PSD).

This type of gear is also known as "sun-and-planets", because it consists of a number of "planet" gears surrounding a central "sun" gear. The planet gears are on shafts fixed to a "planet carrier", which revolves around the same axis like the sun. The planet gears are surrounded by and meshed with an inside-out gear called the "ring". Also this revolves around the same axis like everything else [17], [26], [96].

Fig. 5.9 shows a schematic representation of the power split device adopted in the Toyota Prius vehicle.

The Prius internal combustion engine (ICE) is connected to the planet carrier. As it rotates, the planets mesh with and tend to push both the sun gear (in the middle) and the ring gear (around the outside) in the same direction like the planet carrier. By a careful choice of the size (and hence of the number of teeth) of the sun and the ring

gears, Toyota has arranged 72% of the torque to go to the ring and 28% to go to the sun.

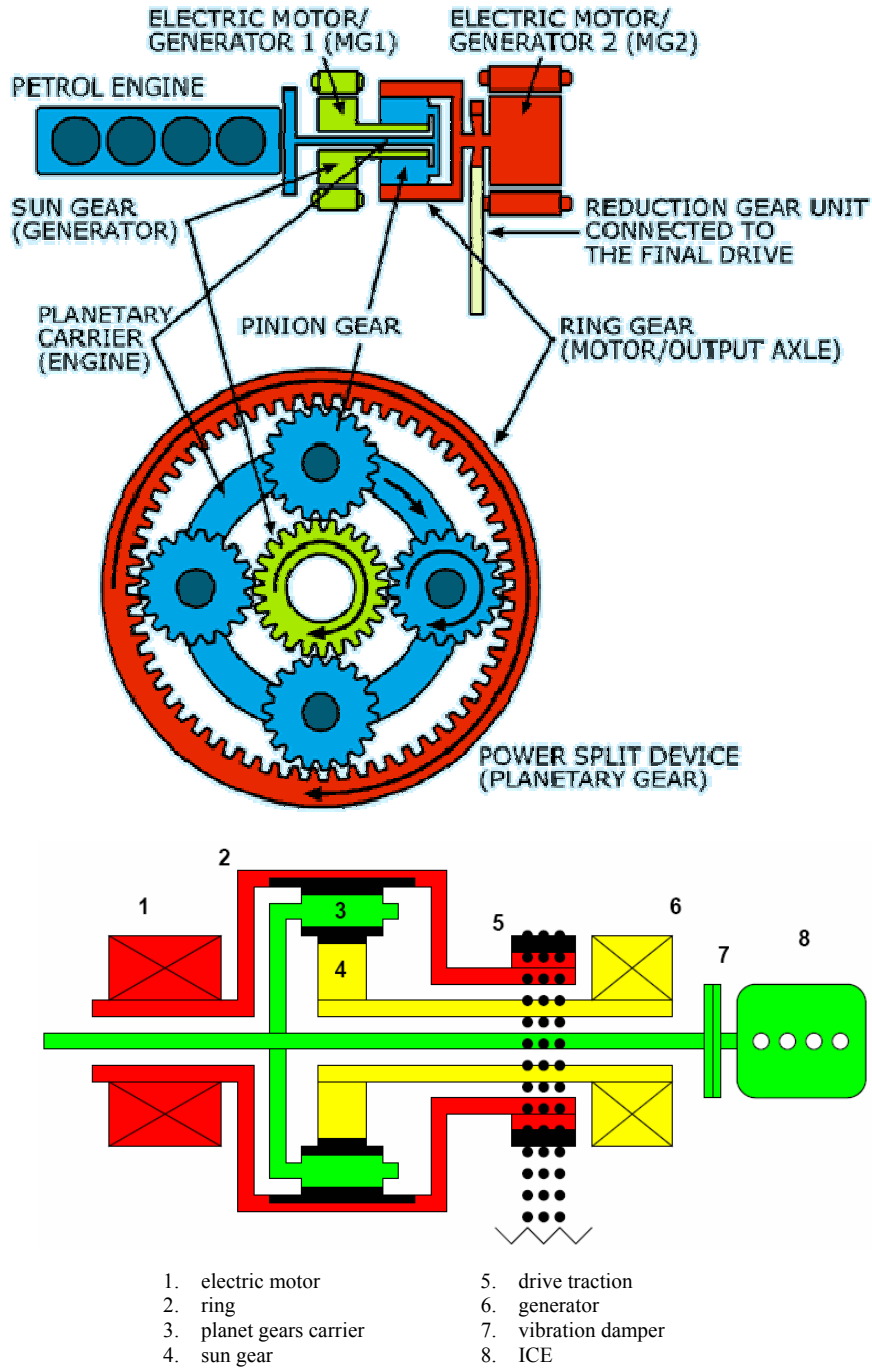


Fig. 5.9: Schematic representation of the CVT in the Toyota Prius

For a given speed profile of the vehicle, the engine speed is related to the generator speed and the electric motor speed by means of the following relation (Willis law):

$$n_g = n + \frac{1}{\tau}(n_e - n) \quad (5.4)$$

with:

$$\begin{cases} n_e = F_r n_w \\ n_w = v/R \end{cases} \quad (5.5)$$

The CVT system presents, for the kinematic relation (5-4), two degree-of-freedom. From a dynamic point of view, every torque applied to a single device of the CVT must be balanced from the other devices.

From a kinematic point of view, Fig. 5.10 shows the graphic relation among the planet gears carrier (ICE), the sun gear (ISA) and the gear (drive traction) speeds, for different operative conditions of the vehicle.

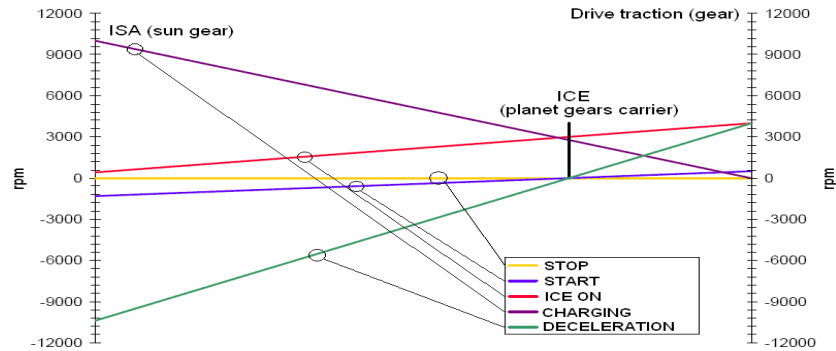


Fig. 5.10: Graphic relation among speeds in the CVT.

5.2.7 ISA model

The electric generator (ISA) of the considered Toyota Prius (NHW10 model) is a 500 V PM brushless, 8 poles, which provides 15 kW at 6000 rpm.

At the starting of the engine, the generator is controlled as a motor to drive the engine to the fitted speed for the jump starting.

Because of the adopted sampling time, also the generator modeling is reduced to a static nonlinear map. This map relates the mechanical power P_G in input to the generator with the electric power P_{B2} in output from the generator. It gives the efficiency of the generator for all the operative conditions:

$$\eta_g = f_g(P_{B2}, n_g) \quad (5.6)$$

$$P_G = \frac{P_{B2}}{\eta_g} \quad (5.7)$$

Fig. 5.11 shows the efficiency map of the brushless generator, as a function of electric power and of the generator speed.

Fig. 5.12 shows the maximum electric power and the maximum torque developed by the generator, over the whole range of speed.

Like a relationship between P_G and P_{B2} , hereafter it will be adopted the maximum efficiency curve in the operative region delimited by the maximum electric power curve (Fig. 5.12):

$$P_{B2} = f_{g, \eta_{gmax}}(n_g) \quad (5.8)$$

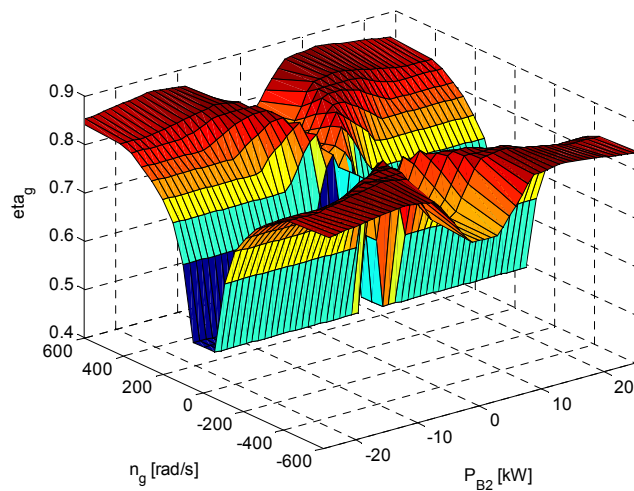


Fig. 5.11: the four-quadrant efficiency map of the generator.

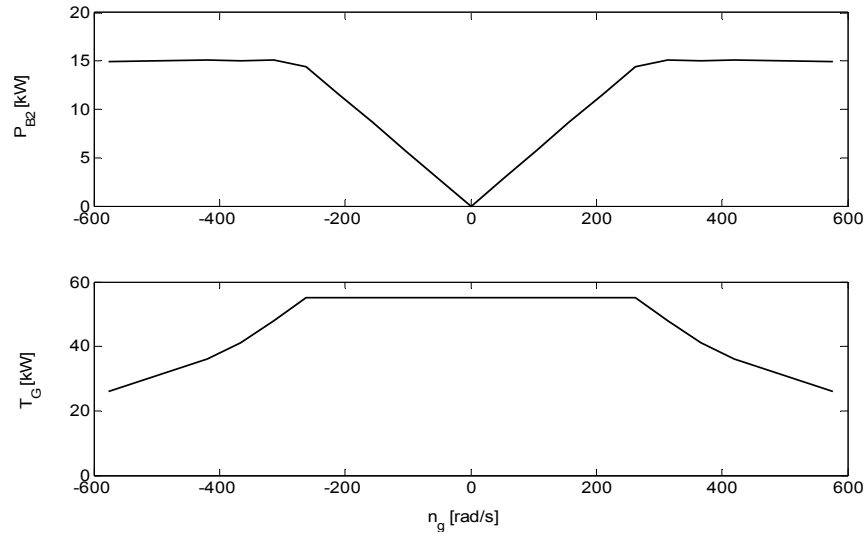


Fig. 5.12: maximum electric power and torque of the generator.

5.2.8 Battery model

The Toyota Prius battery is a sealed 240-cell nickel metal hydride (NiMH) battery providing 300 volts, 4.3 MJ capacity.

In the following, as made for lead-acid batteries (chapter 4), the battery has been considered as a voltage source U_b controlled by the output current i_b and its state of charge Q (SOC), with a series resistance R_b .

In particular, the voltage U_b and the resistance R_b in the following are given by equations (4.7) and (4.8) [80].

The power P_B in input or in output from the battery is the algebraic addition of the power P_S (positive in the charging mode, negative in the discharging mode) actually stored in the battery and the battery losses $P_{B,loss}$ that are supposed like a polynomial (quadratic) function of P_S , and they are positive for both the charging and discharging conditions (equations (4.9), (4.10)).

The battery energy level E_s is given by:

$$E_S(t) = E_S(0) + \int_0^t P_S(\tau) d\tau \quad (5.9)$$

The state of charge, at instant t , is defined as:

$$Q(t) = \frac{E_s(t)}{C_b} \quad (5.10)$$

The model is completely assigned if R_b in charging and discharging mode (Figs. 5.13, 5.14) and U_b (Fig. 5.15) are assigned over the whole SOC range [94]-[95].

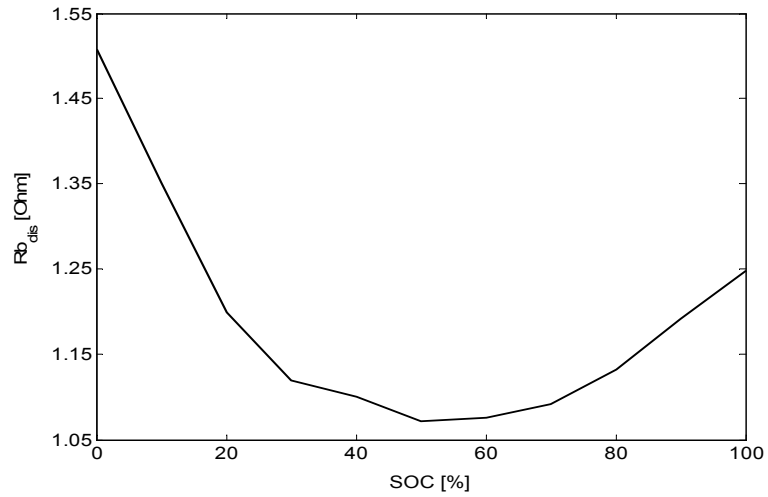


Fig. 5.13: the Toyota Prius battery equivalent resistance in discharging mode.

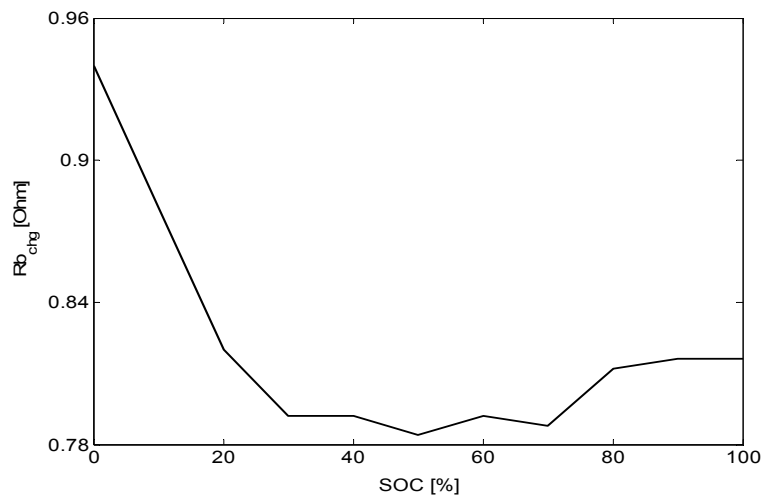


Fig. 5.14: the Toyota Prius battery equivalent resistance in charging mode.

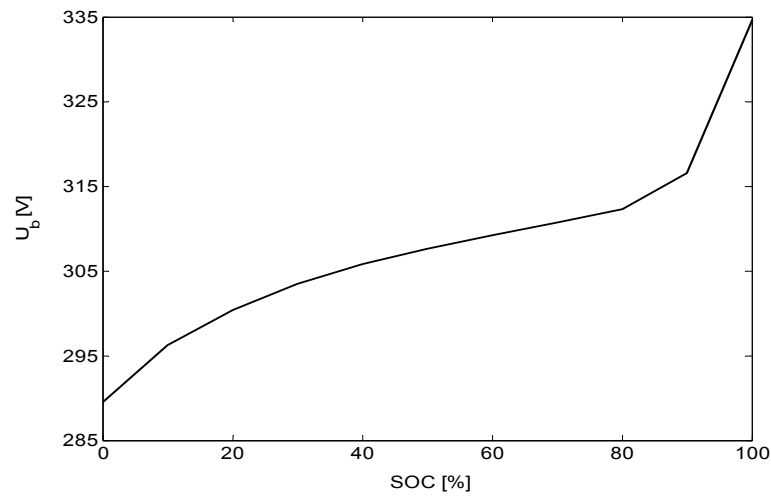


Fig. 5.15: the Toyota Prius battery open-circuit voltage.

5.2.9 Schematic of the power bus

In Fig. 16, a schematic of a possible electrical power bus of a hybrid electric vehicle is represented, with some of the electrical loads actually available on modern hybrid/conventional vehicles, such as: throttle-by-wire, power steering, anti-lock braking, rear-wheel steering, air-conditioning, ride-height adjustment, active suspension, electrically heated catalyst, and so on [2].

The electric power profile adopted for the modelling of the on-board electrical loads has been computed with the *Critical Loads Activation Sequences Maker* tool, that is part of *Evaluator* suite (see chapter 3) [82]. This tool generates, by means of a stochastic approach, different sequences of loads activation and gives, as output, a set of critical operative conditions suitable for testing the power source system. A behavioral model is adopted for several electrical loads, a circuital model is adopted for other loads (electric window winders, radiator fan, air-conditioned fan, electric windscreen wiper, rear window wiper, EPAS).

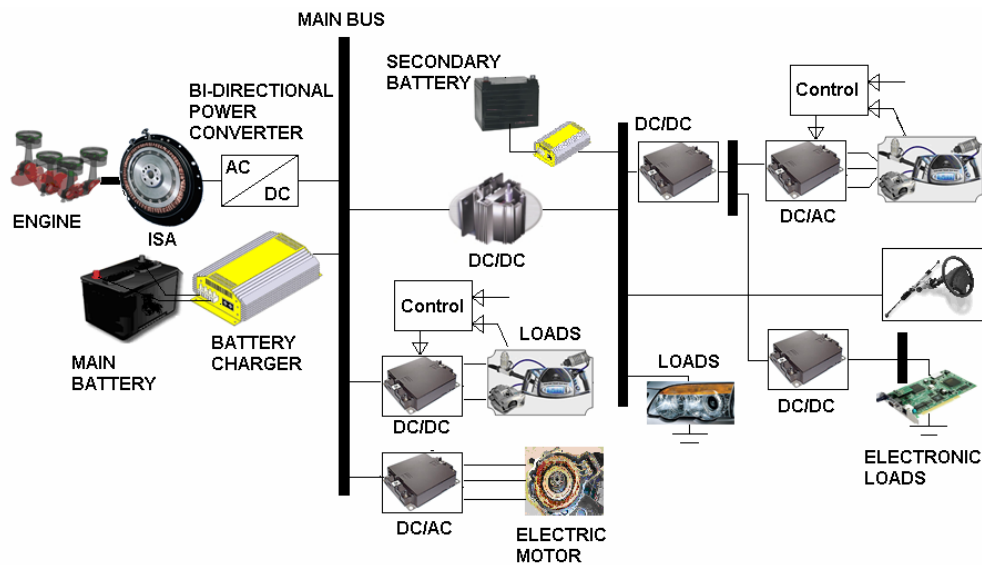


Fig. 5.16: a modern hybrid vehicle electrical power bus architecture.

5.3 Analytic formulation of the proposed optimal control strategy

For a fixed drive cycle and electrical loads power profile, the aim of the proposed strategy is to be able to split the power for the propulsion between the thermal and electric path, redistributing power of the battery and the generator, in order to reduce the fuel consumption and the engine emissions, unaffected the drivability of the vehicle, the comfort of the driver and the on-board electrical loads supplies, keeping as constant as possible the SOC of the battery. These targets can be achieved shifting the engine operating point versus regions with the maximum efficiency, realizing an optimal power split between engine and electric motor [92].

Nevertheless, in order to unaffected the drivability of the vehicle, both the ISA generator output power P_{B2} and the electric motor output power P_E must be adequately controlled. In fact, the electric motor and the generator are coupled to the engine by means of CVT (Fig. 5.2) therefore, controlling their generated powers, the operating power and speed of the combustion engine will be influenced.

The battery can be recharged even by means of re-generative braking; this is possible by controlling the electric motor as a generator during the braking mode.

The action of the proposed strategy implicates that the battery is not used, like in a conventional vehicle, only to supply key-off loads and to assist the alternator against peak-power demands, but it is also used to satisfy the request of the electric motor

for propulsion.

The power P_B flows in output or in input from the battery depending on the necessity of the control strategy to shift the engine operating point versus regions with maximum efficiency.

Let us consider T_s the sampling time of the control strategy, indicating with k the k -*mo* sampling period and considering the equations (5.1), (5.4), (5.6)-(5.7), (4.9)-(4.10), the energetic model of the vehicle, in discrete time, is given by the following system of equations (the generic quantity $f(k) \equiv f(kT_s)$):

$$\left\{ \begin{array}{l} P_{B2}(k) = P_B(k) + P_L(k) + P_{B1}(k) \quad (\text{electrical node}) \\ P_M(k) + P_E(k) = P_G(k) + P_D(k) \\ n_g(k) = n(k) + \frac{1}{\tau} [F_r n_w(k) - n(k)] \end{array} \right\} (\text{mechanical node})$$

$$\left\{ \begin{array}{l} P_{B2}(k) = f_{g,\eta_{gmax}}(n_g(k)) \\ P_G(k) = \frac{P_{B2}(k)}{f_g(P_{B2}(k), n_g(k))} \\ P_E(k) = P_{B1}(k) \left[f_e(P_{B1}(k), n_e(k)) \right]^{sign(P_{B1}(k))} \\ P_B(k) = P_S(k) + \beta P_S^2(k) \end{array} \right. \quad (5.11)$$

with the following conventional signs:

- $P_G > 0$ if in output from the mechanical node;
- $P_D > 0$ if in output from the mechanical node;
- $P_M > 0$ if in output from the engine;
- $P_B > 0$ if in output from the electrical node;
- $P_{B1} > 0$ if in output from the electrical node;
- $P_{B2} > 0$ if in output from the generator;
- $P_E > 0$ if in output from the electric motor.

At the instant k , the system (5.11) is of 6 equations in 8 unknown quantities. It can be resolved respect to arbitrary two quantities.

In the following, all the quantities will be expressed respect to the battery storage power P_S and the engine speed n . This consents to write also the power P_M as

function of P_S and n :

$$P_M(k) = f_M(n(k), P_S(k), P_S(k-1), \dots, P_S(1)) \quad (5.12)$$

Indicating with T_c the period of the considered drive cycle, the total fuel used and emissions at the end of the cycle is given by:

$$F = \int_0^{T_c} f_{tot}(t) dt \quad (5.13)$$

with:

$$f_{tot} = k_1 \dot{m}_f(P_M, n) + k_2 \dot{m}_{HC}(P_M, n) + k_3 \dot{m}_{CO}(P_M, n) + k_4 \dot{m}_{NOx}(P_M, n) \quad (5.14)$$

where k_1, k_2, k_3, k_4 are defined constant weights [92].

The goal of the control strategy is to minimize the cost function (5.14) [28], [92].

Because the ranges of the different quantities involved in the power diagram (Fig. 5.2) are limited by physics underlying or by engineering design, the control strategy can be formulated as a nonlinear optimization problem subject to constraints. In particular, the following inequality constraints must be imposed:

$$\begin{aligned} n_{min} &\leq n \leq n_{max} \\ n_{gmin} &\leq n_g \leq n_{gmax} \end{aligned} \quad (5.15a)$$

$$\begin{aligned} P_{Mmin} &\leq P_M \leq P_{Mmax} \\ P_{Emin} &\leq P_E \leq P_{Emax} \\ P_{Smin} &\leq P_S \leq P_{Smax} \end{aligned} \quad (5.15b)$$

The battery is constrained to have the same amount of energy at the start and at the end of the drive cycle:

$$\Delta SOC = 0 \Leftrightarrow E_s(T_c) = E_s(0) \quad (5.16)$$

By considering the basic assumptions and the equation (5.12), in discrete time the relation (5.14) can be expressed as a function of the battery storage power and the engine speed only, as follows:

$$f_{tot}(P_M(k), n(k)) = f_{tot}(n(k), P_S(k), P_S(k-1), \dots, P_S(1)) \quad (5.17)$$

Considering equation (5.4), the following kinematics constraints:

$$\begin{aligned} n_{min}(k) &\leq n(k) \leq n_{max}(k) \\ n_{gmin}(k) &\leq n_g(k) \leq n_{gmax}(k) \end{aligned} \quad (5.18)$$

can be translated to constraint on n only:

$$n'_{min}(k) \leq n(k) \leq n'_{max}(k) \quad (5.19)$$

with:

$$n'_{min}(k) = \max \left\{ n_{min}(k), \frac{n_{gmin}(k) - \frac{n_e(k)}{\tau}}{1 - \frac{1}{\tau}} \right\} \quad (5.20a)$$

$$n'_{max}(k) = \min \left\{ n_{max}(k), \frac{n_{gmax}(k) - \frac{n_e(k)}{\tau}}{1 - \frac{1}{\tau}} \right\} \quad (5.20b)$$

Referring to the system of equations (5.11), the following dynamics constraints:

$$\begin{aligned}
 0 &\leq P_M(k) \leq P_{Mmax}(n(k)) \\
 -P_{Emax}(n_e(k)) &\leq P_E(k) \leq P_{Emax}(n_e(k)) \\
 P_{Smin}(k) &\leq P_S(k) \leq P_{Smax}(k)
 \end{aligned} \tag{5.21}$$

can be translated to constraint on P_M and P_S only:

$$\begin{aligned}
 P'_{Mmin}(k) &\leq P_M(k) \leq P'_{Mmax}(k) \\
 P_{Smin}(k) &\leq P_S(k) \leq P_{Smax}(k)
 \end{aligned} \tag{5.22}$$

with:

$$\begin{aligned}
 P'_{Mmin}(k) &= \max\{0, P_D(k) + P_G(k) - P_{Emax}(n_e(k))\} \\
 P'_{Mmax}(k) &= \min\{P_{Mmax}(n(k)), P_D(k) + P_G(k) + P_{Emax}(n_e(k))\}
 \end{aligned} \tag{5.23}$$

In this way, the optimization problem statement is expressed with the following equations (N is integer and it is the ratio between the length of the drive cycle T_c and the sampling time T_s):

$$\min_{\begin{matrix} n(1), \dots, n(N) \\ P_s(1), \dots, P_s(N) \end{matrix}} F = \min \left\{ T_s \sum_{k=1}^N f'_{tot}(P_s(k), n(k)) \right\} \tag{5.24}$$

subject to (5.19), (5.22) and to the following equality constraint:

$$\sum_{k=1}^N P_S(k) = 0 \tag{5.25}$$

The final formulation of the minimization with physical constraints is then:

$$\begin{aligned}
 \min_{\substack{F \\ \left[\begin{array}{c} n(1), \dots, n(N) \\ P_s(1), \dots, P_s(N) \end{array} \right]}} &= \min \left\{ T_s \sum_{k=1}^N f_{tot}(P_s(k), n(k)) \right\} \\
 \text{physical} & \\
 \text{constraints:} & \left\{ \begin{array}{l} n'_{min}(k) \leq n(k) \leq n'_{max}(k) \\ P'_{Mmin}(k) \leq P_M(k) \leq P'_{Mmax}(k) \\ P_{Smin}(k) \leq P_S(k) \leq P_{Smax}(k) \\ \sum_{k=1}^N P_S(k) = 0 \end{array} \right. \forall k = 1, \dots, N \quad (5.26)
 \end{aligned}$$

The problem is now formulated as a finite dimensional nonlinear optimization problem. Because all functions involved in the problem are convex functions, the formulated problem is a nonlinear convex problem with inequality and equality constraints [28], [87], [92]. The solution of this problem is given from the Kuhn-Tucker (KT) conditions [87]: for a nonlinear convex problem, KT equations are both necessary and sufficient for a global solution point.

Let us consider the problem of minimizing a function $F(\mathbf{x})$ subject to m equality constraints $G_i(\mathbf{x})=0$ ($i \in [1, m]$), and p inequality constraints $H_j(\mathbf{x}) \leq 0$ ($j \in [1, p]$).

If \mathbf{x}_0 is a local minimum for the constrained problem and if it is a regular point, the KT conditions ensure that there is a vector $\boldsymbol{\lambda} = [\lambda_i, \lambda_j]$, $i \in [1, \dots, m], j \in [1, \dots, p]$, with $(m+p)$ components, such that:

$$\left\{ \begin{array}{l} \nabla_x L(\mathbf{x}_0, \boldsymbol{\lambda}) = 0 \\ \lambda_i G_i(\mathbf{x}) = 0 \quad \text{for } i \in [1, m]; \quad \lambda_j H_j(\mathbf{x}) = 0 \quad \text{for } j \in [1, p] \\ G_i(\mathbf{x}) = 0 \quad \text{for } i \in [1, m]; \quad H_j(\mathbf{x}) = 0 \quad \text{for } j \in [1, p] \\ \lambda_j \geq 0 \quad \text{for } j \in [1, p] \end{array} \right. \quad (5.27)$$

where:

$$L(\mathbf{x}, \boldsymbol{\lambda}) = F(\mathbf{x}) + \sum_{i=1}^m \lambda_i G_i(\mathbf{x}) + \sum_{j=1}^p \lambda_j H_j(\mathbf{x}) \quad (5.28)$$

is the Lagrange function and ∇ is the linear operator nabla. Expression (5.28) represents a more generalized form of the Lagrange function adopted in chapter 4.

The eqs. (5.27) are also sufficient if the problem is convex. In our case we have:

$$\mathbf{x} = \left[n(1), \dots, n(k), \dots, n(N), P_S(1), \dots, P_S(k), \dots, P_S(N) \right]_{(1 \times 2N)} \quad (5.29)$$

$$G_i(\mathbf{x}) = \sum_{k=1}^N P_S(k) \quad \text{for } i=1$$

$$H_j(\mathbf{x}) = \begin{cases} n(j) - n'_{max}(j) & \text{for } j \in [1, N] \\ -n(j) + n'_{min}(j) & \text{for } j \in [N+1, 2N] \\ P_M(j) - P'_{Mmax}(j) & \text{for } j \in [2N+1, 3N] \\ -P_M(j) + P'_{Mmin}(j) & \text{for } j \in [3N+1, 4N] \\ P_S(j) - P_{Smax}(j) & \text{for } j \in [4N+1, 5N] \\ -P_S(j) + P_{Smin}(j) & \text{for } j \in [5N+1, 6N] \end{cases} \quad (5.30)$$

Here λ is a vector of $1 \times (1+6N)$ components, $m=1$, $p=6N$.

Now the solution of the problem (5.26), with related physical constraints, reduces to solve numerically the system of equations (5.27), with \mathbf{x} , $G_i(\mathbf{x})$, $H_j(\mathbf{x})$ defined by (5.29), (5.30).

The solution of the KT equations forms the basis for many nonlinear programming algorithms [28], [88], [92]. These algorithms attempt to compute the Lagrange multipliers directly. These methods are commonly referred as Sequential Quadratic Programming (SQP) methods, since a QP subproblem is solved at each major iteration. In particular in this thesis, as for conventional vehicles application (chapter 4), the Schittkowski method has been adopted [28], [89], [92]. The method allows to closely mimic Newton's method for constrained optimization just as it is done for unconstrained optimization. At each major iteration, an approximation is made of the Hessian of the Lagrangian function using a quasi-Newton updating method. This is then used to generate a QP subproblem whose solution is used to form a search direction for a line search procedure [90].

5.4 Case-study: an application to a real vehicle

In order to test the suggested control strategy, two sets of simulations have been developed: the first one refers to the application of the proposed strategy when a zero variation of SOC is imposed from start to the end of the drive cycle. The second one refers to a comparison between the proposed strategy and the energy management strategy actually implemented in Toyota Prius, as it is simulated by means of the ADVISOR[®] tool [92].

The adopted new European drive cycle (NEDC) [91] is reported in Fig. 5.17.

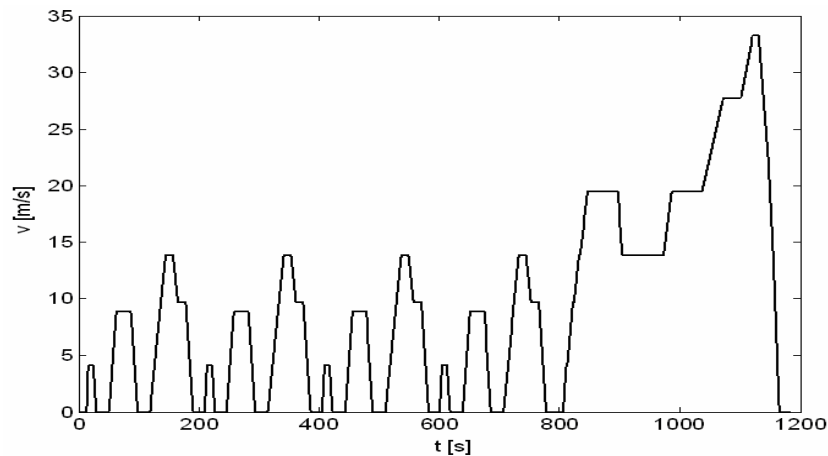


Fig. 5.17: New European drive cycle (NEDC).

The parameters of the considered system are reported in Table 5.1.

Fig. 5.18 shows the electrical loads power profile. This profile has been computed with *Evaluator* a computer-aided suite (see paragraph 5.2.9 and chapter 3). All-electric compressor for cooling is not included in the considered loads, as it has been introduced in the 2004 model only.

The considered static maps for ICE, generator and electric motor are reported in Figs. 5.4, 5.5, 5.7, 5.11. The battery model implements data deduced from Figs. 5.13-5.15.

Fig. 5.19 shows the drive train power, which is derived by the vehicle speed profile and the vehicle parameters (Table 5.1).

<i>Symbol</i>	<i>Quantity</i>	<i>Value</i>	<i>Unit</i>
SIMULATION TIME:			
T_c	Drive cycle length	1180	s
T_s	Sample time	1	s
VEHICLE:			
m	Mass (full load)	1700	kg
A	Frontal area	1.746	m ²
C_d	Air drag coefficient	0.3	
C_r	Rolling resistance coeff.	0.009	
ρ	Air density	1.2	kg/m ³
g	Gravity	9.81	m/s ²
R	Wheel radius	0.287	m
F_r	Final drive ratio	3.93	
τ	CVT ratio	-30/78	
BATTERY:			
U_b	Voltage	288	V
C_b	Capacity	6	Ah/cell
$S.O.C._0$	Initial S.O.C.	70%	
P_{Smax}	Maximum charging power	25	kW
ICE:			
P_{Mn}	Nominal power	43	kW
n_n	Nominal speed	4000	rpm
T_{Mn}	Nominal torque	101.7	Nm
ELECTRIC MOTOR:			
P_{En}	Nominal power	30	kW
n_{En}	Nominal speed	1000	rpm
T_{En}	Nominal torque	300	Nm
V_{En}	Nominal voltage	500	V
GENERATOR:			
P_{B2n}	Nominal power	15	kW
n_{gn}	Maximum speed	6000	rpm
V_{gn}	Nominal voltage	500	V

Table 5.1: New European drive cycle (NEDC).

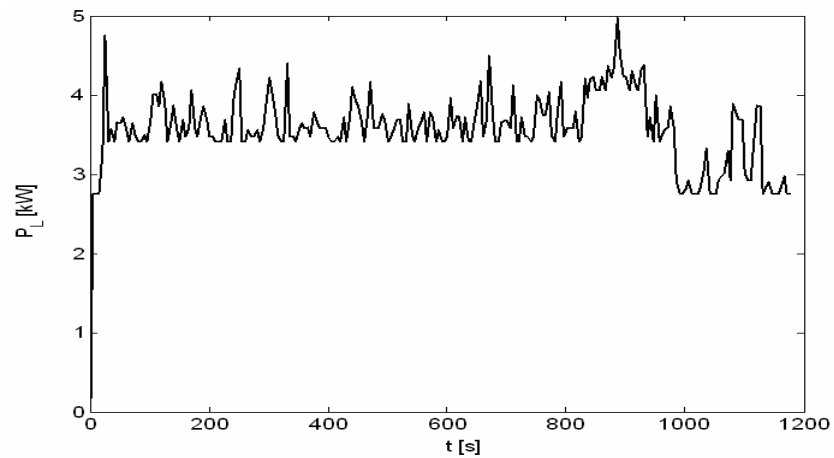


Fig. 5.18: Critical electrical loads power profile used for the simulation.

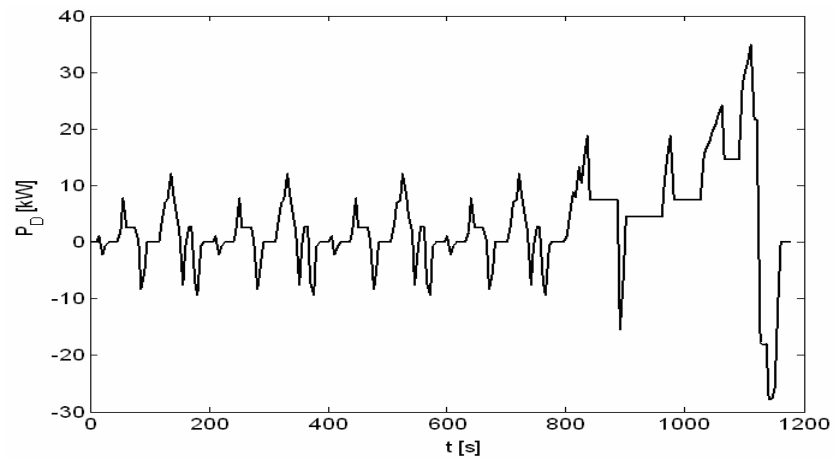


Fig. 5.19: Drive train power.

5.4.1 Simulations and results of the proposed strategy

In the following, the profile of the main quantities of the vehicle obtained from the power split control resulting by the proposed strategy, are reported [92].

Figs. 5.20-5.28 show respectively the ICE speed, the ICE power, the electric motor mechanical power, the generator speed, the battery storage power (with relative bounds), the generator power, the fuel rate, the emissions rates and the battery SOC resulting by the proposed strategy.

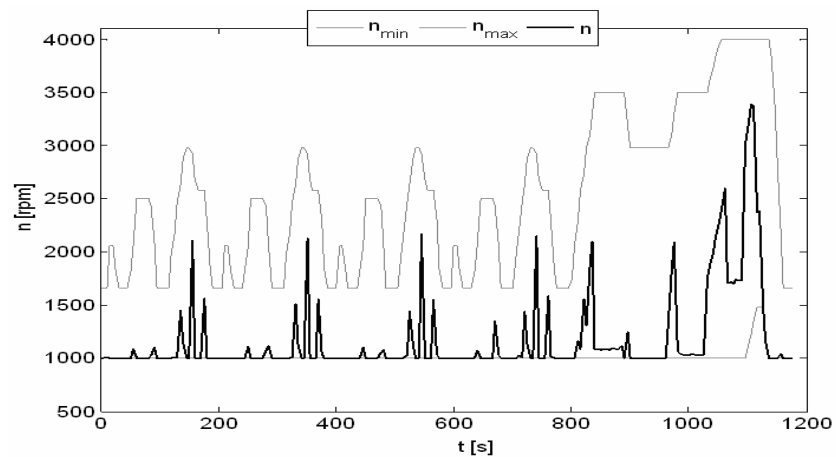


Fig. 5.20: optimal ICE speed and related bounds.

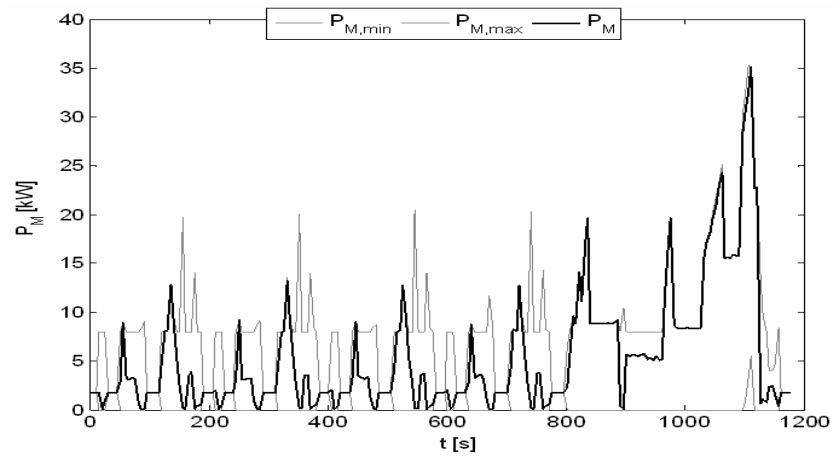


Fig. 5.21: optimal ICE power and related bounds.

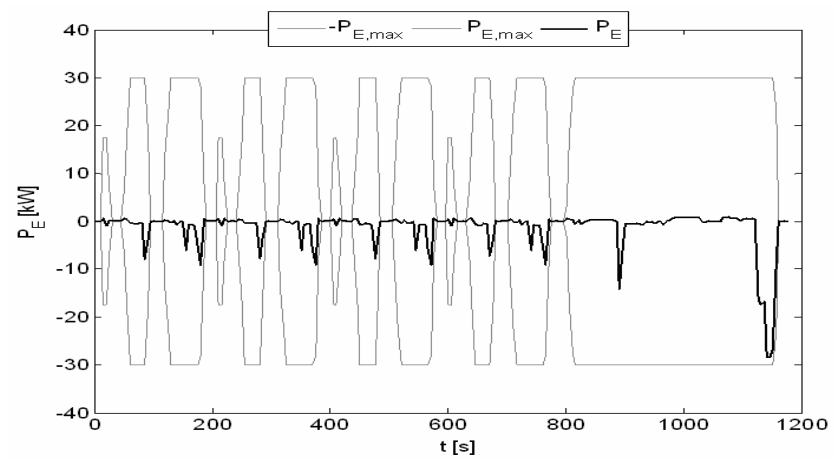


Fig. 5.22: optimal electric motor mechanical power and related bounds.

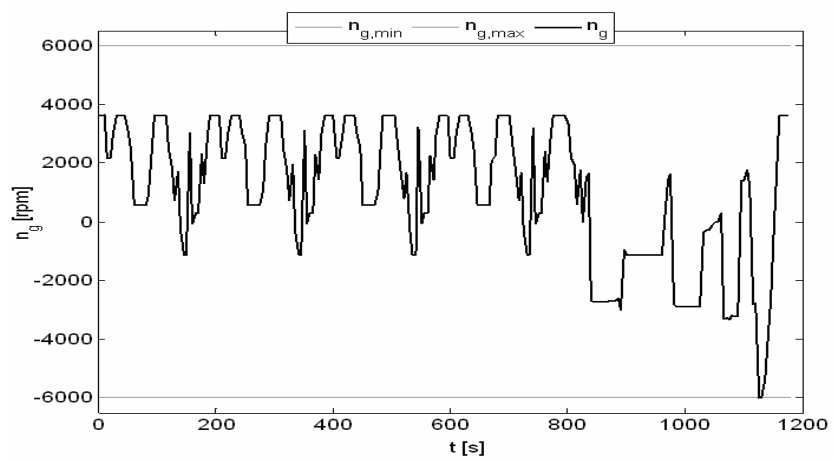


Fig. 5.23: optimal generator speed and related bounds.

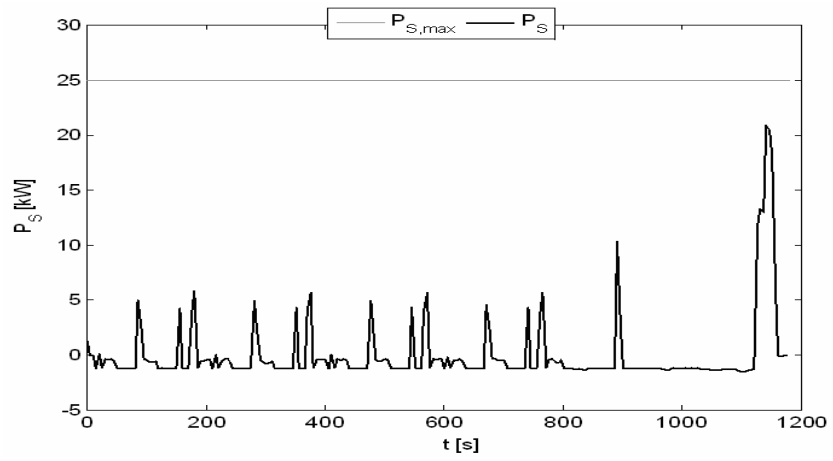


Fig. 5.24: optimal battery storage power and related bounds.

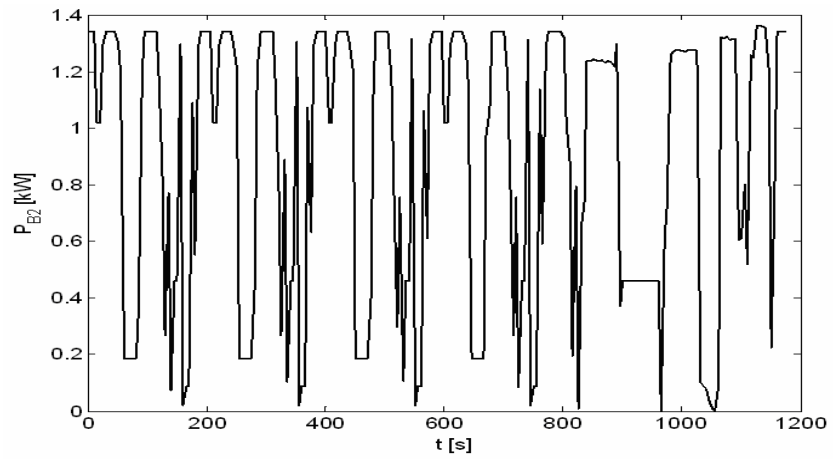


Fig. 5.25: optimal generator electric power.

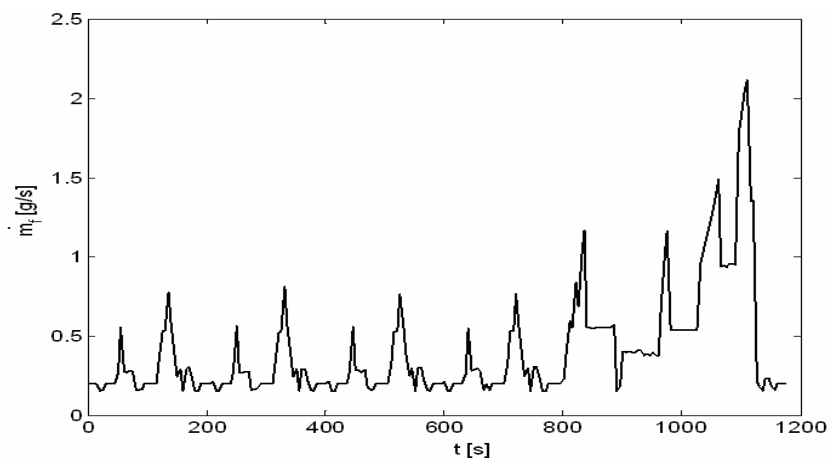


Fig. 5.26: optimal fuel consumption rate.

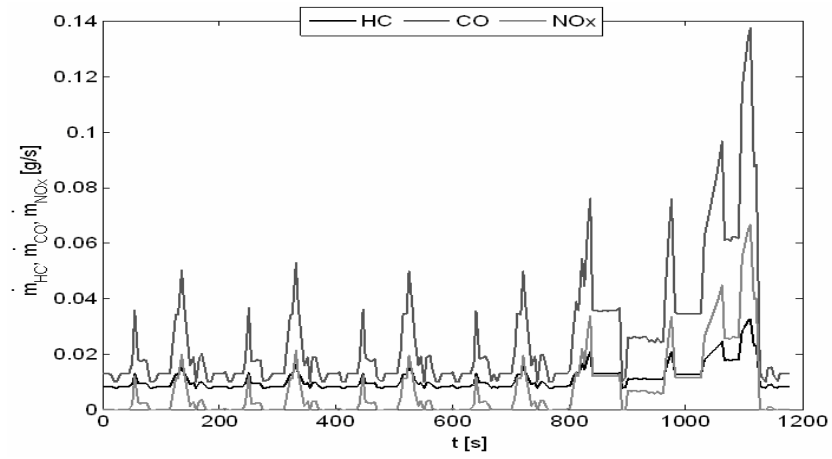


Fig. 5.27: optimal emissions rate.

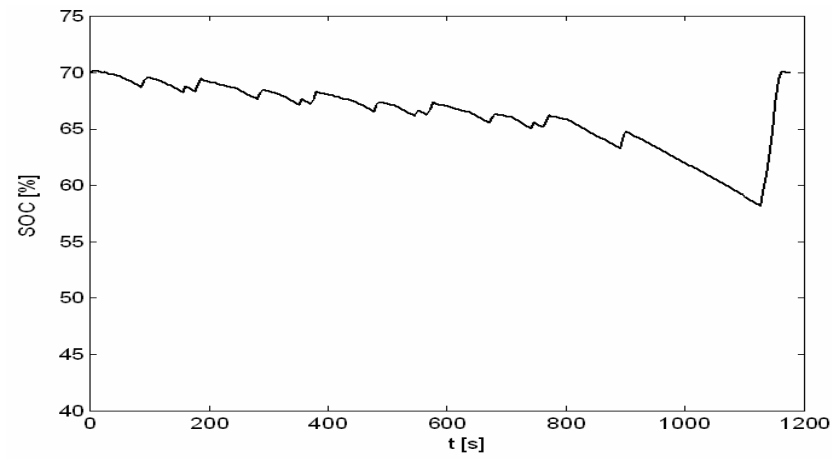


Fig. 5.28: optimal battery SOC profile.

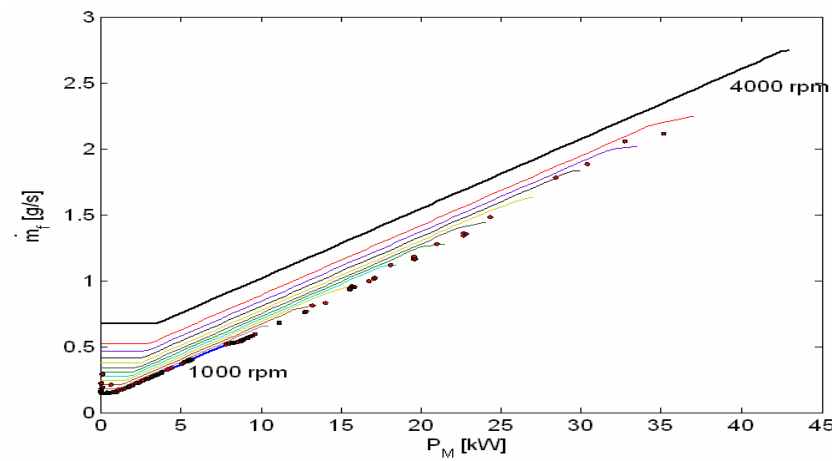


Fig. 5.29: optimal operative points of ICE in the cycle.

Fig. 5.29 shows the operative points of the ICE during the NEDC drive cycle, resulting from the proposed optimization strategy, reported on the fuel map.

5.4.2 Comparisons with ADVISOR simulations results

ADVISOR[®] (Ver. 2004) is a well-known computational tool for automotive applications. With ADVISOR it is possible to simulate several commercial hybrid vehicles, particularly it is possible to simulate the Toyota Prius NHW10 model, for a desired drive cycle, with an imposed electrical loads power profile.

In the ADVISOR's model of Prius, the realistic Hybrid Powertrain Control Strategy is implemented; it realizes several operative modes, depending on the state of the vehicle [26] (see chapter 2).

The numerical results of ADVISOR simulations, carried out under the same operative conditions adopted for our optimization strategy, show that the SOC at the end of the drive cycle is lower than the initial SOC, differently from the results of the proposed strategy.

Therefore, for a correct comparison between ADVISOR and the proposed strategy results, it is necessary to impose as equality constraint for the proposed strategy the following:

$$\Delta SOC_{OS} = \Delta SOC_{ADVISOR} \quad (5.31)$$

instead of the (5.16).

The constraint (5.25) changes consequently as follows (correction on SOC constraint in the optimization algorithm):

$$T_s \sum_{k=1}^N P_S(k) = C_b \Delta SOC_{ADVISOR} \quad (5.32)$$

Figs. 5.30-5.35 show the results of the comparisons between ADVISOR and our strategy (referred as Optimization Strategy - OS in the figures).

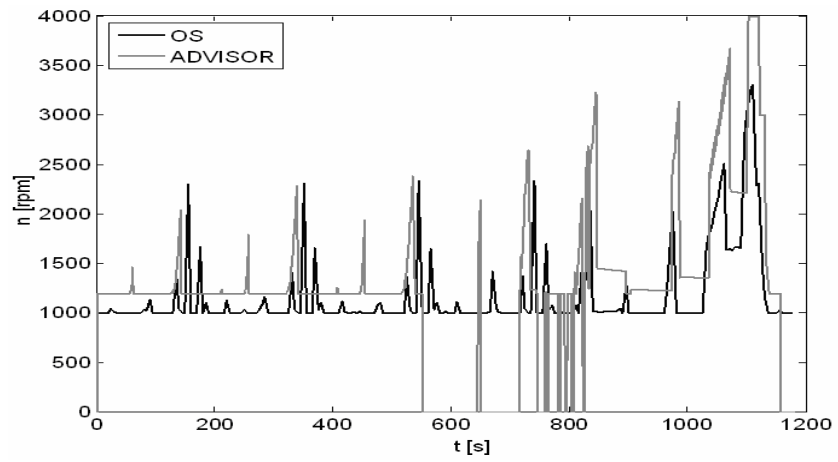


Fig. 5.30: OS vs. ADVISOR ICE speed.

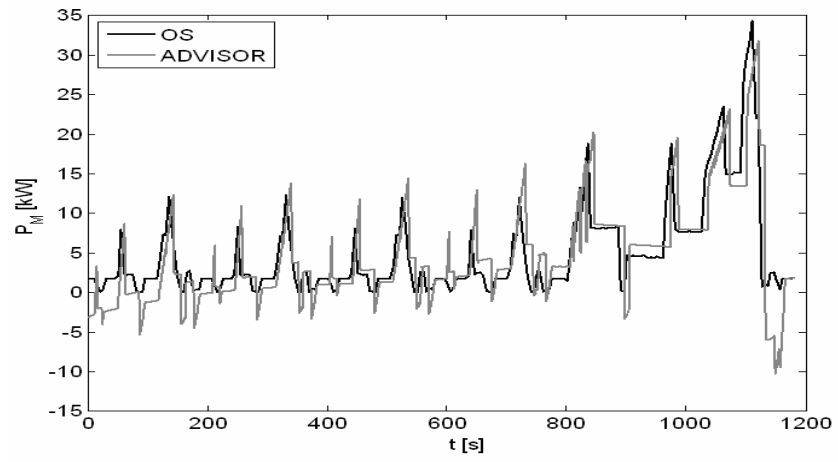


Fig. 5.31: OS vs. ADVISOR ICE power.

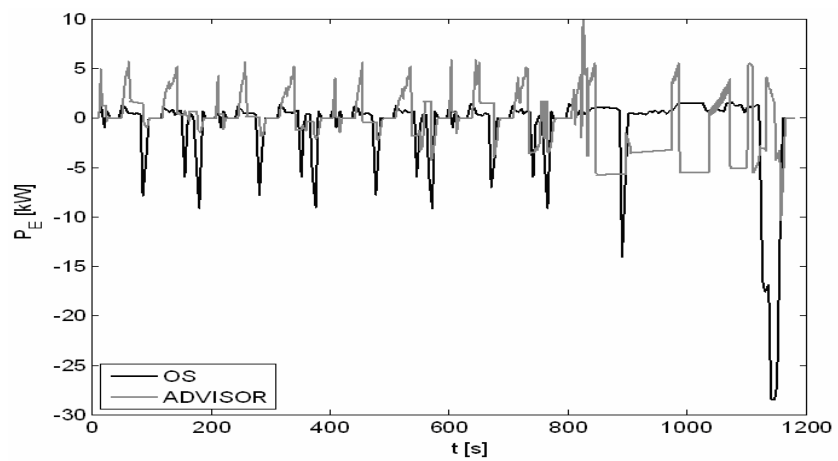


Fig. 5.32: OS vs. ADVISOR electric motor mechanical power.

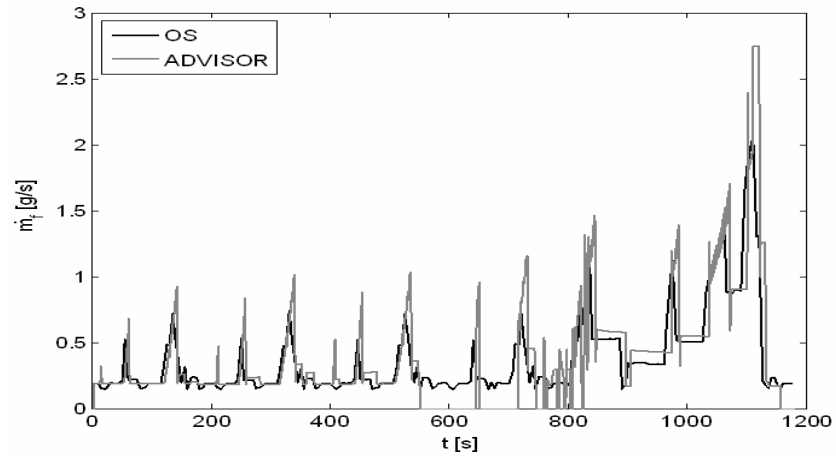


Fig. 5.33: OS vs. ADVISOR fuel rate profile.

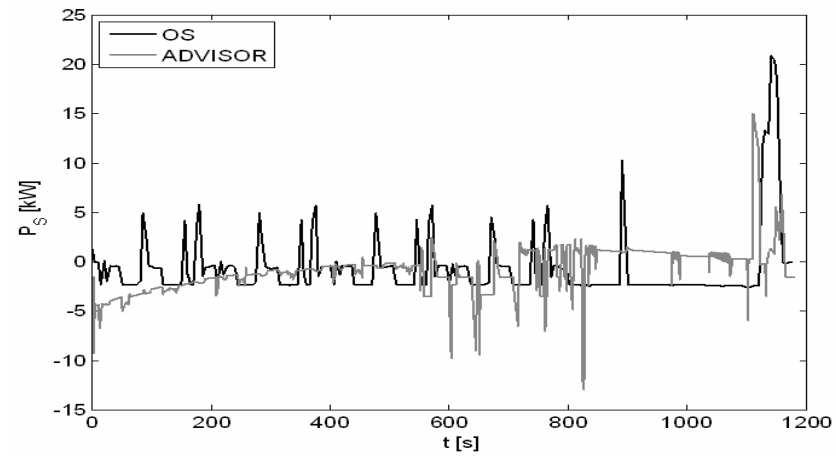


Fig. 5.34: OS vs. ADVISOR battery storage power.

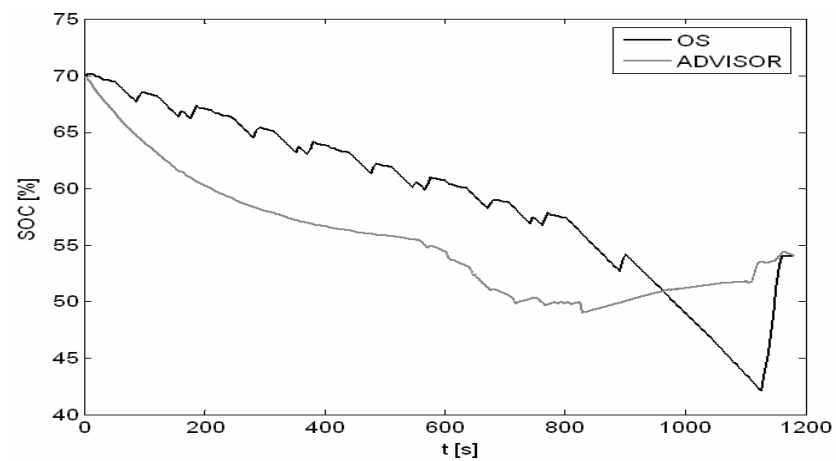


Fig. 5.35: OS vs. ADVISOR battery SOC profile.

As it can be noted from Fig. 5.34, the philosophy of the battery's service is quite different for the two strategies. In fact, such figure shows how the control strategies often impose different sign for the battery storage power.

As it can be noted from Fig. 5.35, the variation of the SOC between the start and the end of the cycle is the same for both the strategies but not zero, according to the constraint (5.32).

Table 5.2 presents the results of comparison, regarding to the global consumptions and the emissions.

	PROPOSED STRATEGY	ADVISOR	% SAVING
FUEL [g]	442.3	459	3.6%
HC [g]	12.7	15.9	20%
CO [g]	28.8	33.1	13%
NO _x [g]	7.5	9.5	21%

Table 5.2: the comparison results.

The results show that with the proposed optimization strategy, operating with the same reduction of the SOC at the end of the considered drive cycle, a 3.6% reduction in fuel consumption and 20%, 13%, 21% reduction in engine emissions (HC, CO, NO_x) can be obtained respect to the real consumptions and emissions of the Toyota Prius thermal engine, as emerged from the ADVISOR simulations [92].

Conclusions

Motivations at the bases of the performed research have been the following:

1. the growing electric power demand in road light vehicles, caused by the expected increase in “comfort” and performances from users, and for the consequent trend towards expanding electrical loads and replacement of more engine driven mechanical and hydraulic systems with electrical systems, that is going the power demand from actual 1kW, for conventional vehicles, towards 5kW for innovative vehicles.
2. the necessity of limiting fuel consumption and pollutant emissions at a tolerable level, due to economic reasons (for the first) and government measures (for the second).

Both the above motivations have required the development of enhanced solutions of architectures and control of conventional or hybrid propulsion vehicles’ electrical power system.

This activity has been splitted in the following two lines of research:

- 1) A comparative evaluation for the choice of an enhanced architecture of the electrical power system in new conventional or hybrid vehicles.
- 2) Implementation of an innovative and enhanced management algorithm for the control of the electrical power system.

The first research line has given as result the implementation of a comparative technique based on a stochastic philosophy.

Starting from the following architecture indexes: size, weight, cost, efficiency and reliability of every components and of the whole system, electric service quality, this technique gives a global index that defines the adaptability of analyzed architecture to the specific automotive application.

As result of the second research line, a new energy management strategy has been developed. It has been implemented in simulation on a real power-split hybrid vehicle and it has shown to be able to split the power for the propulsion between the thermal and electric path, redistributing power of the battery and the generator, in order to reduce the fuel consumption and the engine emissions, preserving the drivability of the vehicle, the comfort of the driver and the on-board electrical loads supplies, keeping as much as possible constant the SOC of the battery.

The energy management strategies based on the global optimization methods don't offer a real-time solution because they assume that the drive cycle is entirely known. In addition, they require a lot of computational time and a fine tuning of their parameters, therefore their use is restricted to single experiments and for a fixed drive cycle.

Nevertheless, their results can be very interesting, because they could be used as a benchmark for the performance of other strategies, or to derive rules for the rule-based strategies.

For these reasons, possible future works of the research would concern the employment of the solutions of the fuel consumption and pollutant emissions global minimization problems for the derivation of rules for real-time rule-based energy optimization strategies. Possible real-time strategies could adopt neural networks, trained with data resulting from the application of the proposed off-line optimization method to several critical drive cycles and critical loads activation sequences, for a specific vehicle.

Possible future works are:

1. to complete the modelling process of the power bus of the vehicle with the modelling of other innovative electrical loads, as to realize a more reliable comparative evaluation for the choice of the most suitable architecture for the current applications;

2. to extend the study and testing of the optimal real-time management strategy for conventional and hybrids vehicles, in particular for the rule-base techniques, implemented by neural networks (outputs of the off-line global optimization problem for several drive cycles and loads activation sequences are used as benchmark for a real-time rule based algorithm).

References

- [1] IPCC, 2007: "Climate Change 2007: Mitigation. Contribution of Working Group III to the Fourth Assessment Report of the Intergovernmental Panel on Climate Change [B. Metz, O.R. Davidson, P.R. Bosch, R. Dave, L.A. Meyer (eds)], Cambridge University Press, Cambridge, United Kingdom and New York, NY, USA, chapters 4, 5.
- [2] A. Emadi, M. Ehsani, J. M. Miller, "Vehicular Electric Power Systems: Land, Sea, Air, and Space Vehicles", Copyright © 2004 by Marcel Dekker, Inc.
- [3] J. M. Miller, A. Emadi, A. V. Rajarathnam, and M. Ehsani, "Current status and future trends in more electric car power systems", in Proc. of 1999 IEEE Vehicular Technology Conference, Houston, TX, May 1999.
- [4] A. Emadi, M. Ehsani, and J. M. Miller, "Advanced silicon rich automotive electrical power systems", 181 Digital Avionics Systems Conference on Air, Space, and Ground Vehicle Electronic Systems, St. Louise, Missouri, Oct. 1999.
- [5] J. G. Kassakian, H. C. Wolf, J. M. Miller, and C. J. Hurton, "Automotive electrical systems-circa 2005", IEEE Spectrum, pp. 22-27, Aug. 1996.
- [6] J. M. Miller, D. Goel, D. Kaminski, H. P. Schoner, and T. Jahns, "Making the case for a next generation automotive electrical system", Convergence Transportation Elect. Association Congress, Dearborn, MI, Oct. 1998.
- [7] J. M. Miller, P. R. Nicastrì, "The next generation automotive electrical power system architecture: Issues and challenges", 17th Digital Avionics Systems Conference on Air, Space, and Ground Vehicle Electronic Systems, Bellevue, WA, Oct./Nov. 1998.
- [8] L. A. Khan, "Automotive electrical systems: architecture and components", 18th Digital Avionics Systems Conference on Air, Space, and Ground Vehicle Electronic Systems, St. Louise, Missouri, Oct. 1999.

- [9] J. G. Kassakian, "The future of power electronics in advanced automotive electrical systems", Proc. of IEEE Power Electronics Specialist Conf., 1996, pp. 7-14.
- [10] J. G. Kassakian, H. C. Wolf, J. M. Miller, and C. J. Hurton, "Automotive electrical systems circa 2005", IEEE Spectrum, Aug. 1996.
- [11] Kassakian, J.G., "Automotive electrical systems-the power electronics market of the future", Applied Power Electronics Conference and Exposition, 2000. APEC 2000. Fifteenth Annual IEEE Volume 1, 6-10 Feb. 2000 Page(s):3 - 9 vol.1.
- [12] Rajashekara, K., "42 V architecture for automobiles", Electrical Insulation Conference and Electrical Manufacturing & Coil Winding Technology Conference, 2003. Proceedings.
- [13] N. A. Kelling, P. Leteinturier, "X-by-Wire: Opportunities, Challenges and Trends", SAE Paper No. 2003-01-0113, March 3-6, 2003.
- [14] Bretz, E.A., "By-wire cars turn the corner", Spectrum, IEEE, Volume 38, Issue 4, April 2001 Page(s):68 – 73.
- [15] P. Bolognesi, O. Bruno, A. Landi, L. Sani, L. Taponecco, "Electric Machines and Drives for X-by-Wire Systems in Ground Vehicles", 10th European Conference on Power Electronics and Applications - EPE2003, vol. CD-Rom, pp. 1-16, Tolosa 2003.
- [16] Isermann, R.; Schwarz, R.; Stolzl, S., "Fault-tolerant drive-by-wire systems", Control Systems Magazine, IEEE Volume 22, Issue 5, Oct. 2002 Page(s):64 – 81.
- [17] Miller, J.M., "Hybrid electric vehicle propulsion system architectures of the e-CVT type", Power Electronics, IEEE Transactions on, Volume 21, Issue 3, May 2006 Page(s):756 – 767.
- [18] G. Maggetto and J. Van Mierlo, "Electric and electric hybrid vehicle technology: A survey", in Proc. IEE Semin. Elect., Hybrid and Fuel Cell Veh. (Ref. No. 2000/050), Apr. 11, 2000, pp. 1–11.
- [19] F. A. Wyczalek, "Hybrid electric vehicles (EVS-13 Osaka)," in Proc. Northcon, Nov. 4–6, 1996, pp. 409–412.

- [20] C. C. Chan, Y. S. Wong, "Electric vehicles charge forward," *IEEE Power Energy Mag.*, vol. 2, no. 6, pp. 24–33, Nov./Dec. 2004.
- [21] R. Nesbitt, C. Muehlfeld, S. Pandit, "Power-split hybrid electric vehicle control with electronic throttle control (ETC)", presented at the SAE Int., Powertrain and Fluid Systems Conf. and Exhibition, Pittsburgh, PA, Oct. 2003, Paper 2003-01-3280.
- [22] M. Kamiya, "Development of Traction Drive Motors for the Toyota Hybrid System," 2005 International Power Electronics Conference, Toki Messe in Niigata, Japan, April 4–8, 2005.
- [23] Syed, F. U.; Kuang, M. L.; Czubay, J.; Ying, H., "Derivation and Experimental Validation of a Power-Split Hybrid Electric Vehicle Model", *Vehicular Technology, IEEE Transactions on*, Volume 55, Issue 6, Nov. 2006 Page(s):1731 – 1747.
- [24] D. Hermance, S. Sasaki, "Hybrid electric vehicles take to the streets", *IEEE Spectrum*, vol. 35, no. 11, pp. 48-52, November 1998.
- [25] Chan, C.C., "The state of the art of electric and hybrid vehicles", *Proceedings of the IEEE* Volume 90, Issue 2, Feb. 2002 Page(s):247 – 275.
- [26] <http://www.toyota.com/prius/>
- [27] M. Balenovic, T. Backx, "Model-based predictive control of a threeway catalytic converter", *Proc. IEEE Conference on Control Applications*, Mexico City, pages 626–631, 2001.
- [28] F. Esposito, V. Isastia, S. Meo, "Energy management Strategy for Automotive Electric Power System", *Przeglad Elektrotechniczny (ISSN 0033-2097)*, vol. 2006, n. 2, pp. 26-31, Selected paper from International Conference on Power Electronics and Intelligent Control for Energy Conservation, PELINCEC 2005.
- [29] Jong-Seob Won; Langari, R.; Ehsani, M., "An energy management and charge sustaining strategy for a parallel hybrid vehicle with CVT", *Control Systems Technology, IEEE Transactions on*, Volume 13, Issue 2, Mar 2005 Page(s):313 – 320.
- [30] A. M. Singer-Englar, R. J. Kamisky and others, "Design and Development of a Parallel Hybrid Powertrain for a High-Performance Electric Sport Utility Vehicle", SAE paper n. 2005-01-3827.

- [31] Pisu, P.; Rizzoni, G., “A supervisory control strategy for series hybrid electric vehicles with two energy storage systems”, *Vehicle Power and Propulsion*, 2005 IEEE Conference, 7-9 Sept. 2005 Page(s):8 pp.
- [32] Kelly, K.J.; Mihalic, M.; Zolot, M., “Battery usage and thermal performance of the Toyota Prius and Honda Insight during chassis dynamometer testing”, *Battery Conference on Applications and Advances*, 2002. The Seventeenth Annual, 15-18 Jan. 2002 Page(s): 247 – 252.
- [33] T. C. Moore, A. B. Lovins, “Vehicle design strategies to meet and exceed PNGV goals”, SAE Paper No. 951906, 1995.
- [34] D. Buntin, J. W. Howze, “A switching logic controller for a hybrid electric/ICE vehicle”, in *Proc. of the American Control Conf.*, vol. 2, Seattle, WA, June 1995, pp. 1169-1175.
- [35] N. Jalil, N. A. Kheir, M. Salman, “A rule-based energy management strategy for a series hybrid vehicle”, in *Proc. of the American Control Conf.*, vol. 1, Albuquerque, NM, June 1997, pp. 689-693.
- [36] C. Liang, W. Qingnian, L. Youde, M. Zhimin, Z. Ziliang, L. Di, “Study of the electric control strategy for the power train of hybrid electric vehicle”, in *Proc. of the IEEE International Vehicle Electronics Conf. (IVEC '99)*, vol. 1, Changchun, China, September 1999, pp. 383-386.
- [37] E. Cerruto, A. Consoli, A. Raciti, A. Testa, “Energy flows management in hybrid vehicles by fuzzy logic controller”, in *Proc.*, 7th Mediterranean Electrotechnical Conf., vol. 3, Antalya, Turkey, April 1994, pp. 1314-1317.
- [38] E. Cerruto, A. Consoli, A. Raciti, A. Testa, “Fuzzy logic based efficiency improvement of an urban electric vehicle”, in *20th International Conf. on Industrial Electronics, Control and Instrumentation (IECON '94)*, vol. 2, Bologna, Italy, September 1994, pp. 1304-1309.
- [39] E.-S. Koo, H.-D. Lee, S.-K. Sul, J.-S. Kim, “Torque control strategy for parallel hybrid vehicle using fuzzy logic” in *Proc. of the 33rd IEEE Industrial Applications Society Annual Meeting*, vol. 3, St. Louis, MO, October 1998, pp. 1715-1720.
- [40] A. Brahma, B. Glenn, B. Guezennec, T. Miller, G. Rizzoni, G. Washigton, “Modeling, performance analysis and control design of a hybrid sport-utility

- vehicle”, in Proc. of the 1999 IEEE International Conf. on Control Applications, Kohara Coast-Island of Hawaii, HI, August 1999, pp. 1715-1720.
- [41] J.-S. Won, R. Langari, “Fuzzy torque distribution control for a parallel hybrid vehicle”, *Expert Systems: The International Journal of Knowledge Engineering and Neural Networks*, vol. 19, no. 1, pp. 4-10, February 2002.
- [42] N. J. Schouten, M. Salman, N. Kheir, “Fuzzy logic control for parallel hybrid vehicles”, *IEEE Trans. on Cont. Syst. Technology*, vol. 10, no. 3, pp. 460-468, May 2002.
- [43] M. Salman, N. J. Schouten, N. A. Kheir, “Control strategies for parallel hybrid vehicles”, in Proc. of the American Control Conf., Chicago, IL, June 2000, pp. 524-528.
- [44] S. Delprat, T. M. Guerra, and J. Rimaux, “Control strategies for hybrid vehicles: Optimal control”, in Proc., Vehicular Technology Conf. (VTC 2002-Fall), vol. 3, Vancouver, Canada, September 2002, pp. 1681-1685.
- [45] A. Kleimaier, D. Schroder, “Optimization strategy for design and control of a hybrid vehicle”, in Proc., 6th International Workshop on Advanced Motion Control, Nagoya, Japan, March 30 - April 1 2000, pp. 459-464.
- [46] H. Mosbech, “Optimal control of hybrid vehicle,” in Proc., International Symp. on Automotive Technology & Automation (ISATA '80), vol. 2, Turin, Italy, September 1980, pp. 303-320.
- [47] M. Oprean, V. Ionescu, N. Mocanu, S. Beloiu, C. Stanciu, “Dynamic programming applied to hybrid vehicle control,” in Proc. of the International Conf. on Electric Drives (ICED 88), vol. 4, Poiana BRA W SOV, Romania, September 1988, pp. D2/10/1-20.
- [48] A. Brahma, Y. Guezennec, G. Rizzoni, “Optimal energy management in series hybrid electric vehicles,” in Proc. of the American Control Conf., Chicago, IL, June 2000, pp. 60-64.
- [49] J. Bumby, I. Forster, “Optimisation and control of a hybrid electric car”, *IEE Proceedings*, vol. 134. Part D, no. 6, pp. 373-387, November 1987.
- [50] C. Kim, E. NamGoong, S. Lee, T. Kim, H. Kim, “Fuel economy optimization for parallel hybrid vehicles with CVT,” SAE Paper No. 1999-01-1148, 1999.

- [51] E. D. Tate, S. P. Boyd, “Finding ultimate limits of performance for hybrid electric vehicles” SAE Paper No. 2000-01-3099, 2000.
- [52] G. Paganelli, M. Tateno, A. Brahma, G. Rizzoni, and Y. Guezennec, “Control development for a hybrid-electric sport-utility vehicle: Strategy, implementation and test results”, in Proc. of the American Control Conf., vol. 6, Arlington, VA, June 2001, pp. 5064-5069.
- [53] J.-S. Won, R. Langari, M. Ehsani, “Energy management strategy for a parallel hybrid vehicle”, in Proc. of International Mechanical Engineering Congress and Exposition (IMECE '02), New Orleans, LA, November 2002, pp. IMECE2002-33 460.
- [54] S.-I. Jeon, S.-T. Jo, Y.-I. Park, J.-M. Lee, “Multi-mode driving control of a parallel hybrid electric vehicle using driving pattern recognition”, Journal of Dynamic Systems, Measurement, and Control, vol. 124, pp. 141-149, March 2002.
- [55] S. Delprat, T. Guerra, J. Rimaux, “Optimal control of a parallel powertrain: From global optimization to real time control strategy”, in Proc. 18th Electric Vehicle Symposium EVS 18, Berlin, Germany, 2001.
- [56] J. Seiler, D. Schröder, “Hybrid vehicle operating strategies”, in Proc. 15th Electric Vehicle Symposium EVS 15, Bruxelles, France, 1998.
- [57] G. Paganelli, T. Guerra, S. Delprat, J. Santin, E. Combes, M. Delhom, “Simulation and assessment of power control strategies for a parallel hybrid car”, J. Automobile Eng., vol. 214, pp. 705–718, 2000.
- [58] G. Paganelli, S. Delprat, T. Guerra, J. Rimaux, J. Santin, “Equivalent consumption minimization strategy for parallel hybrid powertrains”, in Proc. Fall VTC-01 Conference Sponsored by VTS (Vehicular Technology Society) and IEEE, Atlantic City, NJ, 2001.
- [59] G. Paganelli, G. Ercole, A. Brahma, Y. Guezennec, and G. Rizzoni, “General supervisory control policy for the energy optimization of charge-sustaining hybrid electric vehicles”, Special Issue of JSAE Review, vol. 22, no. 4, pp. 511–518, 2001.
- [60] V. Johnson, K. Wipke, D. Rausen, “HEV control strategy for real-time optimization of fuel economy and emissions”, SAE, Paper no. 2000-01-1543.

- [61] M. Back, M. Simons, F. Kirschbaum, V. Krebs, “Predictive control of drivetrains”, in Proc. 15th IFAC World Congress 2002, Barcelona, Spain, 2002.
- [62] West, M.J.; Bingham, C.M.; Schofield, N., “Predictive control for energy management in all/more electric vehicles with multiple energy storage units”, Electric Machines and Drives Conference, 2003. IEMDC'03. IEEE International, Volume 1, 1-4 June 2003 Page(s):222 - 228 vol. 1.
- [63] Rajagopalan, A.; Washington, G.; Rizzoni, G.; Guezennec, Y., “Development of Fuzzy Logic and Neural Network Control and Advanced Emissions Modeling for Parallel Hybrid Vehicles”, NREL/SR-540-32919, December 2003.
- [64] Afridi, K.K.; Tabors, R.D.; Kassakian, J.G., “Alternative electrical distribution system architectures for automobiles”, Power Electronics in Transportation, 1994. Proceedings , 20-21 Oct. 1994, Pages:33 - 38.
- [65] J. Shen, A. Masrur, V. K. Garg, J. Monroe, “Automotive Electric Power and Energy Management – A System Approach”, Business Briefing: global automotive manufacturing & technology 2003.
- [66] I.A. Khan, “Power electronics in automotive electrical systems”, Power Electronics in Transportation, 1996. IEEE, 24-25 Oct. 1996 Page(s):29 – 38.
- [67] M.A. Masrur, D.S. Sitar, V.A. Sankaran, “Can an AC (alternating current) electrical system replace the present DC system in the automobile? An investigative feasibility study. I. System architecture”, Vehicular Technology, IEEE Transactions on, Volume 47, Issue 3, Aug. 1998 Page(s):1072 – 1080.
- [68] M.A. Masrur, D.S. Sitar, V.A. Sankaran, “Can an AC (alternating current) electrical system replace the present DC system in the automobile? An investigative feasibility study. II. Comparison and tradeoffs”, Vehicular Technology, IEEE Transactions on, Volume 47, Issue 3, Aug. 1998 Page(s):1081 – 1086.
- [69] P. R. Nicastrì, H. Huang, “42V PowerNet: Providing the Vehicle Electrical Power for the 21st Century”, SAE Paper 2000-01-3050.
- [70] M. Ehsani, N. Shidore, Y. Gao, “On board power management”, Power Electronics in Transportation, 2004, Page(s):11 – 17.

- [71] Neubert, J., “Powering up”, IEE Review , Volume: 46 , Issue: 5 , Sept. 2000, Pages:21 - 25.
- [72] A. Graf, “Semiconductors in the 42V PowerNet”, Intertech, 42V Automotive Systems Conference, Chicago, September 17-18, 2001.
- [73] F. Schmidt, “Draft specification of a dual voltage vehicle electrical power system 42V/14V”, Consortium of Advanced Automotive Electrical/Electronic Components and Systems Boston, MA, Mar. 1997.
- [74] J.G. Kassakian, J.M. Miller, N. Traub, “Automotive electronic power up”, IEEE Spectr., vol. 37, pp. 34-39, May 2000.
- [75] F. Klotz, A. Graf, “Driving small motors at 42 V powernet”, 42 Volt Technology-SAE SP-1619, Mar. 2001.
- [76] H. Thiemer, “Influence of automotive 42 V powernet on small PM DC motors”, Electric Machines and Drives Conference, 2001. IEMDC 2001. IEEE International, 2001 Page(s):591 – 593.
- [77] S. M. Lukic, A. Emadi, “Effects of Electrical Loads on 42V Automotive Power Systems”, SAE Paper 2003-01-2257.
- [78] P. VanOverschee, B. De Moor, “Subspace Identification of Linear Systems: Theory, Implementation, Applications”, Kluwer Academic Publishers, 1996.
- [79] G. Cimmino, “Sistemi EPAS (electric power assisted steering) per autoveicoli”, M.S. Thesis, Federico II University of Naples, 2005.
- [80] L. Piegari, R. Rizzo, “Experimental evaluation of charge laws for road vehicle batteries”, Vehicle Electronics Conference, 2001. IVEC 2001. Proceedings of the IEEE International, 25-28 Sept. 2001 Page(s):17 – 20.
- [81] S. Iovieno, “Una metodologia per l’analisi del sistema di generazione a bordo dei veicoli di trasporto su gomma”, M.S. Thesis, Federico II University of Naples, 2004.
- [82] V. Isastia Cimino, S. Meo, F. Esposito, “An optimization technique for the choice of advanced automotive electrical systems”, 5th IASTED International Conference on POWER AND ENERGY SYSTEMS (EuroPES 2005), June 15-17, 2005, Benalmádena, Spain.
- [83] Wierzbicki, M. Makowski, J. Wessels, “Model-based decision support methodology with environmental applications”, Kluwer Academic Publishers,

- Dordrecht, series: Mathematical modeling and applications, 2000, ISBN 0-7923-6327-2.
- [84] Massam, B.H., “Multi-Criteria decision making techniques in planning”, Oxford Pergamon, 1988.
- [85] SABER[®] MAST Language User Guide, Books 1, 2, Version Y-2006.06, Synopsys.
- [86] SABER[®] Simulator Guide Reference Manual, Version Y-2006.06, Synopsys.
- [87] S. Boyd, L. Vandenberghe, “Convex Optimization”, Cambridge University Press 2004.
- [88] Fletcher, R., “Practical Methods of Optimization”, John Wiley and Sons, 2000.
- [89] Schittkowski, K., “NLQPL: A FORTRAN-Subroutine Solving constrained Nonlinear Programming Problems”, Annals of Operations Research, Vol. 5, pp 485-500, 1985.
- [90] T. Coleman, M. A. Branch, A. Grace, “Optimization Toolbox User’s Guide”, The MathWorks, Inc.
- [91] NEDC, European Council Directive, 70/220/EEC with amendments.
- [92] S. Meo, F. Esposito, “An Optimal Energy Management Strategy for Power-Split Hybrid Electric Vehicles”, International Review of Electrical Engineering (IREE), Vol. 1, n. 5, pp. 619-632, 2006.
- [93] <http://www.cleangreencar.co.nz/page/prius-history>
- [94] Kelly, K.J., Rajagopalan, A., “Benchmarking of OEM Hybrid Electric Vehicles at NREL”, NREL/TP-540-31806, NREL, Golden, CO, August 2001.
- [95] ADVISOR[®] Data files.
- [96] P. Setlur, J.R. Wagner, D.M. Dawson, B. Samuels, Nonlinear control of a continuously variable transmission (CVT), Control Systems Technology, IEEE Transactions on, Volume 11, Issue 1, Jan. 2003 Page(s):101 – 108.